

Nonlinear Model Predictive Control of a Hybrid Diesel-Electric Marine Propulsion Plant

Vasileios Karystinos

Diploma Thesis



School of Naval Architecture and Marine Engineering
National Technical University of Athens

Supervisor: Assistant Prof. George Papalambrou

Committee Member : Prof. N. Kyrtatos

Committee Member : Prof. K. Kyriakopoulos

July 2019

Acknowledgments

This work has been carried out at the Laboratory of Marine Engineering (LME) at the School of Naval Architecture and Marine Engineering of the National Technical University of Athens, under the supervision of Assistant Professor George Papalambrou.

I would first like to thank my thesis supervisor Assistant Professor George Papalambrou for giving me the chance and motivation to work on this topic. I would also like to thank him for his patience, continuous support and immense knowledge. His guidance helped me in all the time working on this thesis.

I would like to thank Professor Nikolaos Kyrtatos for providing the opportunity to work with the full-scale hybrid diesel-electric marine propulsion powertrain of LME. Access to LME experimental facilities was essential in order to verify theoretical concepts from a practical perspective and evaluate experimentally the designed control system. I also thank him for being a member of my supervisors committee.

I would also like to thank Professor Konstantinos Kyriakopoulos for evaluating my work and being a member of my supervisors committee.

I would like to express my sincere gratitude to Mr. Nikolaos Planakis, PhD candidate of School of Naval Architecture and Marine Engineering for his contribution to the experimental validation of control system performance. I am extremely thankful to him for sharing expertise, and sincere and valuable guidance and encouragement extended to me.

I take this opportunity to express gratitude to all LME fellow members for their help and support.

I am also sincerely grateful to my family, for the unceasing encouragement, support, motivation and attention throughout my studies.

I also place on record, my sense of gratitude to one and all, who directly or indirectly, have lent their hand in this venture. This accomplishment would not have been possible without them. Thank you.

Abstract

In this thesis, the implementation of nonlinear model predictive control in a hybrid diesel-electric marine power plant is investigated. Initially, modeling procedure of the components of the power plant is been presented. For each component (engine, electric motor/generator, battery), several models where investigated. The aim is to find models which are accurate and computationally efficient, so that the controller would be able to solve the optimization problem in real time. Moreover, dynamic analytic models where also reviewed in order to set up a reliable simulation for the controller.

Nonlinear Model Predictive Control (NMPC) is a sophisticated model based control method which can handle nonlinear multi-variable problems with constraints by solving the optimization problem of minimizing an objective function over a finite horizon. The developed controllers were evaluated regarding the performance with simulations in a virtual hybrid diesel-electric set-up in Simulink. Moreover, the development of an efficient observer for the applied load estimation by implementing a Moving Horizon Estimation (MHE) scheme is also examined. MHE is a technique which approaches the full estimation problem using a finite measurement horizon.

Finally, the performance of the developed controllers was experimentally verified on the hybrid propulsion plant HIPPO-2 at LME. The experiments were conducted for various load profiles, and the controllers were evaluated regarding the their ability to track the contextually reference and satisfy the predefined constraints.

List of Figures

1.1	Wärtsilä HY-2 Diesel-Mechanical Configuration.	14
2.1	The HIPPO-2 hybrid diesel-electric testbed of LME.	18
2.2	HIPPO-2 speed and torque outputs.	19
2.3	Engine CAT C9.3.	20
2.4	Loading diagram of CAT C9.3.	20
2.5	ABB Electric Motor 90 kW.	21
2.6	ABB Electric Brake 315 kW.	21
2.7	ABB ACS 800 controlling panels.	22
2.8	The HIPPO-2 dSpace monitoring and control board.	23
2.9	The general arrangement of data acquisition system for HIPPO-2.	24
2.10	Relation between air fuel ratio and emissions, from [9].	26
2.11	Typical Configuration of a Diesel Engine, from [10].	27
2.12	Block Diagram of diesel engine model for simulations from [12].	28
2.13	Fuel Consumption vs Speed and Torque Map.	31
2.14	CAT [®] C 9.3 engine and SCANIA DC13-081A model, experiment and simulation comparison results.	32
2.15	MISO parametric model for Fuel Rate estimation, compared to simulation data (Case A)	36
2.16	MISO parametric model for Fuel Rate estimation, compared to experimental data (Case B)	37
2.17	Willans model fitting results, compared to test data from manufacturer.	41
2.18	Willans model comparison with experimental data.	41
2.19	Typical Li-ion Discharge Voltage Curve from [28]	43
2.20	Equivalent circuit of quasi-static battery model	44
2.21	Block diagram of quasi-static battery model	46
2.22	Equivalent circuit of PNGV battery model	47
2.23	Block diagram of PNGV battery model	48
2.24	Battery model comparison results obtained from Simulink	50
3.1	Concept of Model Predictive Controller [39].	55
3.2	ACADO Code Generation Structure [55].	64
4.1	Block Diagram of engine direct torque control scheme of HIPPO 2 with battery consideration.	69
4.2	Simulink set up of Marine Hybrid Diesel Electric Propulsion Plant	70
4.3	Block Diagram of indirect fuel rate scheme	71
4.4	Simulation results of Fuel Rate control with and without control horizon NMPC	74
4.5	Simulation results of Fuel Rate control with and without adaptive NMPC	75
4.6	Block Diagram of direct SE control scheme	76

4.7	Simulation results engine control with Fuel Consumption Rate constraint . . .	79
4.8	Block Diagram of direct SE control scheme with battery consideration . . .	80
4.9	Simulation results of direct engine control with consideration of battery . . .	82
4.10	Block Diagram of direct SE control scheme with battery consideration and MHE estimator	84
4.11	Simulation results and comparison of MHE-NMPC scheme with and with- out SE feedback from the MHE	86
4.12	Vessel operation profile	87
4.13	Simulation results of NMPC and MHE performance during transient pro- peller load	88
5.1	Exp 1: Applied EB torque, EM torque and ICE torque.	91
5.2	Exp 1: Measured fuel rate consumption and reference, λ value and EM requested power.	92
5.3	Exp 1: NOx concentration, EGR valve command and Exhaust Gas Mass Flow.	92
5.4	Exp 2a: Applied EB torque, EM torque and ICE torque.	96
5.5	Exp 2a: Measured fuel rate consumption and reference, λ value and EM requested power.	96
5.6	Exp 2a: NOx concentration, EGR valve command and Exhaust Gas Mass Flow.	97
5.7	Exp 2b: Applied EB torque, EM torque and ICE torque.	97
5.8	Exp 2b: Measured fuel rate consumption and reference, λ value and EM requested power.	98
5.9	Exp 2b: NOx concentration, EGR valve command and Exhaust Gas Mass Flow.	98
5.10	Exp 2b: Near constraint (ICE torque) operation.	99
5.11	NOx production for static reference in g/kWh (Exp 2a)	101
5.12	NOx production for dynamic reference in g/kWh (Exp 2a)	101
5.13	Exp 3a: Applied EB torque, EM torque and ICE torque.	106
5.14	Exp 3a: Measured fuel rate consumption and reference, λ value and EM requested power.	107
5.15	Exp 3a: NOx concentration, EGR valve command and Exhaust Gas Mass Flow.	107
5.16	Exp 3b: Applied EB torque, EM torque and ICE torque.	108
5.17	Exp 3b: Measured fuel rate consumption and reference, λ value and EM requested power.	109
5.18	Exp 3b: NOx concentration, EGR valve command and Exhaust Gas Mass Flow.	109
5.19	Exp 3c: Applied EB torque, EM torque and ICE torque	110
5.20	Exp 3c: Measured fuel rate consumption and reference, λ value and EM requested power.	111
5.21	Exp 3c: NOx concentration, EGR valve command and Exhaust Gas Mass Flow	111
5.22	Exp 5b: NOx production for static reference in mg/s and g/kWh	113
5.23	Exp 5c: NOx production for dynamic reference in mg/s and g/kWh	114

List of Tables

2.1	Engine simulation model and HIPPO 2 engine characteristics comparison.	28
2.2	PNGV ECM parameters [38]	48
2.3	PNGV and quasi-static ECM parameters for simulation	49
4.1	HIPPO's 2 measured signal sample times and time delays relative to load application.	69
4.2	PNGV and quasi-static ECM parameters for simulation	81
5.1	Index of experiments which were conducted on HIPPO 2 test-bed	89
5.2	Comparison Hybrid vs ICE sole operation for the same load cycle	102
5.3	PNGV and quasi-static ECM parameters for experiment	105
5.4	Comparison Hybrid vs ICE sole operation for the same load cycle and battery configuration.	113
A.1	Nomenclature for engine model [12].	120
A.2	Constant that were applied for engine model [12].	121
A.3	Parameters that were applied for engine model [12].	122

Contents

List of Figures	7
List of Tables	9
1 Introduction	13
2 Propulsion Plant Description and Modeling	17
2.1 HIPPO-2 Experimental Test-Bed	18
2.2 Diesel Engine Modeling	25
2.2.1 Introduction	25
2.2.2 Modeling	26
2.3 Electric Motor/Generator Modeling	38
2.3.1 Introduction	38
2.3.2 Modeling	39
2.4 Battery Modeling	42
2.4.1 Introduction	42
2.4.2 Modeling	43
2.4.3 Model Comparison	48
2.5 HIPPO-2 Modeling of dynamics	51
3 NMPC - MHE Theory and Application	53
3.1 Nonlinear Model Predictive Control Theory	54
3.1.1 NMPC Problem Formulation and solution via Real Time Iteration	56
3.1.1.1 Nonlinear MPC scheme (NMPC)	56
3.1.1.2 Sequential Quadratic Programming (SQP) for NMPC	56
3.1.1.3 The Real Time Iteration approach (RTI)	58
3.1.1.4 Global optimality for the NMPC solution	59
3.1.1.5 Application to continuous-time systems	60
3.2 Moving Horizon Estimation Theory	61
3.2.1 MHE Problem Formulation	62
3.3 NMPC and MHE Implementation	64
4 Controllers Design and Simulations	65
4.1 NMPC Strategy and Implementation	67
4.2 Propulsion Plant Simulation	69
4.3 Indirect Control of ICE	71
4.3.1 Fuel Rate control	71
4.4 Direct Control of ICE	76
4.4.1 Engine Speed Reference Tracking	76
4.4.2 Engine Speed Reference Tracking with Battery Consideration	80
4.5 Load Estimation - MHE	83

4.6	Marine Application: Propeller Loading	87
5	Experimental Results	89
5.1	Experiment 1: Indirect Fuel Rate Control	90
5.1.1	Controller Set Up	90
5.1.2	Experimental Results	91
5.1.3	Results Analysis	93
5.2	Experiments 2a and 2b: Direct Engine Speed Control	94
5.2.1	Controller Set Up	94
5.2.2	Experimental Results	95
5.2.3	Result Analysis	100
5.3	Experiments 3a, 3b and 3c: Direct Engine Speed Control with Battery Consideration	104
5.3.1	Controller Set Up	104
5.3.2	Experimental Results	105
5.3.3	Results Analysis	112
6	Conclusions and Future Work	115
	Appendices	117
A	Simulation Engine Model Symbols and Parameters	119
	Bibliography	123

Chapter 1

Introduction

Problem Formulation

Over the past two decades, within the wider international debate on climate change, industries are on a great pressure to reduce their environmental impact. In this context, there are requirements for marine industry to reduce emissions of greenhouse gases, most notably carbon dioxide although other exhaust gases and the components, such as the nitrogen oxides (NO_x), are also included. Furthermore, a regulatory framework is implemented by the IMO, MARPOL Annex VI, in order to enforce the above reductions, by setting operational and design limitations. For instance, engines manufactured after 2011 and with output power over 130 kW required to limit their specific NO_x emissions. In environmentally "sensitive" sea regions, even lower limits apply. Moreover, the vessel design efficiency is also examined, via the EEDI index. This efficiency depends on the total CO₂ related emissions, the ship would emit in order to complete the required transportation work. Indicatively, by 2030 the ships which will be constructed are required to have 30 % reduced EEDI than 2013 [1]. Although, this regulation aimed to increase the hull efficiency, a trend is to regulate it via the efficiency of the propulsion plant (e.g. "slow steaming"). Most of the marine propulsion and powering plants employ diesel engines as their main power supplier. However, considering that diesel engines have almost reach their thermal capabilities and they are rather pollutant machines, the usage of novel technological advancements, in order to achieve the above reductions, seems to be inevitable.

According to [2] several promising technologies have been proposed. Some of them aim to decrease the power demand, (i.e. by optimizing the efficiency of the hull and propeller) and others to increase the efficiency of power plant itself. Regarding the second manner, a lot of new recent technologies promise to reduce both emissions and fuel consumption. A number of these efforts, are related with optimizing the existing diesel engines performance regarding the emissions, directly (e.g. the EGR), or indirectly (e.g. SCR). Moreover, alternative fuels (e.g. LNG and bio-fuels) and renewable sources of power have been also proposed. Furthermore, advances in battery technologies regarding their capacitance and efficiency, have already made possible the first fully battery depended ships, employing both high energy efficiency and zero emissions. However, battery cost and limited capacitance still pose barriers which have to be overcome. An interesting solution which aims to combine the proven availability and operational efficiency of conventional propulsion manner, and the benefits of novel technologies is Hybrid Propulsion and Energy Conversion. Hybrid propulsion is an option where one or more modes of powering the ship can be utilized to optimize performance for economic, environmental or operational reasons. A common hybrid configuration is that the different powering modes feed a common elec-

trical bus bar from which power can be drawn for various purposes. This, however, is not necessarily the case since many examples of mechanical linkages between independent power sources have been designed and operated in ships, both past and present [2]. The key factor in order to achieve respectable higher efficiency is the control strategy. For instance, studies have shown that a 10-35% fuel and emission reduction is possible in battery deployment and intelligent use of DC configurations by implemented appropriate control strategies [1].

Literature Review

Over the recent years, there is an increasing number of hybrid marine applications. These systems have extra degrees of freedom leading to increased complexity of the propulsion system. However, the control implementations for these systems are based mostly in traditional control strategies, e.g. fixed combinator curves, fixed frequency generators, rule based control of batteries etc. [1]. Research have shown, though, that conservative control strategies which apply to advance architectures, will probably lead to a insignificant fuel and emission reduction. However, control strategies progress regarding marine applications, is not so advanced. Although, strategies with significant increase efficiency have been proposed, most of them lack of impact analysis.

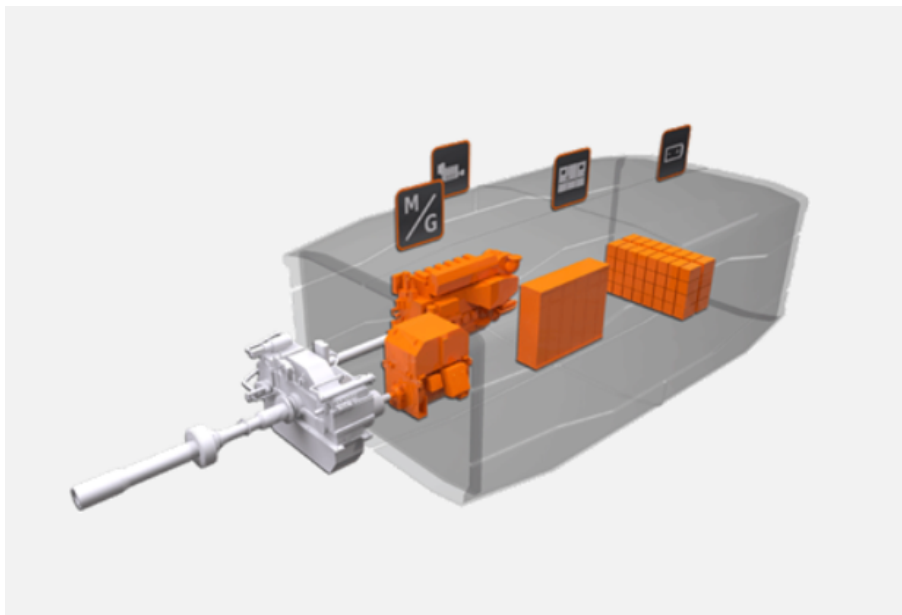


Figure 1.1: Wärtsilä HY-2 Diesel-Mechanical Configuration.

Hybrid propulsion, can be reviewed in accordance with the implemented configuration. There are applications which the main propulsive system is conventional one, such as a diesel engine, the electric motor is connected to the main shaft line. The main idea is that diesel engine is supposed to provide the propulsive power in higher speeds and loads, in which the efficiency is greater. Additionally the electric Motor would provide the propulsive power in lower speeds, in which the the diesel efficiency is significantly lower. In [3], an interesting application is suggested for a naval frigate application in which the the electrical part serves as shaft generator in partial loads, increasing in this way the efficiency by covering the electric supply demand directly from the engine with a higher

efficiency. The implemented control strategy was speed and voltage droop control, combining field oriented control for the electric machines. An another interesting application which refers to parallel operation of the electric motor and diesel engine is presented in [4], which the motor assists the engine so as to maintain a specific air-fuel ratio λ reference. In that way, during transient operations, the thermal loading of the engine is decreased, and consequently the NOx emissions drops. In [5], the above is implemented via Model Predictive Control.

An another interesting implementation is the use of hybrid power supply. Besides diesel engines and diesel generators, batteries could be implemented as a secondary power source. In this way, the high efficiency of diesel engines in high loads is fully exploited, while in partial and low loads, the propulsion is conducted by the electric part with high efficiency. Two approaches are conceived for this scheme. The first is referred as heuristic control strategy, in which the battery charge is provided offshore. In [6], a rule based strategy which greatly reduce the fuel consumption for hybrid harbor tugs is suggested. The other approach suggests that the battery should be recharged during the operation by the primary mover. According to [6], an equivalent fuel consumption strategy is proposed which aims to drop the fuel consumption, by applying linear programming.

Thesis structure

In this work, *hybrid diesel-electric ship propulsion* is examined from the point of the implemented control strategy, with respect to minimizing the produced emissions during transient loads. In particular, Nonlinear Model Predictive Control (NMPC) configuration for the closed-loop control of a parallel Hybrid diesel-electric powertrain is investigated. The main purpose is to implement an efficient control scheme which reduces NOx emissions for the Hybrid powertrain HIPPO-2 of Laboratory of Marine Engineering (LME). Two control schemes were followed. The first employs indirect control of the engine by regulating the electric torque, in order to manipulate the fuel consumption dynamically during transient loading. In the second scheme, both engine and electric motor are controlled directly from the NMPC so as the rotational shaft speed to follow a predefined reference, in respect to certain constraints. In this case, the aim is to reduce the engine dynamics in order to reduce the NOx propagation, and smooth the engine operation. Moreover, battery employment is also considered and implications regarding the above strategy when capacitance is rather small are investigated. Finally, an efficient observer for the engine operation is proposed and a simulation of the controller-observer scheme in a marine application is illustrated.

The structure of the thesis is as follows: in chapter 2 the experimental facility is presented, along with the installed engine sensors and the data acquisition system and its modeling approach is described. In chapter 3, a brief theory review of NMPC and MHE techniques is illustrated. In chapter 4, control design and simulation results are presented. Results from experimental testings of the controllers on HIPPO 2 testbed are shown in chapter 5. Finally, the conclusions of this work are presented in chapter 6.

Chapter 2

Propulsion Plant Description and Modeling

In this chapter, the experimental hybrid powertrain facility *HIPPO-2*, where the controllers were applied and tested, is presented. The facility is composed of three major components, *Internal Combustion Engine (ICE)*, *Electric Motor/Generator (EM)* and *Electric Brake (EB)*, which applies the load torque to the system. In addition, a *virtual Battery (B)* was also considered, which was simulated in parallel during the experimental test via the control platform. The model predictive control scheme, requires to model the above components so as to simulate and solve the optimization control problem. Here the model schemes for each component are presented. Furthermore, modeling was not confined in the NMPC application, and reliable models for a dynamic simulation set-up were also reviewed and implemented.

2.1 HIPPO-2 Experimental Test-Bed

The HIPPO-2 hybrid diesel-electric power plant consists of an internal combustion engine (ICE) in serial connection to an electric motor (EM). In this configuration, the rotational speed of the ICE and the EM are identical and the supplied torques add together to maintain the total torque demand applied by an electric motor brake (EB). In Fig. 2.1 and 2.2 the experimental hybrid powertrain of LME is presented, along with a schematic representation of the speed and torque outputs.

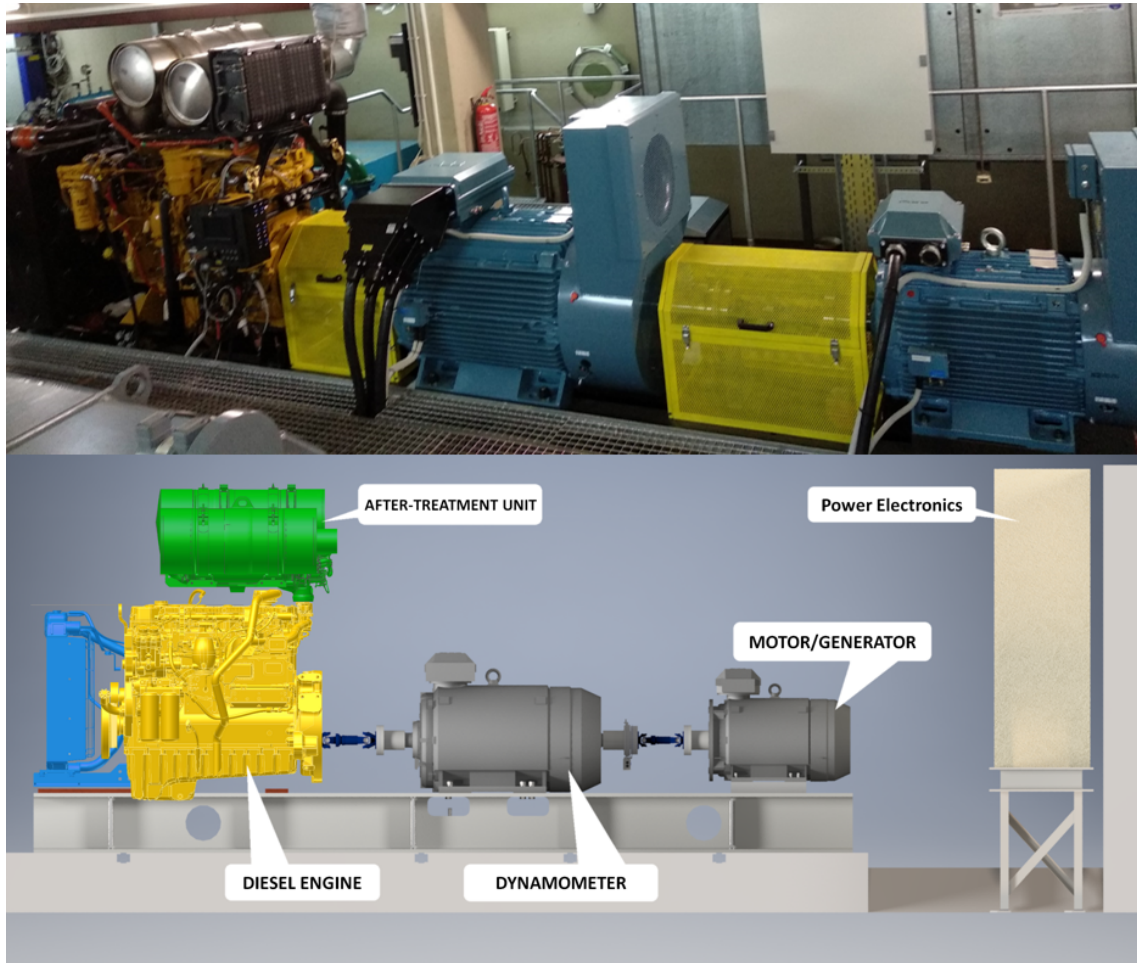


Figure 2.1: The HIPPO-2 hybrid diesel-electric testbed of LME.

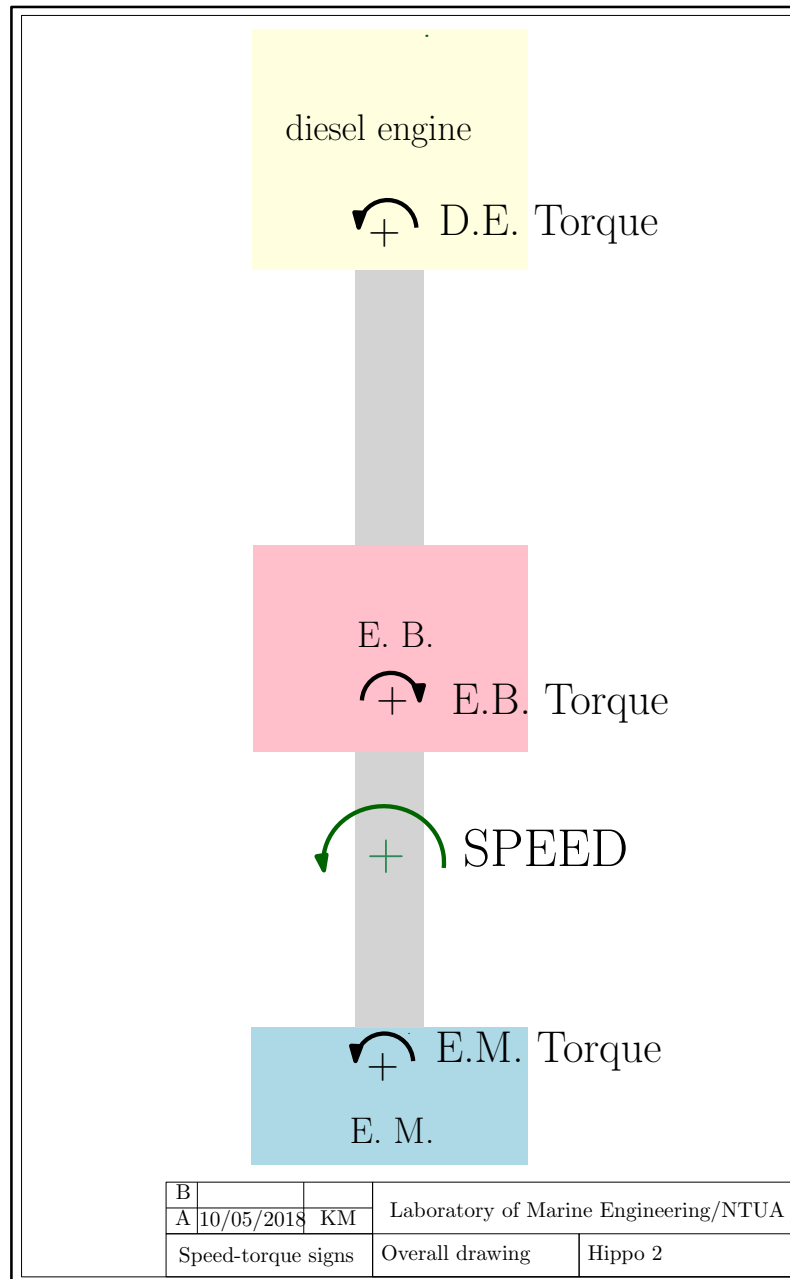


Figure 2.2: HIPPO-2 speed and torque outputs.

HIPPO-2 Integration

The ICE is a turbocharged CATERPILLAR® 6-cylinder 9.3-liter 4-stroke industrial diesel engine, model C9.3 ACERT™, (shown in Fig. 2.3), producing 261 kW at 1800-2200 rpm and maximum torque 1596 Nm at 1400 rpm. The loading diagram of engine is shown in 2.4 (Rating C). According to the speed reference and the deviation of speed measurement, the electronic control unit (ECU) of the ICE controls the fuel injection in the cylinders in closed loop control, using controller in the form of look-up tables. The engine is designed to meet U.S. EPA Tier 4 Final, EU Stage IV emission standards. Exhaust Gas Recirculation (EGR) and Selective Catalyst Reducer (SCR) systems for NO_x reduction, are also incorporated, along with a Diesel Particulate Filter (DPF).

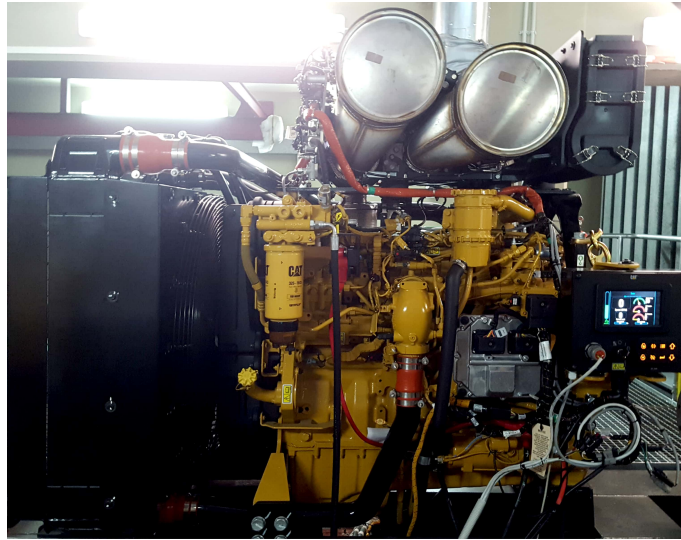


Figure 2.3: Engine CAT C9.3.

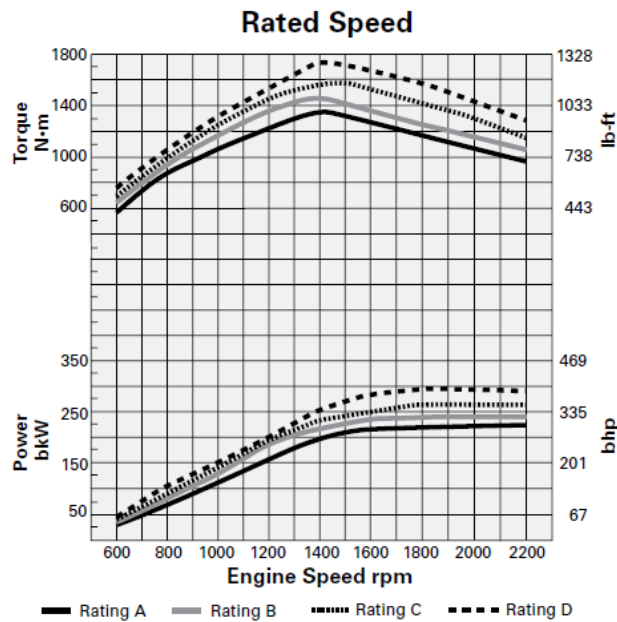


Figure 2.4: Loading diagram of CAT C9.3.

The EM is a standard AC induction 3-phase motor (shown in Fig. 2.5), with a rated power of 90 kW at 1483 rpm, type M3BP 280SMB 4 IMB3/IM1001, manufactured by ABB®. The EM can operate both as motor, to assist the engine, and as generator to store energy.



Figure 2.5: ABB Electric Motor 90 kW.

The EB is a standard AC induction 3-phase motor manufactured also by ABB®, type M3BP 355SMB 4 IMB3/IM1001, with 315 kW load capacity, operating at 1488 rpm. The EB is shown in Fig. 2.6.



Figure 2.6: ABB Electric Brake 315 kW.

The 3 motors are connected in series, thus the operating speed range of HIPPO-2 is from 600 to 2200 rpm, with maximum load of 341 kW (ICE and EM combined power).

ABB® industrial drives

The speed and torque outputs for both EM and EB are being controlled and supervised by ABB® drives. The type of ABB driver which has been used for EB and EM is ACS800 (fig 2.7) with power capabilities of 390 kW and 100 kW respectively.



Figure 2.7: ABB ACS 800 controlling panels.

The data acquisition and the control of the ABB engines are achieved through ACS800 panels and CANopen bus protocol.

System Sensors

The system operation is monitored via a number of sensors. The NO_x and λ values are provided by a *SmartNO_x* sensor in the manifold downstream of the turbocharger (TC). Fuel mass flow measurements are provided by two ABB® Coriolis flow-meters, one at supply and one at return fuel lines. Intake manifold pressure is also measured. The fuel mass flow from the diesel tank as well the fuel return are measured by two identical Coriolis flowmeters manufactured by ABB. Between EM and EB, a torque meter, HBM T10F, is installed, which measures the EM torque.

Description of Data Acquisition System

The data acquisition system of HIPPO 2 consists of:

1. DSpace Microautobox II
2. CAN bus
3. RCAN modules

4. ABB Drivers
5. Signaling Cables for I/O
6. Ethernet cable

The platform for Data Acquisition and control of the powertrain is based on the dSpace Micro Autobox II DS1401/1511 (Fig. 2.8) controller board, with rapid control prototyping capability, programmed under the MATLAB/Simulink environment.



Figure 2.8: The HIPPO-2 dSpace monitoring and control board.

The simplicity of communication topography is depicted in figure 2.9. dSpace Micro Autobox II is a real-time system for performing fast function prototyping in fullpass and bypass scenarios. It operates without user intervention, just like an ECU. It has the ability to connect with many sensors from the testbed through of its Analog, Digital and CAN ports. In fact, with dSMA II it is possible to read all the data from any sensor which is mounted on C9.3 diesel as well on ABB electric motor through CAN bus. The backbone of CAN bus is a twisted pair cable; in the particular case 3 CAN channels from dSpace are used. The first is CAN A from CAT engine's ECU and is connected to CAN 2 in dSMA II connector, the second is ABB CAN from RCAN modules which is connected to CAN 3 in dSMA II; the third CAN channel, CAN 4, has been installed for future use and is connected to AT's ECU. The CAT C9.3 engine together with the two ABB motors have almost 150 sensors and 700 signals that can be acquired and used for monitoring every parameter of the HIPPO-2 test bench. It is very important for the prototype test bench to have the capability to monitor a diverse set of parameters for basic engine, TC, AT as well as for those parameters related to the operation of electric drives. Taking into consideration all the above complexity of sensing, the most efficient way of connecting and controlling the motors is through CAN bus.

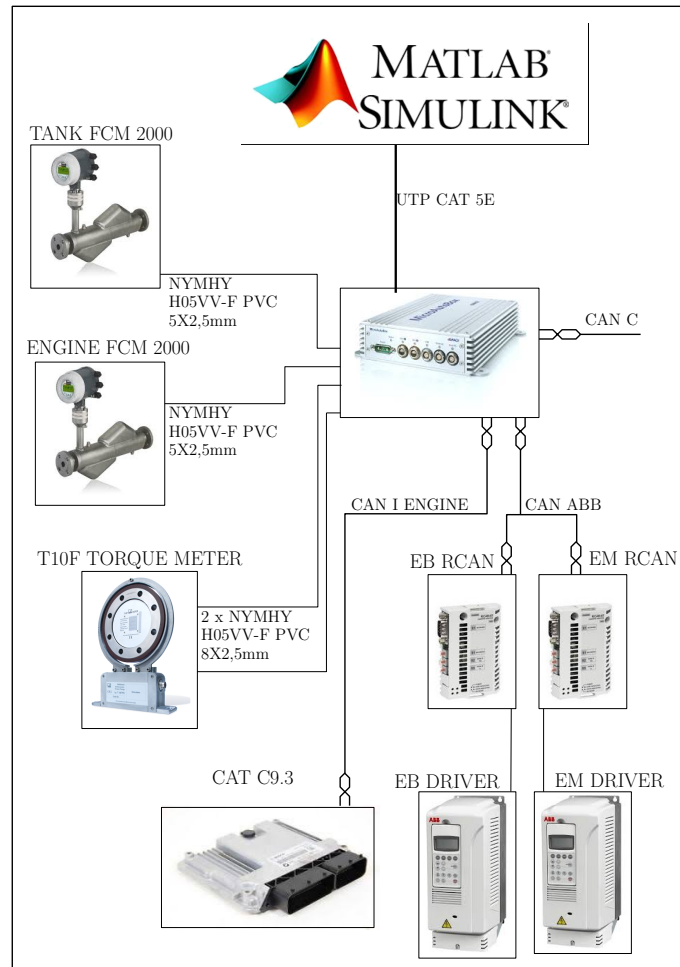


Figure 2.9: The general arrangement of data acquisition system for HIPPO-2.

2.2 Diesel Engine Modeling

2.2.1 Introduction

Internal Combustion Engines (ICE) are heat engines in which production of mechanical power from the chemical energy, contained in the fuel, is conducted. This energy is released by burning the fuel with an oxidizer, usually air, inside a combustion chamber. ICEs can be distinguished into two categories. The *continuous-combustion*, in which the flow of fuel-oxidizer is steady and a steady flame is maintained, for instance gas turbines and jet engines, and the *intermittent-combustion engines*, where ignition of air and fuel is periodic, also they are commonly referred to as a reciprocating engine. Gasoline piston engines and diesel engines are examples of the second group. In the present work, the main propulsion machine, is a *Four-Stroke Diesel Engine*, and therefore only this ICE category is further discussed.

The main attributes of diesel engines and consequently the reason of their dominance as the main powering device in industry over the past century, is their high power/weight ratio and their relatively high thermal efficiency [7]. Four stroke turbocharged Diesels can reach efficiency of approximately 40 %. Two key factors are responsible for the above [8]. The first is the increased compression ratio. When the working fluid is compressed, its temperature rises, leading to increased thermal efficiency. Since, the compressed fluid is consisted only from oxidizer (air), there is no self-ignition problem. The fuel eject and ignites, at the desired crankshaft angle. The second is that diesel engine can operate with lean mixtures of air and fuel in cylinder, such that throttling of the intake air can be completely avoided, something which is possible due to extremely hot air in cylinder. Consequently, the high thermal efficiency is maintained to a certain degree for part load operations.

The operation of diesel engines is associated with two major drawbacks [8]. The first is related to the low power-density they exhibit. This occurs from the fact that the mixture inside the combustion chamber is always lean, and thus less fuel can be burned in atmospheric conditions inside a cylinder. Moreover, engine maximum speed is relatively low due to mechanical limitations. This problem is sufficiently addressed with super or turbocharging the engine, namely, compressing the air before enters the cylinder, allowing more fuel to be burnt, in this way. The second disadvantage refers to issues of the exhaust gas purification. Apart of the ideal products of combustion, which are water (H_2O) and carbon dioxide (CO_2), several by-products are also produced. A part of them are harmful to environment or cause health problems to humans. Therefore, numerous legislation frameworks, aiming to reduce the above effects, have been applied since the early 1970s for the automotive, and the late 1990s for marine industry [9], implementing limits to their concentration in the exhaust gases. The main pollutants that the above limits apply are nitrogen oxides (NO_X), unburned hydrocarbons (HC), carbon monoxide (CO) and soot. Key factors for the concentration of above is ratio of air-fuel compared to stoichiometric (λ) and the cylinder temperature. The typical relation of air-fuel ratio and the emissions above is shown in Figure 2.10.

Although, Diesel engines have lower raw emissions than Otto, their working principle (i.e. lean operation), exclude the solution of the the three-ways-catalysts, since this system requires stoichiometric air-fuel ratios. Consequently, other technologies have developed, in order to restrict the above emissions, continually lowering fuel consumption and optimizing performance at the same time. These options after-treat the exhaust gas (e.g.

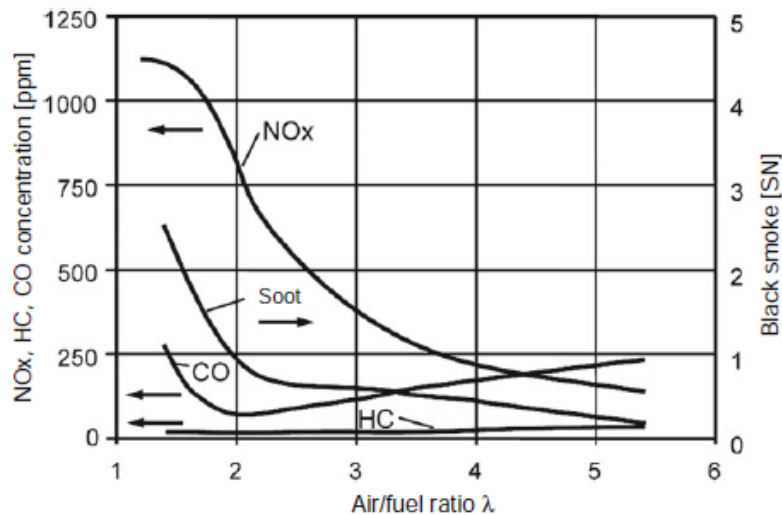


Figure 2.10: Relation between air fuel ratio and emissions, from [9].

Selective Catalyst Reducer - SCR), or affect the operation of engine itself (e.g. Exhaust Gas Re-circulation - EGR).

Obviously, Diesel engines are complex systems, which can be resolved to several sub-systems, all of which interact with each other in a direct or in an indirect way. In Figure 2.11, a block diagram derived from [10] is presented, showing a typical configuration of a diesel engine. The main components of a diesel engine are the *Intake* and the *Outlet Receiver*, the *Compressor*, the *Turbine*, the *Intercooler*, the *EGR* and the *Cylinders*.

Diesel engine behavior at transients operations

Most of the engine-oriented literature is focused on steady state operation, although transient applications represent a large portion of the engine operating patterns (e.g. maneuvering conditions for ships), or even the majority of operations (e.g. automotive vehicles). In recent years, due to the latest regulatory framework regarding the engine emissions, more attention is given concerning this operation mode. According to literature [59], during transient loading profiles, gaseous and noise emissions typically exceed their acceptable values following the extreme, non-linear and non-steady-state conditions experienced during dynamic engine operation. For instance, 50% of NOx emissions from automotive engines during the European Driving Cycle stem from periods of acceleration, whereas instantaneous particulate matter and NOx emissions during load increase transients have been measured to be 1 to 2 orders of magnitude higher than their respective quasi-steady values.

2.2.2 Modeling

Since diesel engines have been a main source of power for the industry and transportation for over a century, several modeling approaches have been conducted. [8,10–15]. According to [8], diesel models can be distinguished between *distributed* or *lumped* parameters, *crank resolution* or *cycle average*, *mean value* or *discrete event* and *operation analysis* or *control design oriented* models. In the present study, the aim is to build a model which can predict the dynamic behavior of a diesel engine (e.g. the Fuel Oil Consumption in speed

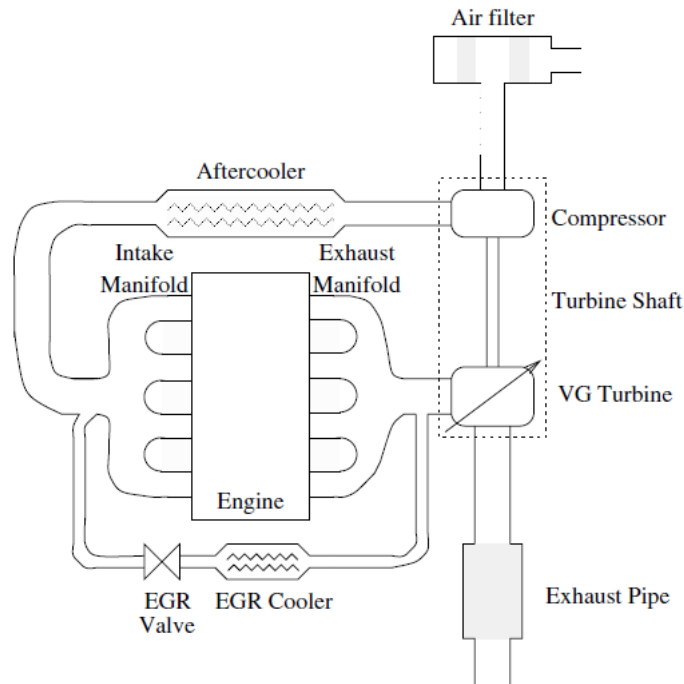


Figure 2.11: Typical Configuration of a Diesel Engine, from [10].

control mode), but not too complex in order to be able to be resolved by the optimizer in real time. Furthermore, in order to develop and test the controller behavior, a dynamic mean value model of the CAT C9.3 ACERT engine¹, or at least a equivalent type and size engine model, is required. Considering the above, two model types were reviewed and are presented in this section: a *simple mean value, cycle average, analysis model* for simulation and a *non-linear, parametric, dynamic model* in order to be integrated in the controller.

Dynamic Diesel engine model for simulations

The model, which was used for simulations and is described below, was derived from [12], and it is a simplification of the model proposed in [11], i.e. the turbine geometry is fixed, EGR valve is considered closed and turbine and compressor equations were simplified in order to be continuously differentiable. The model is very accurate since the most significant relative error of the important intake manifold pressure dynamics is 7% at higher speeds and 2% at the lower, compared to the real engine. The model describes a six-cylinder 12.7-l SCANIA diesel engine. This engine type is resembling CAT C 9.3 ACERT, and thus it can be used for developing and testing the controllers. The SCANIA characteristics, compared to CAT C9.3, are shown in the table 2.2.2.

The block diagram of the model is shown in Figure 2.12. The model consists of two control volumes, intake and exhaust manifold, and four restrictions, compressor, engine, turbine, and wastegate. The states of the model are four, engine speed, ω_{ice} , inlet manifold pressure, p_{im} , exhaust manifold pressure, p_{em} , and turbocharger speed, ω_{tc} . Its inputs are the external load, the injected fuel and the waste-gate valve command. For shake

¹CAT C9.3 is used at the HIPPO-2 test-bed

<i>Specification</i>	<i>CAT C9.3 ACERT</i>	<i>SCANIA DC13-081A</i>
Type	4-Stroke-Cycle Diesel	4-Stroke-Cycle Diesel
Cylinders	6 In-Line	6 In-Line
Bore [mm]	115	130
Stroke [mm]	149	160
Displacement [L]	9.3	12.7
Compression Ratio	17.0:1	17.3:1
Maximum Power [bkW]	261	257
Rated Speed [rpm]	1800-2200	1500-2100
Specific Consumption [g/kWh] (at Full Load and 1800 rpm)	204	196

Table 2.1: Engine simulation model and HIPPO 2 engine characteristics comparison.

of simplicity, waste-gate valve is assumed to be closed for all cases. The mathematical formulation of the model is described below.

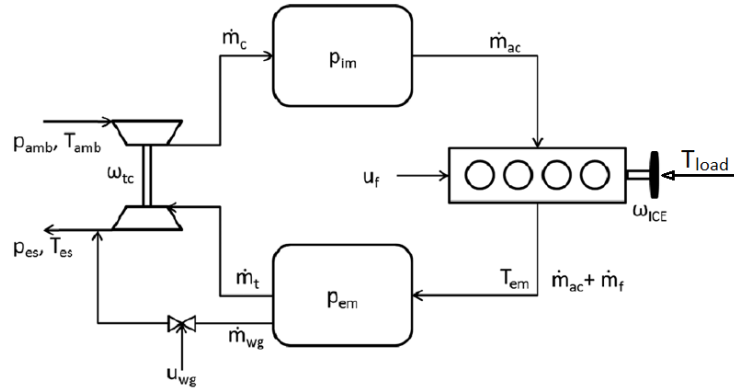


Figure 2.12: Block Diagram of diesel engine model for simulations from [12].

The governing differential equations for shaft and turbocharger rotational speed are derived from the Newton's 2nd Law. The pressure states were modeled as isothermal procedures via the ideal gas law and mass conservation.

$$\frac{d\omega_{ice}}{dt} = \frac{1}{J_{engine}} (T_{ice} - T_{load}) \quad (2.2.1)$$

$$\frac{dp_{im}}{dt} = \frac{R_a T_{im}}{V_{im}} (\dot{m}_c - \dot{m}_{ac}) \quad (2.2.2)$$

$$\frac{dp_{em}}{dt} = \frac{R_e T_{em}}{V_{em}} (\dot{m}_{ac} + \dot{m}_f - \dot{m}_t - \dot{m}_{wg}) \quad (2.2.3)$$

$$\frac{d\omega_{tc}}{dt} = \frac{P_t - P_c}{\omega_{tc} J_{tc}} - w_{fric} \omega_{tc}^2 \quad (2.2.4)$$

Where $m_{c/ac/f/t/wg}$ denotes massflow, $T_{im/em}$ manifold temperatures, $J_{engine/tc}$ inertias, $V_{im/em}$ manifold volumes, $R_{a/e}$ gas constants, $P_{t/c}$ turbine/compressor powers, T_{ice}

engine torque, and T_{load} mechanical load on shaft. The rest of engine components, which are compressor massflow and power; intake manifold pressure, engine torque, and exhaust temperature; exhaust manifold pressure, wastegate massflow, turbine massflow, are modeled with nine algebraic sub-models. Their mathematical representation is given below. Note that symbols and constants are explained in Appendix A, along with their numerical values.

Compressor: The compressor model consists of two sub-models, one for the massflow and one for the power consumption

$$\Pi_{c,max} = \left(\frac{\omega_{tc}^2 R_c^2 \Psi_{max}}{2c_p T_{amp}} + 1 \right)^{\frac{\gamma_a}{\gamma_a - 1}} \quad (2.2.5)$$

$$m_{c,corr} = m_{c,corr,max} \sqrt{1 - \left(\frac{\Pi_c}{\Pi_{c,max}} \right)^2} \quad (2.2.6)$$

$$\dot{m}_c = \frac{m_{c,corr} p_{amb} / p_{ref}}{\sqrt{T_{amb} / T_{ref}}} \quad (2.2.7)$$

$$\Pi_c = \frac{\dot{m}_c c_{pa} T_{amb} \left(\Pi_c^{\frac{\gamma_a - 1}{\gamma_a}} \right)}{\eta_c} \quad (2.2.8)$$

Engine Gas Flow: The engine gas flow model consists of two submodels, one for air flow and one for fuel flow.

$$\dot{m}_{ac} = \frac{n_{vol} p_{im} \omega_{ice} V_D}{4\pi R_a T_{im}} \quad (2.2.9)$$

$$\dot{m}_f = \frac{10^{-6}}{4\pi} u_f \omega_{ice} n_{cyl} \quad (2.2.10)$$

$$\lambda = \frac{\dot{m}_{ac}}{\dot{m}_f} \frac{1}{(A/F)_s} \quad (2.2.11)$$

In [12], it is noted that λ should be above $\lambda_{min} = 1.2$ in order to avoid smoke problems. Furthermore, it is suggested that a new variable should be used in order to avoid discontinuities

$$\varphi_\lambda = \dot{m}_{ac} - \lambda_{min} \dot{m}_f (A/F)_s \quad (2.2.12)$$

Engine Torque: The net torque of the engine, T_{ice} , is modeled using three torque components and one efficiency model.

$$T_{ice} = T_{ig} - T_{fric} - T_{pump} \quad (2.2.13)$$

$$\eta_{ig} = \eta_{ig,ch} \left(1 - \frac{1}{r_c^{\gamma_{cyl} - 1}} \right) \quad (2.2.14)$$

$$T_{ig} = \frac{u_f 10^{-6} n_{cyl} q_{HV} \eta_{ig}}{4\pi} \quad (2.2.15)$$

$$T_{fric} = \frac{V_D}{4\pi} 10^5 (c_{fr1} \omega_{ice}^2 + c_{fr2} \omega_{ice} + c_{fr3}) \quad (2.2.16)$$

$$T_{pump} = \frac{V_D}{4\pi} 10^5 (p_{em} - p_{im}) \quad (2.2.17)$$

Exhaust Temperature: The engine out temperature model is based on ideal gas Seiliger cycle. The engine out temperature and the exhaust manifold temperature are assumed to be equal.

$$q_{in} = \frac{\dot{m}_f q_{HV}}{\dot{m}_f + \dot{m}_{ac}} \quad (2.2.18)$$

$$x_p = 1 + \frac{q_{in} x_{cv}}{c_{va} T_{im} r_c^{\gamma_a - 1}} \quad (2.2.19)$$

$$T_{em} = \eta_{sc} \Pi_e^{1 - \frac{1}{\gamma_a}} r_c^{1 - \gamma_a} x_p^{\frac{1}{\gamma_a} - 1} \left(q_{in} \left(\frac{1 - x_{cv}}{c_{pa}} + \frac{x_{cv}}{c_{va}} \right) + T_{im} r_c^{\gamma_a - 1} \right) \quad (2.2.20)$$

Turbine: The turbine model consists of two sub-models. The turbine massflow is modeled with the standard restriction model and considering that half of the expansion occurs in the rotor and the other half in the stator. Also a simplification is conducted, considering that the useful pressure ratio over turbine is the squared pressure ratio, something which is not completely true for high speeds and torque (a reason for the greater error at these conditions).

$$\Pi_t^* = \sqrt{\Pi_t} \quad (2.2.21)$$

$$\Psi_t(P_i^*) = \sqrt{\frac{2\gamma_e}{\gamma_e - 1} \left((\Pi_t^*)^{\frac{2}{\gamma_e}} - \Pi_t^* \right)^{\frac{\gamma_e + 1}{\gamma_e}}} \quad (2.2.22)$$

$$\dot{m}_t = \frac{p_{em}}{\sqrt{R_e T_{em}}} \Psi_t A_{t,eff} \quad (2.2.23)$$

$$P_t = \dot{m}_t c_{pe} T_{em} \eta_t \left(1 - \Pi_t^* \right)^{\frac{\gamma_e - 1}{\gamma_e}} \quad (2.2.24)$$

Wastegate: Although, wastegate valve considered to be closed during the simulations, for the sake of completeness, the nonphysical model of wastegate is presented.

$$\Psi_{wg} = c_{wg,1} T_{em} \sqrt{1 - \Pi_{wg}^{cwg,2}} \quad (2.2.25)$$

$$\dot{m}_{wg} = \frac{p_{em}}{\sqrt{R_e T_{em}}} \Psi_{wg} u_{wg} A_{wg,eff} \quad (2.2.26)$$

Moreover, the model was further modified, so as its speed controller to resemble the one of HIPPO-2. As previously referred, engine control at HIPPO 2 can be implemented

in two ways. The first module is direct torque control of the engine, via open loop control of engine inputs, probably with the use of lookup tables. In the simulation scheme, engine has two inputs, the injected fuel and the shaft speed. Using a PI controller, and measuring the resulted injected fuel mass, a reference map for the injected fuel with torque and the shaft speed as reference inputs, was constructed. The second control model is speed control. This was easily implemented with an additional PI controller before the torque reference map. Furthermore, fuel consumption maps for the steady state operating condition were created for control purposes. The fuel consumption maps, along with Speed - Torque limits and simulation results are shown in the following Figures 2.13 and 2.14.

Considering the results presented in Figure 2.14, the dynamic behavior of the simulation model is almost the same to this of the experimental engine, from control perspective. In essence, the simulation model was used for developing, testing and tuning the NMPC successfully.

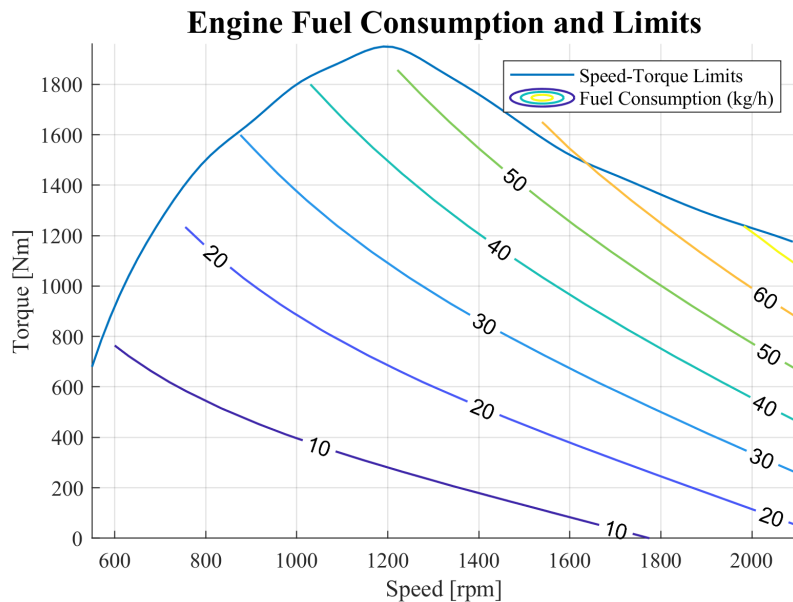


Figure 2.13: Fuel Consumption vs Speed and Torque Map.

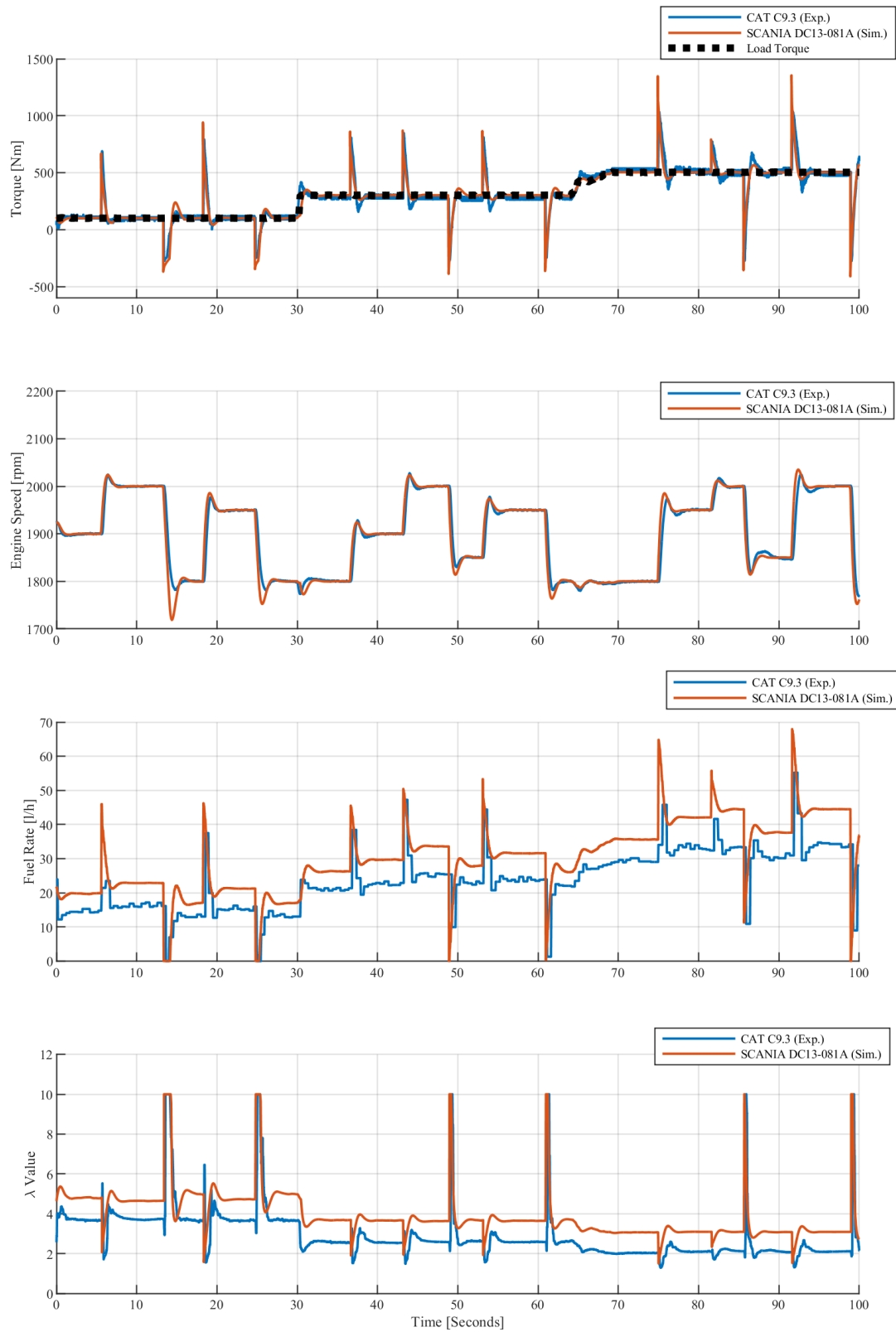


Figure 2.14: CAT[®] C 9.3 engine and SCANIA DC13-081A model, experiment and simulation comparison results.

Parametric Engine Model

Although the previous model was relatively simple, continuously differentiable (i.e. can be solved from optimization software) and can successfully capture the system dynamics, a real time optimization controller, (as the NMPC), would not be able to solve the model in the short periods of time the problem requires (e.g. around 0.1 seconds). Thus, other model approaches were considered, in order to model the engine for the control purpose. An interesting approach of control oriented modeling of the dynamic behavior of an engine for applications, such as the NMPC, is presented in [13]. The idea is to model the state differential equations of the system with the use of polynomials of certain degree, by fitting data acquired from the system. Parametric approaches have been used before [8], [15], however they referred to steady state conditions.

The mathematical approach of the model is rather simple. The dynamic response is acquired via the continuous time polynomial expression of (2.2.27).

$$\dot{x} = \theta^T f_l(x, u) \quad (2.2.27)$$

where x is the vector of the states, u is the vector of inputs, θ is the matrix of polynomial coefficients, which have to be estimated, and $f_l(x, u)$ is the vector of the polynomial terms of l order. For instance, if $x \in \mathbb{R}^1$, $u \in \mathbb{R}^1$ and $l = 2$ then the polynomial terms are:

$$f_2(x, u) = [1 \quad x \quad u \quad xu \quad x^2 \quad u^2] \quad (2.2.28)$$

In this work, polynomials of 2nd and 3rd degree were used, of one or two inputs and one output. If inputs, outputs and its derivatives are available, the coefficient θ can be estimated through linear least squares. In [13], it is suggested that if the derivatives of the output cannot be measured directly, filtered derivatives can approximate \dot{x} . In fact, by applying $1/(s + \tau)$ in (2.2.27), the following is obtained.

$$\left\{ \frac{s}{Ts + \tau} \right\} x = \theta^T \left\{ \frac{1}{Ts + \tau} \right\} f_l(x, u) \quad (2.2.29)$$

An even more simpler approach of the above is the parametric model to describe the steady state condition. The parametric equations describe the engine quantities directly, and not via their derivatives. Essentially, these models occur, by fitting steady state engine maps to polynomial equations. The advantage of these models is that they are rather simple, and computationally efficient, since in contrast to the previous, no integration is needed. However they are unable to describe the dynamic engine behavior.

Parametric Online Adaptation

The above polynomial models can provide a close estimation of the engine dynamic or quasi-static behavior, which is rather satisfactory for NMPC application. However, in many cases high fidelity system approach is required (e.g. so as the controlled variable not to have permanent offset from the reference) or their characteristics are *time variant*. As a result, the above models may be insufficient for model based control. A modification of the parametric models, which can address these requirements, is to estimate the affine terms of the polynomial model online. The procedure which was followed and that is described below, is referred to at [16], and a NMPC oriented application is presented at [13]. The above parametric model can be re-written as

$$z = \theta(t)^T \phi \quad (2.2.30)$$

where the term $\theta(t)$ denotes that the affine term is time variant, $z = \{(s/(Ts + \tau))\} x$ and $\phi = \{1/(Ts + \tau)\} f_l(x, u)$. It is assumed that at a time instant, equation (2.2.30) is used to obtain an estimation of system states \hat{z} , using the previously estimated affine terms. Then, the real output of the system is measured, and the normalized estimation error ϵ is then calculated as

$$\epsilon = \frac{z - \hat{z}}{m^2} = \frac{z - \theta(t)^T \phi}{m^2} \quad (2.2.31)$$

where $m^2 = 1 + n_s$ is the normalizing signal, so as the term $\phi/m \in \mathbb{L}_\infty^2$. Typical values are $n_s^2 = \phi^T \phi$ or $n_s^2 = \phi^T P \phi$ and $P = P^T > 0$. The above equation is re-written considering the parameter error: $\tilde{\theta} \triangleq \theta(t) - \theta^*$, where θ^* is the real system parameter

$$\epsilon m = -\frac{\tilde{\theta}^T \phi}{m} \quad (2.2.32)$$

The signal which occurs from the above equation, according to [16], is a reasonable measure of error $\tilde{\theta}$, because for any piece-wise continuous signal vector ϕ (not necessarily bounded), large ϵm implies large $\tilde{\theta}$. Therefore, the online affine estimation scheme can be transformed to a cost function minimization problem via *gradient method*. A simple appropriate quadratic cost function is

$$J(\theta) = -\frac{\epsilon^2 m^2}{2} = \frac{(z - \theta^T \phi)^2}{2m^2} \quad (2.2.33)$$

Because of the property of m , $J(\theta)$ is convex over θ for every time instant t (i.e. the problem is well posed). Also convexity guaranties that there is a single global minimum, in which $\epsilon = 0$. The proofs of the previous statements can be found in [16]. Minimization of the trajectory $\theta(t)$ is generated from the differential equation

$$\dot{\theta} = -\Gamma \nabla J(\theta) \quad (2.2.34)$$

where $\Gamma = \Gamma^T > 0$ is a scaling matrix that is referred as *Adaptive Gain*. Also the following applies

$$\nabla J(\theta) = -\frac{(z - \theta^T \phi)\phi}{m^2} = -\epsilon \phi \quad (2.2.35)$$

and consequently the adaptive law, which is reffered as *gradient algorithm*, is given by:

$$\dot{\theta} = \Gamma \epsilon \phi \quad (2.2.36)$$

The only tuning parameter of the above is the Γ matrix. The larger its values are the faster the algorithm converge to minimum.

In the present work, the above method is applied in order to fit experimental data, obtained directly from measurements, in order to model the engine operation for the NMPC. Since the measured outputs are digital signals, which can be sampled with low frequency, direct derivative calculation is not suggested. In order to validate the method, two fitting examples with both the regular and the adaptive scheme were tested, as follows.

²the definition is: if $x \in \mathbb{L}_\infty$ then $\|x\|_\infty \triangleq \sup_{t \geq 0} |x(t)|$

Case A: MISO System (Simulation Data)

The first parametric model is about a MISO system, which can predict the Fuel Oil Consumption, of SCANIA simulation model, given the torque load and the speed. The polynomial is of second order, and no filtering was used since there is no noise, data are smooth and derivatives can be obtained directly. At Figure 2.15, the results for fitting model compared to the high fidelity model are shown, for two data-sets, one which is the fitting dataset, while the other one which was obtained for validation. Note that validation data are more "raw" (i.e. steps) than the fitting data, in order to test the limits of the method. The results are quite satisfactory.

Case B: MISO System (Experimental Data)

This model, also, refers to a MISO system with the same purpose. The major difference here is that the datasets were acquired directly from the experimental CAT C9.3 engine. Therefore, filtering was inevitable due to disturbances and since they are digital signals (discrete), derivatives cannot be calculated directly. However, the time constant T of the transfer function, was very small (around 0.01 s, meaning that data were already smooth enough. The results are shown at Fig. 2.16.

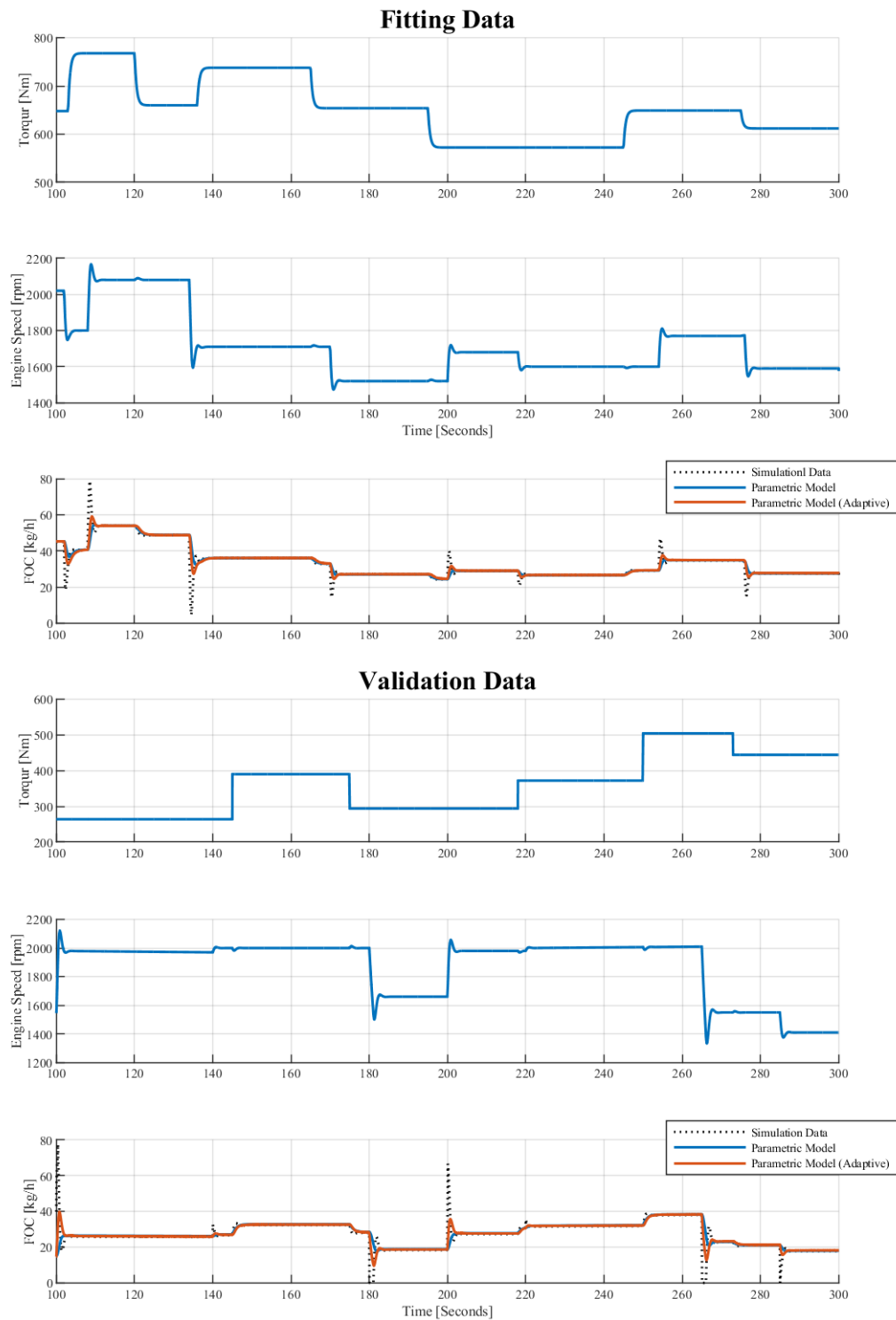


Figure 2.15: MISO parametric model for Fuel Rate estimation, compared to simulation data (Case A)

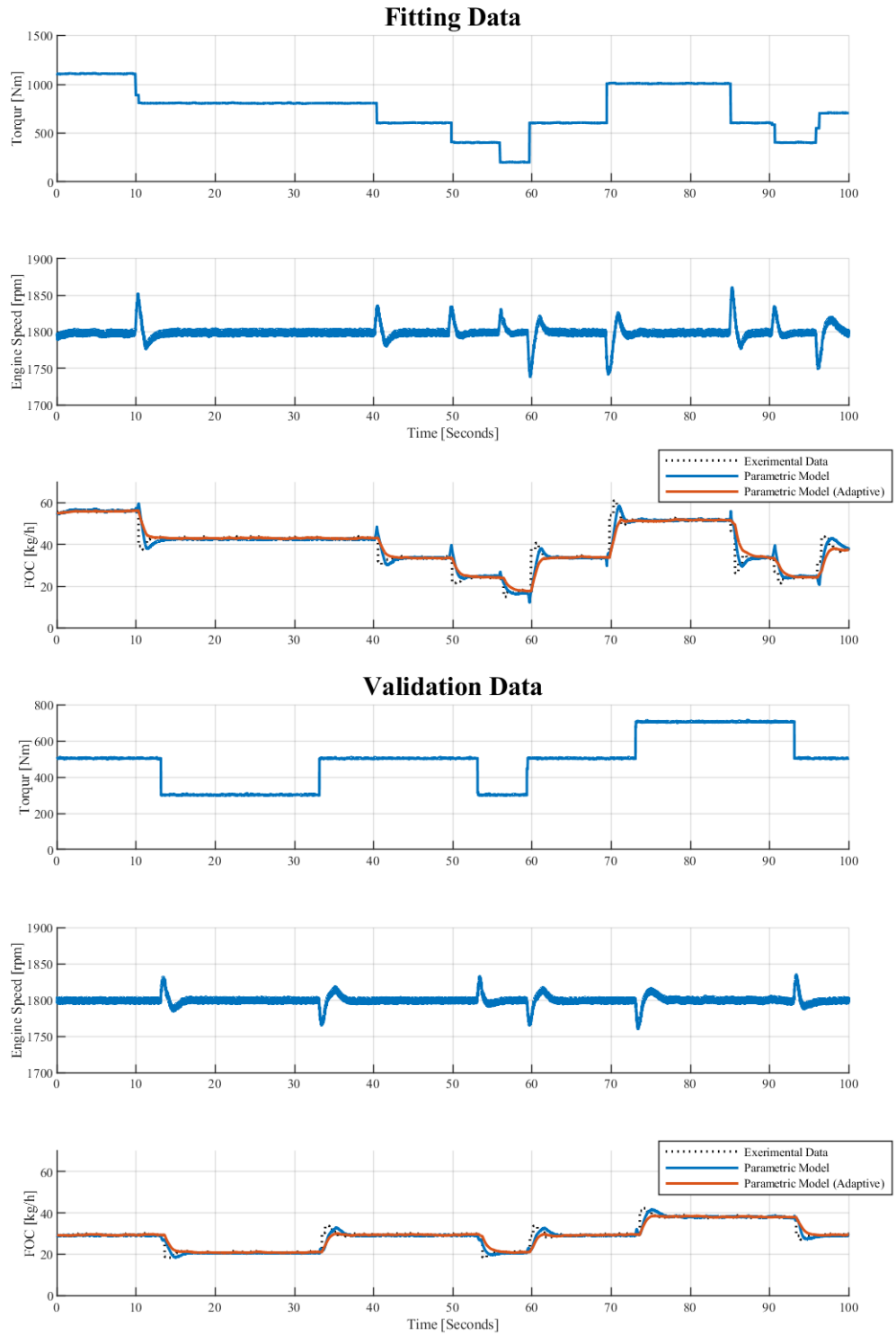


Figure 2.16: MISO parametric model for Fuel Rate estimation, compared to experimental data (Case B)

2.3 Electric Motor/Generator Modeling

2.3.1 Introduction

Electric Machines can convert electric energy to mechanical energy and vice versa. The machines which conduct the first are called *Electric Motors* and the machines which do the opposite *Electric Generators*. They were first developed at the mid of 19th century and since that time, they have been an important component of the infrastructure. Their development is considered to be crucial for the future, since these machines do not produce emissions during energy conversion to electricity. The operation of both machines is based on using the electromagnetic forces which are consequences of Faraday's law and of Lorentz's law. The former describes the induction of an electromotive force in conductors being in relative motion with respect to a magnetic field. The latter describes the force generated on a current carrying conductor inside a magnetic field.

In hybrid propulsion plants, the electric machines are a key component, and usually they are reversible (i.e. they can operate both as motor and generator). The operation of these machines, according to [17], can be distinguished into three modes, one motoring and two generating, which are: (1) to convert the electrical power from the battery into mechanical power to drive the vehicle, (2) to convert the mechanical power from the engine into electrical power to recharge the battery, or (3) to recuperate mechanical power available at the drive train to recharge the battery (regenerative braking). Of course, in a marine hybrid plant the latter is not so common during operation, except maneuvering or special cases (e.g. during propeller ventilation the electric part can absorb and store to battery a portion of kinetic energy in order to reduce over-speeding). Desirable characteristics, for electric machines operating in a hybrid propulsion plant are [17]: high efficiency, low cost, high specific power, good controllability, fault tolerance, low noise, and uniformity of operation (low torque fluctuations).

The electric machines which are used in propulsion plants are *rotating machines*, with two major components, the stator and the rotor. The latter is connected to the moving part of the machine (output shaft), in which the acting torque is applied. These electric machines are categorized into two major types according to current supply, direct current (DC) motors and alternating-current (AC) motors. For each category there are others sub-categories. At the experimental test-bed HIPPO 2, the motor is an AC asynchronous squirrel cage motor, and therefore only this motor type will be further described.

In AC motors in general, AC voltage is applied to stator, creating a rotating magnetic field in the stator windings, which are, for three phase motors, one or more sets of three. This magnetic field changes its orientation according to sign of current flowing in the windings, which is continuously varying, and consequently the orientation of the magnetic field keeps varying, resulting in a rotating magnetic field. The speed of the rotating magnetic field is called the synchronous speed. It equals the pulsation of the three-phase AC voltage divided by the number of poles. In asynchronous AC machines (also called induction motors), the rotor does not rotate with the same speed of the magnetic field when load to shaft is applied. The rotor usually hosts a set of conductors with end rings, an arrangement known as "squirrel cage". Electromotive force and thus current is induced in the rotor windings by the interaction of the conductors with the rotating magnetic field. The rotor becomes an electromagnet with alternating poles, attracted by those of the rotating magnetic field of the stator.

Control of these motors is conducted with sophisticated electronics (inverters), and various control schemes have been applied in the past, such as the Scalar Control (V/f Control), the Field Oriented Control, Sliding Control Mode (SMC) and the Direct Torque Control (DTC). The industrial Drive which controls the AC motor of HIPPO 2 is using the DTC control scheme. This type of control is based on the mathematical approach of induction machines, and therefore various parameters, such as stator resistance, mutual inductance, saturation co-efficiency, etc. are required. The control variables are output torque and stator magnetic flux. DTC is able to control more accurate and has the fastest response time, does not need feedback devices and has reduced mechanical failure. The disadvantage is that due to the inherent hysteresis of the comparator, higher torque and flux ripple exist [18].

2.3.2 Modeling

AC motor modeling approaches are divided into two major categories, the quasi-static and the dynamic modeling. AC machines are essential dynamic, although, rarely dynamic models are used for hybrid plant simulation and its control orientated applications [17]. However, in the present work, both approaches were reviewed and it was decided that quasi-static approach should be used for both simulation and the model based control application. A brief presentation of the dynamic model which have been studied and the reason why is rejected are analyzed below.

The dynamic model is usually based on the two phased (d-q) equivalent circuit of the machine, in which each electrical quantity is described by its direct and quadratic component. The reference frame of the model can be synchronous to stator, to rotor, or steady. The dynamic approach is use the correct physical casualty of the AC motor, meaning that model inputs are the 3-phase Voltage and shaft(rotor) speed, and the outputs are the electromagnetic Torque and the 3-phase current. Although the above model might seem simple, its mathematical description is quite complex. The dynamic model which was reviewed [19] for this work, is consisted from four differential equation and ten algebraic equations. The model was constructed in Simulink, fitted with HIPPO-2 AC Motor parameters and tested. The results were more than satisfactory, since they have lees than 1% deviation from the manufacturer's test data. Another point that should be mentioned is that the system response was quite fast. However the above model does not fully describe the system's dynamics. In order to do so, another key component has to be modeled, which is the Industrial drive which controls the induction machine. The drive uses DTC control scheme, as mentioned before. Simple DTC modeling of approaches can be found in literature (e.g. [20]) or in Simulink Library. The drive uses a more sophisticated approach, which calculates the flux reference in order to save energy or to brake (generate). However, the key point of the drive in respect to the propulsion plant control is its dynamic response. According to the manufacturer [21], the dynamic response of a DTC driven AC motor to 100 % torque step is typically 1–5 milliseconds (ms), which approaches the motor's physical limit. Considering the fact that the NMPC controller is designed to operate with sample time 100 ms, induction machine dynamics can be completely disregarded without any error at all.

From the control engineering point of view, the AC motor quantity which is required for the controller is the power input, given the output torque and rotational speed. Several models which describes the above where revised [17].

Willans Approach

A simple quasi-static model, which connects the output rotating speed and torque with the required power input, is the Willans approach [17]. This model considers that the electrical power input and the mechanical power output, have linear dependency. The model is valid for both motoring and generating modes. Therefore, the expression which describes them is the following:

$$T_m(t) \cdot \omega_m(t) = e \cdot P_m(t) - P_0, \quad P_m \geq 0 \quad (2.3.1)$$

$$T_m(t) \cdot \omega_m(t) = \frac{P_m(t)}{e} - P_0, \quad P_m < 0 \quad (2.3.2)$$

where $P_m(t)$ is the input power, $\omega_m(t)$ is the rotational speed, $T_m(t)$ is the output torque, P_0 represents the power losses occurring after the energy conversion (friction, heat losses, etc.) and e is the “indicated” efficiency, i.e., the maximum efficiency that can be obtained when P_0 is zero. Thus e represents the efficiency of the energy conversion process only (electrical to mechanical energy and vice versa). In contrast with other quasi-static approaches, this model can describe the effect of the “idle” losses P_0 for small values of power. In this circumstance, it may occur that $P_m > 0$ while being $\omega_m \cdot T_m < 0$, that is, even if some mechanical power is available from the downstream powertrain, still the energy source must supply a certain amount of electric power [17].

Moreover, it is suggested that parameters e and P_0 are dependent on motor speed $\omega_m(t)$. However, good average approximations can be found and used without significant error. In order to validate that, a Willans model is fitted to HIPPO’s 2 AC motor data and then its compared to experimental results. The data used for fitting was derived from the manufacturer’s data-sheets for operating points 25 %, 50 %, 75 %, and 100% of maximum load under nominal voltage. The result fitting of Willans model and its comparison with the experimental results is shown at Figs. 2.18 and 2.17.

Considering the above figures, it is clear that model can predict the required Power demand satisfactory enough, for low and high loads for both motoring and generating modes. Therefore, the model was integrated inside the NMPC controller and was also used in simulations.

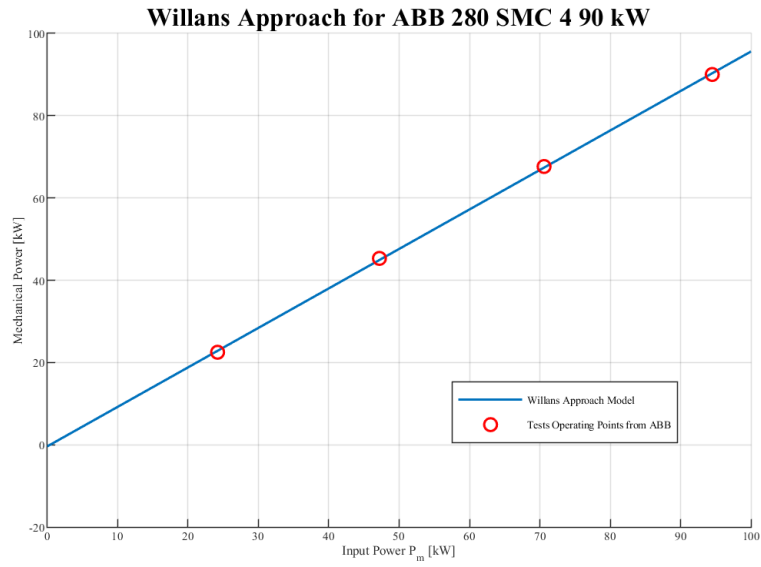


Figure 2.17: Willans model fitting results, compared to test data from manufacturer.

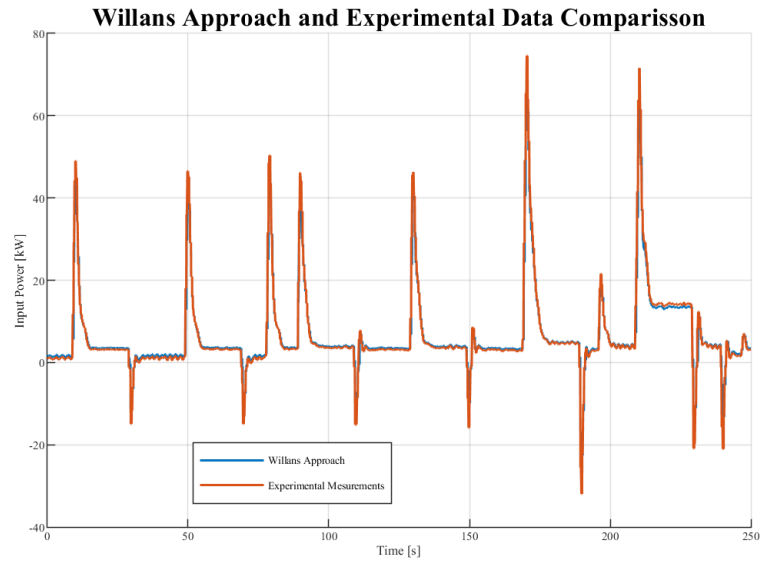


Figure 2.18: Willans model comparison with experimental data.

2.4 Battery Modeling

2.4.1 Introduction

Electrochemical batteries are key components of Hybrid Diesel - Electric Ships and Vehicles (HEV), in general. The main function of these devices, in a hybrid propulsion plant, is to transform and store electrical energy in chemical form, and then re-transform it back to electricity, in order to be used by the electric motors, when it is required.

Each battery cell is characterized by the maximum power it can provide to the propulsion plant, and the nominal capacity. The first refers to the rate of energy a battery can provide to the plant, and it is the product of current and voltage. The latter, defines the amount of electricity a battery can supply, in terms of Coulombs (Ampere-seconds, As) or more often in Ampere-hours, Ah. Also, a dimensionless parameter, the *State of Charge* (SoC), describes the remaining capacity of the battery, and it is expressed as percentage or fraction of the nominal capacity

$$SoC(t) = \frac{Q(t)}{Q_{nom}} \quad (2.4.1)$$

The battery charge, and therefore SoC, is difficult to be measured directly. Subsequently, it is calculated indirectly, from the charge equilibrium which is expressed from

$$\dot{Q}(t) = -I_b(t) \quad (2.4.2)$$

It is common, in case of battery charge, a parameter to be taken into account, the *coulombic or charging efficiency* n_c [22–24] in order to model the fact that a fraction current is not transformed into charge of the battery current due to irreversible, parasitic reactions taking place in the battery. Therefore, the above equation takes the form

$$\dot{Q}(t) = -n_c \cdot I_b(t) \quad (2.4.3)$$

Furthermore, it should be noted that not the whole capacity of the battery can be used in practice [17]. There is *SoC window*, whose limits define the maximum SoC that can be achieved during charging, and the minimum SoC that can be reached during discharging, in order to maximize battery life. This feature is expressed by the specific energy of battery.

Moreover, a group of attributes of a battery pack, operating in a hybrid power plant, are usually required [17], most important of which are

- high specific energy,
- high specific power,
- long calendar and cycle life,
- low initial and replacement costs,
- high reliability,
- wide range of operating temperatures,
- and high robustness.

In case of marine applications, although there is a noticeable trend for hybrid - electric applications and several breakthroughs occurred towards this direction, these are relatively recent, and consequently, there is not sufficient information for the special requirements a battery which is operating in this environment should comply with [25].

A battery is usually composed from a number of cells, in which three major components can be distinguished: two electrodes and a medium. Half reactions are taking place in the electrodes. The cathode is the electrode where reduction, gain of electrons, takes place (the positive during discharging and the negative during charging), and the anode is the part where the oxidation process happens. The cells are connected in parallel or/and in series. The former connection is used to increase the total capacity of the battery, and the latter to increase the voltage, and thus the power production of battery pack [26]

2.4.2 Modeling

Several battery modeling approaches can be found in the literature. These models are commonly categorized as *Electrochemical Models* or *Equivalent Circuit Models, (ECMs)*. Furthermore, other categories for the models arising from the fact that battery behavior can be distinguished in two parts, the linear and the nonlinear section. The first applies for the most part of charge/discharge cycle. This region, in respect to charge, is located from 10-20% to 80-90% of SoC. The regions, when the charge is very low or very high, the behavior is nonlinear. A typical Voltage-SoC diagram which illustrates the above regions is shown in Fig. 2.19. Most of the modeling approaches are referring to the linear region, since the nonlinearities appear mostly outside of the operational limits. However, there are some efforts which try to model the battery behavior in these regions [27].

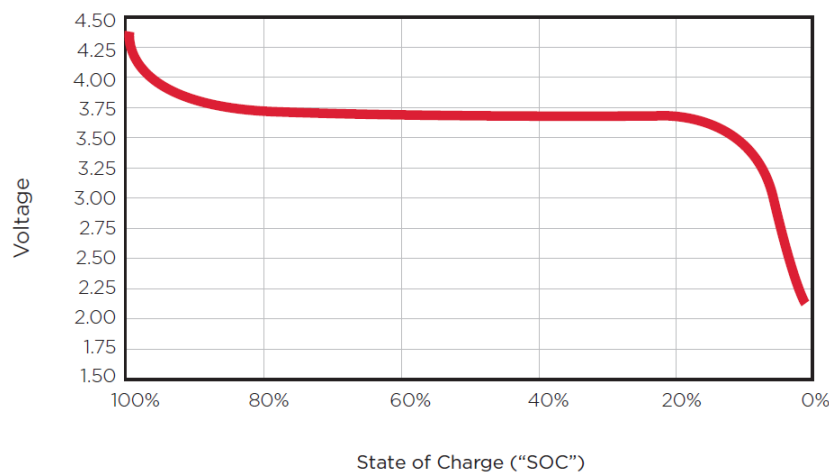


Figure 2.19: Typical Li-ion Discharge Voltage Curve from [28]

In the first case, a set of coupled nonlinear differential equations, is employed in order to describe the pertinent transport, thermodynamic, and kinetic phenomena occurring in the cell. Afterwards, these phenomena are converted into measurable quantities such as cell current and voltage by constructing a relationship between the microscopic quantities, such as electrode and interfacial micro-structure and the fundamental electrochemical studies and cell performance. However, the use of partial differential equations and the large number of unknown parameters, are often lead to high computational cost and great

memory requirements and consequently, these models are not desirable for model control, especially when lot of simulation are required in a restricted time period [29].

In the present work, only ECMs were reviewed [17, 23, 27, 30–34]. However, two models were finally used, a quasi-static and a dynamic approach and therefore, are presented below.

A. Quasi-static Model

This model is based on the equivalent circuit, which is presented in Fig. 2.20, and was originally used for lead acid batteries [17].

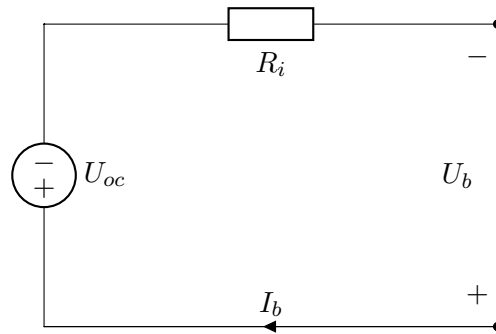


Figure 2.20: Equivalent circuit of quasi-static battery model

The ECM consists of a Voltage Source and a Resistance. The first component refers to *Open Source Voltage (OCV)*, and represents the equilibrium potential of the battery. Since this quantity depends on the charge level, it is parameterized using the following affine relationship

$$U_{oc}(t) = k_2 \cdot SOC(t) + k_1 \quad (2.4.4)$$

The above equation is boiled in the fact that the OCV can be modeled using a permanent voltage source U_C and a capacitor [22], with a capacitance which is calculated using the following equation

$$C_{oc}(t) = \frac{Q}{U} = \frac{Q_{Batt}}{U_{oc}(SOC = 0\%) - U_{oc}(SOC = 100\%)} \quad (2.4.5)$$

From Kirchhoff's Voltage Law and considering (2.4.1), the following expression for the OCV is formed :

$$U_{oc}(t) = U_c + \frac{Q}{C_{oc}} = U_c + \frac{SOC \cdot Q_{nom}}{100 \cdot C_{oc}} \quad (2.4.6)$$

It is clear that by considering $k_1 = U_{oc}$ and $k_2 = Q_{nom}/100 \cdot C_{oc}$, equation (2.4.4) arises. As for the resistance component, this expresses the internal resistance of the battery cell. The internal resistance takes into account several phenomena, but in principle it can be stated that is the combination of three contributions [17], the *Ohmic Resistance* R_o which accounts for the the series of the ohmic resistance in the electrolyte, in the electrodes, and in the interconnections and battery terminals, the *charge-transfer* resistance R_{ct} , which

is associated with the “charge-transfer” (i.e., involving electrons) reactions taking place at the electrodes. and the *diffusion or concentration resistance* R_d , which represents the diffusion of ions in the electrolyte due to concentration gradients. Consequently, the sum of the above is the total internal resistance

$$R_i = R_d + R_{ct} + R_o \quad (2.4.7)$$

In [22], the ohmic resistance is considered as a quadratic function of SoC, the diffusion resistance as a function of the current and the charge-transfer as function of the current and the OCV (and therefore SoC). Due to the significant number of parameters which have to be identified, other approaches can be found in the literature. In [17, 23, 24], the internal resistance is calculated as a function of SoC using an affine relation as for OCV

$$R_i(t) = k_4 \cdot SOC(t) + k_3 \quad (2.4.8)$$

Furthermore, in applications considering simulation for control problems, internal resistance along and OCV can be considered as constant quantities [35]. The terminal battery voltage is calculated via Kirchhoff’s Voltage Law, for the ECM

$$U_b(t) = U_{oc}(t) - R_i(t) \cdot I_b(t) \quad (2.4.9)$$

In the present work, the battery modeling is oriented for control purposes, and therefore, the input variable is the required Power $P_b(t)$, the battery should balance, and the output variable is the SoC of the battery. The relation between the required power, the current and the terminal voltage is

$$I_b(t) = \frac{P_b(t)}{U_b(t)} \quad (2.4.10)$$

Now, combining (2.4.9) and (2.4.10), the following expression for the terminal voltage occurs

$$U_b^2(t) - U_{oc}(t) \cdot U_b(t) + P_b(t) \cdot R_i(t) = 0 \quad (2.4.11)$$

The solution of this equation is [17]

$$U_b(t) = \frac{U_{oc}(t)}{2} + \sqrt{\frac{U_{oc}^2(t)}{4} - P_b(t) \cdot R_i(t)} \quad (2.4.12)$$

And considering (2.4.10), a proportionate equation for battery current is formed

$$I_b(t) = \frac{U_{oc}(t) - \sqrt{U_{oc}^2(t) - 4P_b(t) \cdot R_i(t)}}{2R_i(t)} \quad (2.4.13)$$

Finally the SoC, is calculated by combining (2.4.2) and (2.4.1). As a result, a differential equation for the state of charge is formulated

$$\frac{dSOC}{dt} = -\frac{100}{Q_{nom}} \cdot \frac{U_{oc}(t) - \sqrt{U_{oc}^2(t) - 4P_b(t) \cdot R_i(t)}}{2R_i(t)} \quad (2.4.14)$$

The block diagram of the quasi-static model is presented in Figure 2.21

Battery Operating Limits

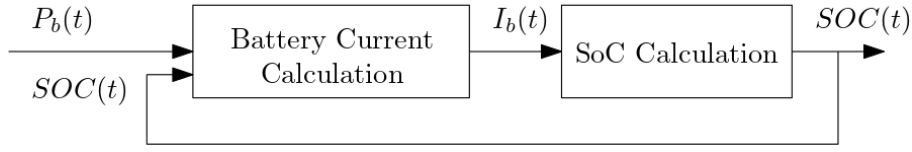


Figure 2.21: Block diagram of quasi-static battery model

The operating limits of the above model, can be derived considering (2.4.12) [17]. For the discharge case, the following limitation are applied: $P_b \geq 0$ and $U_b < U_{oc}$. The power can be calculated as a function of voltage as

$$P_b(t) = \frac{-U_b^2(t) + U_b(t) \cdot U_{oc}(t)}{R_i(t)} \quad (2.4.15)$$

The power is zero for $U_b = 0$ and $U_b = U_{oc}$. If the Voltage is between these two values, the power is positive. The maximum power can be found by differentiate the (2.4.15) with respect to U_b and set to zero as follows

$$\frac{dP_b}{dU_b} = \frac{U_{oc} - 2U_b}{R_i} = 0 \quad (2.4.16)$$

Leading to the following expressions for the maximum power, the battery can provide, and the corresponding voltage and current

$$P_{b,max}(t) = \frac{U_{oc}^2(t)}{4R_i(t)}, \quad U_{b,P_{max}}(t) = \frac{U_{oc}(t)}{2}, \quad I_{b,P_{max}}(t) = \frac{U_{oc}(t)}{2R_i(t)} \quad (2.4.17)$$

It is noteworthy, that the maximum power depends on $|U_{oc}|$ and consequently on SoC . Hence the maximum power is time varying. Furthermore, in practice, batteries are not operating on limits, and voltage is confined in a narrow band around U_{oc} , $U_b \in (U_{b,min}, U_{b,max})$ [17], with $U_{b,min} > U_{b,P_{max}}$ and consequently the maximum battery power is always lower than the corresponding in (2.4.17). In case of charging (mean. $P_b < 0$ and $U_b > U_{oc}$), an equivalent expression with (2.4.17) arises, but with a minus sign in front of the expression.

Also, in case of control schemes involving battery cell components, additional constraints regarding the battery function are applied, such as rate of SoC alteration, maximum current and voltage, etc. [36]. These constraints refer to battery health, and they are usually defined by the manufacturer. In this work, the battery component is virtual i.e. its model running on the software during experimental tests, and therefore, no further analysis is conducted.

Another point worth to be mentioned, is that the above Battery model is *scalable*. A battery configuration, is mostly made up of multiple cells connected in parallel or/and in series, as mentioned above. The quasi-static model for a cell can be modified, in order to model the whole battery, consisted of N_s cells in series and N_p cells in parallel, as follows

$$U_{oc} = N \cdot U_{cell}, \quad R_i = R_{cell} \cdot \frac{N}{N_p} \quad (2.4.18)$$

The total capacity of battery pack is $Q_o = Q_{cell} \cdot N_p$.

Dynamic Model

The scheme which was presented in the previous section can describe the battery operation with satisfactory accuracy, depending on the definition of parameters. However, there are limitations, regarding the operation in transient loads. In this case, a lot of key phenomena occur, which have several implications for battery operation. In order to take into account the above, several dynamic models have been proposed [27,30–32]. The model which have been chosen to be reviewed is the *PNGV* Equivalent Circuit Model [31].

The PNGV ECM is a linear lumped parameter battery model. The ECM of the model is presented in Figure 2.22:

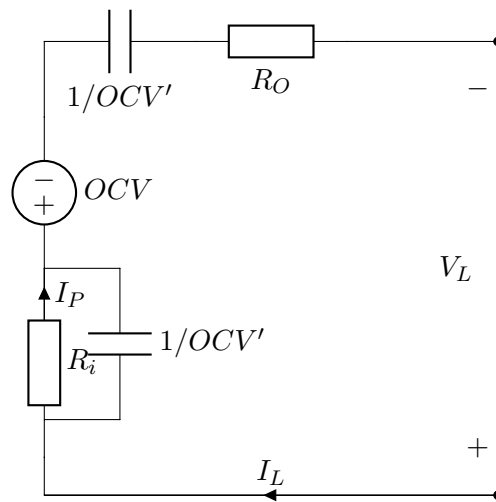


Figure 2.22: Equivalent circuit of PNGV battery model

This modeling approach attempts to predict the battery terminal voltage U_b under pulse conditions, in order to be used for battery system modeling. The model is based on a set of parameters, which can be estimated by conducting several test to the cell, involving, mainly, load pulses in several operating conditions, which are described in the PNGV testing manual [31]. Afterwards, these test results are analyzed and processed accordingly to the PNGV instruction in order to obtain the parameters. The parameters of the model, that should be defined are

- OCV An ideal voltage source that represents “open circuit” battery voltage
- R_O Battery internal “ohmic” resistance
- R_P Battery internal “polarization” resistance (e.g., due to concentration gradients)
- C Shunt capacitance around R_P
- τ Polarization time constant, $\tau = R_P C$
- I_L Battery load current
- I_P Current through polarization resistance

- V_L Battery terminal voltage
- $1/OCV'$ A capacitance that accounts for the variation in open circuit voltage with the time integral of load current I_L . OCV' is not usually equal to the slope of V_L measured open circuit vs. battery state of charge.

Considering the Voltage Kirchhoff's Law, the main relation for the terminal voltage is

$$V_L = OCV - OCV' \int I_L dt - R_O I_L - R_P I_P \quad (2.4.19)$$

The polar current, can be derived by solving the following deferential expression, with a specified initial condition: $I_P = 0$ at $t = 0$:

$$\frac{dI_P}{dt} = \frac{I_L - I_P}{\tau} \quad (2.4.20)$$

The rest of the battery model, occurs by combing the expression (2.4.2) and (2.4.10) in order to calculate the load current and the SoC. The block diagram of the model, is given bellow

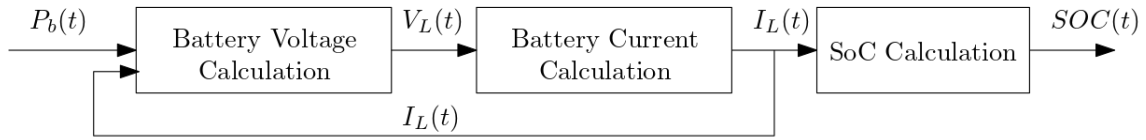


Figure 2.23: Block diagram of PNGV battery model

It is important to bear in mind, that the above parameters are considered to be constant for the given SoC, temperature, etc. In this evidence, in literature [37], it is proposed for each voltage calculation step, the parameters of the PNGV model should be recalculated according to the most recent measurements of SoC and temperature. In this work, due to lack of data and for simplification, this is disregarded.

2.4.3 Model Comparison

In order to illustrate the differences between the reviewed models, a simulation test was conducted, using *Simulink*. For simplification, and since the batteries were virtual, their parameters where consider to be constant and same for charging and discharging. The model parameters were found in [38], and they refer to a Li-ion battery cell of capacitance of 100 Ah and PNGV modeling. The parameters are shown in the table below:

<i>Parameter</i>	<i>Value</i>	<i>Unit</i>
OCV	3.26	Volts
R_O	0.0241	Ohms
R_P	0.0271	Ohms
$1/OCV'$	1760000	Farads
C	96000	Farads

Table 2.2: PNGV ECM parameters [38]

It is obvious that the battery pack will be consisted of several cells as the above. The capacity of the above cell is sufficient (100 Ah), but the nominal voltage is rather low (3.26 V). Therefore, it is decided that 150 cells to be connected in series, with aim of increasing the voltage ($OCV = 652$ V) with the same capacity. The above parameter values are typical for a hybrid propulsion plant with size as HIPPO 2. The rest parameters are emerged, using the fundamentals of circuit analysis. In essence, the ohmic resistance, the diffusion resistance and the OCV where multiplied by the number of cells, and the diffusion and the open source voltage capacitor where divided by the number of cells.

The equivalent parameters of the quasi-static model, where calculated, using the above. The open source voltage was modeled using (2.4.4). The parameters k_1 and k_2 , where calculated using (2.4.6). The internal resistance was considered as the sum of the ohmic resistance and the diffusion resistance, as in (2.4.7), and was considered constant. The final parameters for both the PNGV and quasi static model are shown in Table 2.3.

The simulation lasted 10^5 seconds, during which, the two battery models where submitted to the same pulse loads, simultaneously, which were both positive (discharging) and negative (charging). Soc, terminal voltage and current where measured. The results are shown in Figure 2.24.

<i>Parameter</i>	<i>Value</i>	<i>Unit</i>
<i>PNGV Model</i>		
<i>OCV</i>	652	Volts
<i>R_O</i>	0.4820	Ohms
<i>R_P</i>	0.5420	Ohms
<i>1/OCV'</i>	8800	Farads
<i>C</i>	480	Farads
<i>Quasi - Static Model</i>		
<i>k₁</i>	652	Volts
<i>k₂</i>	40.9091	Volts/% SoC
<i>R_i</i>	1.0240	Ohms

Table 2.3: PNGV and quasi-static ECM parameters for simulation

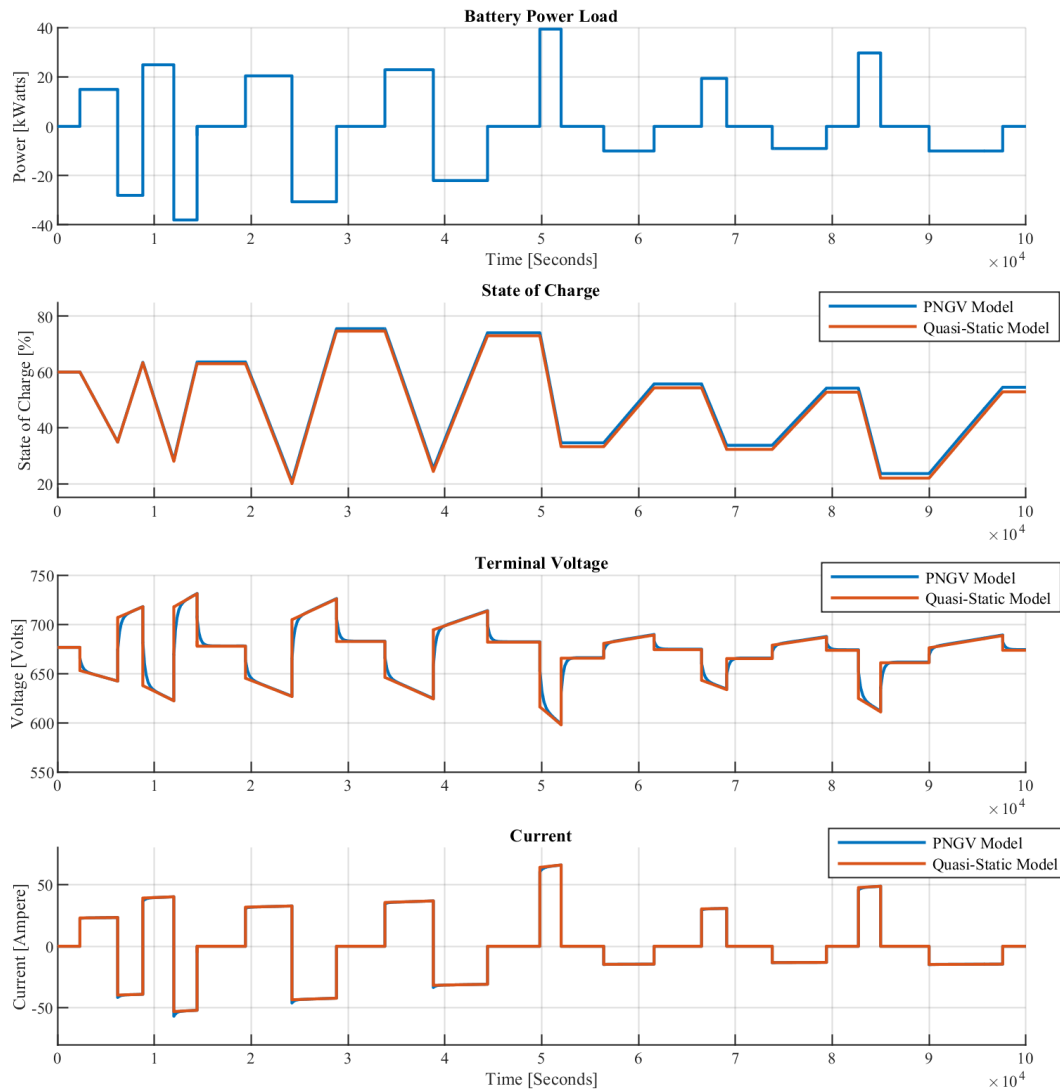


Figure 2.24: Battery model comparison results obtained from Simulink

According to the simulation results, SoC barely differ for the two models, and this deviation is observable only after considerable time period. Voltage and current measurements, indicate that both the dynamic and the quasi-static model converge to the same value, for the same operational condition. Differences appear only at the time when the load is changed. This was expected, since in the PNGV model the dynamic effects of diffusion are addressed, where in the quasi-static model do not. However, these effects are not of considerable magnitude.

All in all, it is decided that the PNGV model was used as virtual battery for both simulations and experiments. The quasi-static was integrated inside the NMPC controller. The reason is, that the only variable of importance considering the battery, for control purposes, is the SoC. For both models, this parameter is nearly the same, and considering the fact that, the prediction horizon will be maximum 2 seconds, quasi-static approach returns excellent results. Moreover, the SoC for the latter model, is calculated using only one differential equation and contains only one algebraic loop.

2.5 HIPPO-2 Modeling of dynamics

In HIPPO-2 experimental testbed, the torque command to CAT C9.3, is given as percentage of the maximum indicated torque. According to the dynamic model which was presented in section 2.2.2 of the present chapter, the gross torque can be modeled using three components, the net torque, the friction torque and the torque which is absorbed for pumping. Assuming that pumping torque, can be described for the particular operating region, from a 2nd degree polynomial, the relation between the command and the output torque is:

$$T_{ICE} = c_1 \cdot uT_{ICE} - (c_2 + c_3 \cdot SE + c_4 \cdot SE^2) \quad (2.5.1)$$

Considering that the engine rating is C, the peak indicated torque according to manufacturer, is 1596 Nm and since in torque control mode, command input is given to the controller as percentage of the peak net torque, it is considered that c_1 is 15.96 Nm/%. The rest coefficients, were fitted from data which was measured from the hybrid test-bed, via least squares method.

The rotational shaft speed, was modeled via the second Newton's Law. Considering the previous relation, the differential equation which describes the dynamics of the system is non-linear, as follows:

$$\frac{d\omega}{dt} = \frac{1}{J}(c_1 \cdot uT_{ICE} + c_{EM} \cdot uT_{EM} - T_{LOAD} - (c_2 + c_3 \cdot SE + c_4 \cdot SE^2)) \quad (2.5.2)$$

Where ω is the rotational speed SE at rad/s , c_{EM} is the coefficient which transforms the control command to Nm. According to manufacturer, 100 % command translates to 579.6 Nm. Therefore, c_{EM} was considered to be 5.796 Nm/%.

Chapter 3

NMPC - MHE Theory and Application

In this chapter, elements of basic theory for the controller (NMPC) and observer (MHE) schemes which were applied are presented. The presentation focuses on the basic problem formulation, and the particular solutions which were implemented in order to solve the problem. Furthermore, the basic functions and attributes of the optimization software (ACADO Toolkit) which was employed to implement the control and observation schemes are also briefly presented.

3.1 Nonlinear Model Predictive Control Theory

Before the Nonlinear Model Predictive Control (NMPC) scheme is analyzed, it is appropriate to describe the basic structure of the finite horizon Optimal Control Problems (OCP). In this class of problems, the optimization is to compute the best control strategy, for the given horizon, which would not violate the physical constraints of the problem and would minimize a specific cost function. The optimal problem can be defined as:

$$\min_{x(\cdot), u(\cdot)} \int_{t_0}^{t_N} F(T_k, x(t_k), u(t_k)) dt_k + E(t_N, x(t_N), x(t_N))$$

subject to

$$\begin{aligned} x(t_0) &= x_0 && \text{(Initial Values)} \\ x_{k+1} &= f(t_k, x(t_k), u(t_k)) && \text{(System Dynamics)} \\ h(x_{t_k}, u_{t_k}) &\leq 0 && \text{(Stage Constraints)} \\ r(x(t_N)) &\leq 0 && \text{(Terminal Constraints)} \end{aligned}$$

where J is the objective function, F is the stage cost function and E is the terminal cost function. The objective function is minimized in interval t_0, \dots, t_N . $x = x_0, \dots, x_n$ denotes the state vector and $u = u_0, \dots, u_m$ denotes the control vector of the system. Solving the problem gives the best sequence of controls u_k that delivers the sequence of states x_k , for every time interval $k = t_0, \dots, t_{N-1}$ satisfying the stage constraints $0 \geq h(x_{t_k}, u_{t_k})$ and ending up in such x_N that satisfies the terminal constraint $0 \geq r(x_{t_N})$.

Model predictive Control (both Linear and Nonlinear) is actually a procedure which aims to solve the above optimal problem. In order to give a better illustration of the procedure, and since the chosen algorithm for this work depends on linear approach, the logic behind both of these schemes is described.

Model Predictive Control (MPC) is an advance, model based, control technique, which is able to deal with multiple input and output constrained linear systems. The basic idea for this scheme is that in by explicit use of a linear system model, given measurements or estimates of the current states of the system and a hypothetical future input trajectory or feedback control policy, the MPC conducts future predictions for the system behavior, for a finite time horizon H_p and plans an optimal control strategy, at the same time, for an also finite time control horizon H_c . The is to minimize an application-appropriate cost function and respect the predefined constraints. From the above control sequence, only the first control input is implemented, while the control and prediction horizon are displaced towards the future (Receding Strategy). Afterwards, the procedure is repeated. The above scheme is conducted in a discrete time framework [39, 40]. An illustrative figure for a MPC application for control of a SISO plant is shown at Fig. 3.1. The ability of handling multi-input/output problems, and the excellent behavior in near constraint conditions, are two attributes, among others which have made this control scheme quite popular the past decades. Furthermore, algorithmic developments have speeded up significantly the implementation of Linear MPC, increasing even further its usage [41, 42].

Nonlinear Model Predictive Control (NMPC) is based on the same idea, however, it can tackle problems with nonlinear dynamics and constraints, and not known to be convex

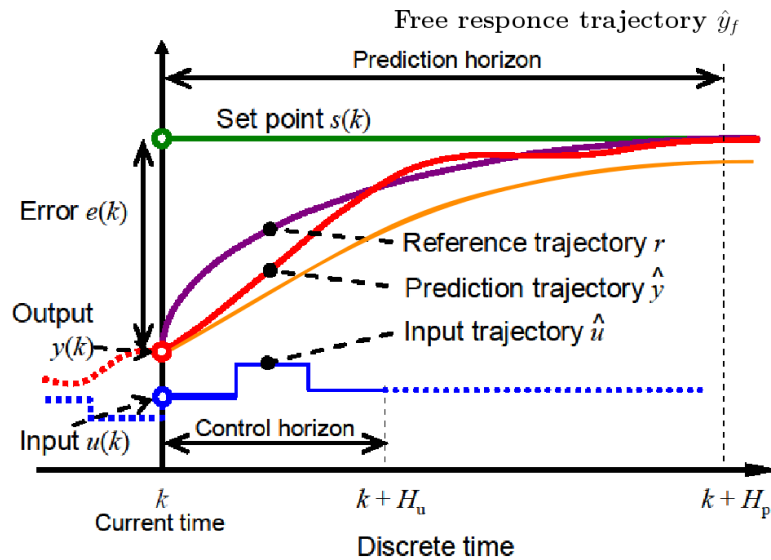


Figure 3.1: Concept of Model Predictive Controller [39].

as well. Due to the increased complexity, these problems are considered to be very difficult to be solved, and it is suggested that there is no global efficient way to solve them, but only a few approaches under a number of compromises. NMPC was first introduced in chemical industry where systems evolve at a very slow rate, giving time to the controller to complete the required calculations. In recent years, development of optimization algorithms and embedded control platforms has greatly reduced the required time for the NMPC algorithms to solve the optimization problem, leading to an increase in implementations and faster applications [43].

In order to implement NMPC controllers, several algorithmic approaches have been proposed [43]. In the present work, it was chosen that the implementation should be conducted via the largely used approach of the *Real Time Iteration (RTI) Scheme* [43]. Key factor to this approach is the observation that the NMPC is required to solve a sequence of OCPs, which solutions are very closely related. In essence, for every time instant the solution to the OCP is close to the previous one, since the differences in system dynamics evolution is not so fast. The convergence of the solution, is achieved via the RTI "on the fly", along with the evolution of system dynamics. According to [43], the RTI due to the fact that the NMPC problem is approached approximately by solving one properly structured linear Quadratic Problem (QP) per sampling time, the NMPC here can be conceived as a special case of linear time-varying MPC, with two main features:

- a. the system dynamics are linearized online, according to the current state and control prediction (rather on trajectory);
- b. numerical integration scheme is employed in order to simulate the system dynamics.

In [43], an intuitive justification for the above is provided, which is referred to as the *real time dilemma*. A brief description of the procedure the RTI implements the NMPC controller is presented in the next section.

3.1.1 NMPC Problem Formulation and solution via Real Time Iteration

3.1.1.1 Nonlinear MPC scheme (NMPC)

The RTI approach for NMPC solvers, is based on the Quadratic Program (QP) structure of MPC for nonlinear systems. In order to illustrate the approach, a time invariant discrete nonlinear dynamic system $x^+ = f(x, u)$, with inequality constraints $h(x, u) \leq 0$, is considered. The NMPC problem can be formulated as:

$$\begin{aligned}
 NLP(\hat{x}_i, \mathbf{x}_i^{ref}, \mathbf{u}_i^{ref}) = \\
 \underset{\mathbf{x}, \mathbf{u}}{\operatorname{argmin}} \sum_{k=0}^{N-1} \begin{bmatrix} x_{i,k} - x_{i,k}^{ref} \\ u_{i,k} - u_{i,k}^{ref} \end{bmatrix}^\top W_{i,k} \begin{bmatrix} x_{i,k} - x_{i,k}^{ref} \\ u_{i,k} - u_{i,k}^{ref} \end{bmatrix} \\
 \text{s.t.} \\
 x_{i,0} = \hat{x}_i, \\
 x_{i,k+1} = f(x_{i,k}, u_{i,k}), \quad k = 0, \dots, N-1 \\
 h(x_{i,k}, u_{i,k}) \leq 0, \quad k = 0, \dots, N-1
 \end{aligned} \tag{3.1.1}$$

At every time instant, the problem provides the NMPC control solutions in the following form:

$$u_i^{NMPC} = u_{i,0}, (\mathbf{x}_i, \mathbf{u}_i) = NLP(\hat{x}_i, \mathbf{x}_i^{ref}, \mathbf{u}_i^{ref}) \tag{3.1.2}$$

The above problem is a structured Nonlinear Program (NLP), which can be solved with various approaches. In this work the *Sequential Quadratic Programming (SQP)* algorithm is used. Here it is important to be noted that the stage cost matrix is considered to be quadratic positive and semi-definitive. According to [43], although more generic costs should be more suitable, by choosing them, closed loop stability and algorithmic problems might occur. Moreover, for sake of simplicity, the terminal cost is omitted.

3.1.1.2 Sequential Quadratic Programming (SQP) for NMPC

The SQP approach for NMPC occurs from QPs delivering Newton directions for performing steps towards the solution starting from an available guess. The iteration is repeated taking (not necessarily full) Newton steps until convergence. At guess $[x_i^{guess}, u_i^{guess}]$, the nonlinear problem is formulated as:

$$\begin{aligned}
 QP_{NMPC}(\hat{x}_i, \mathbf{x}_i^{guess}, \mathbf{u}_i^{guess}, \mathbf{x}_i^{ref}, \mathbf{u}_i^{ref}) = \\
 \underset{\Delta \mathbf{x}, \Delta \mathbf{u}}{\operatorname{argmin}} \sum_{k=0}^{N-1} \frac{1}{2} \begin{bmatrix} \Delta x_{i,k} \\ \Delta u_{i,k} \end{bmatrix} H_{i,k} \begin{bmatrix} \Delta x_{i,k} \\ \Delta u_{i,k} \end{bmatrix} + J_{i,k}^\top \begin{bmatrix} \Delta x_{i,k} \\ \Delta u_{i,k} \end{bmatrix} \\
 \text{s.t.} \\
 \Delta x_{i,0} = \hat{x}_i - x_{i,0}^{guess}, \\
 \Delta x_{i,k+1} = A_{i,k} \Delta x_{i,k} + A_{i,k} \Delta u_{i,k} + r_{i,k}, \quad k = 0, \dots, N-1 \\
 C_{i,k} \Delta x_{i,k+1} + D_{i,k} \Delta u_{i,k} + h_{i,k} \leq 0, \quad k = 0, \dots, N-1
 \end{aligned} \tag{3.1.3}$$

$$\begin{aligned}
 \text{where } \Delta x_{i,k} &= x_{i,k} - x_{i,k}^{ref}, \quad k = 0, \dots, N-1 \\
 \Delta u_{i,k} &= u_{i,k} - u_{i,k}^{ref}, \quad k = 0, \dots, N-1
 \end{aligned}$$

The matrices $A_{i,k}, B_{i,k}, C_{i,k}, D_{i,k}$ are derived from the linearization of system dynamics and dynamic constraints. Contrary to the linear MPC for nonlinear systems, the linearization occurs at the initial guess $[x_i^{guess}, u_i^{guess}]$. Therefore, the sensitivity matrices are:

$$\begin{aligned} A_{i,k} &= \left. \frac{\partial f(x, u)}{\partial x} \right|_{x_i^{guess}, u_i^{guess}} & B_{i,k} &= \left. \frac{\partial f(x, u)}{\partial u} \right|_{x_i^{guess}, u_i^{guess}} \\ C_{i,k} &= \left. \frac{\partial h(x, u)}{\partial x} \right|_{x_i^{guess}, u_i^{guess}} & D_{i,k} &= \left. \frac{\partial h(x, u)}{\partial u} \right|_{x_i^{guess}, u_i^{guess}} \\ r_{i,k} &= f(x_i^{guess}, u_i^{guess}) - x_{i,k+1}^{guess} & h_{i,k} &= h(x_i^{guess}, u_i^{guess}), & J_{i,k} &= W_{i,k} \begin{bmatrix} x_{i,k}^{guess} - x_{i,k}^{ref} \\ u_{i,k}^{guess} - u_{i,k}^{ref} \end{bmatrix} \end{aligned} \quad (3.1.4)$$

The matrix $H_{i,k}$ is the Hessian approximation of the Lagrangian of 3.1.3. The popular Gauss Newton Hessian approximation is given directly by assuming $H_{i,k} = W_{i,k}$. Therefore, the SQP procedure for time instant i , is given by Algorithm 1.

Algorithm 1: SQP for NMPC at discrete time i

Input: current state estimate \hat{x}_i , reference trajectory $(\mathbf{x}_i^{ref}, \mathbf{u}_i^{ref})$ and initial guess $(\mathbf{x}_i^{guess}, \mathbf{u}_i^{guess})$

1 **while** *Not converged* **do**

2 Evaluate $r_{i,j}, h_{i,k}$, and the sensitivities $A_{i,k}, B_{i,k}, C_{i,k}, D_{i,k}, H_{i,k}, J_{i,k}$ using (3.2.5);

3 Construct and solve $QP_{NMPC}(\hat{x}_i, \mathbf{x}_i^{guess}, \mathbf{u}_i^{guess}, \mathbf{x}_i^{ref}, \mathbf{u}_i^{ref})$ as in (3.1.3) to get the Newton direction $(\Delta \mathbf{x}_i, \Delta \mathbf{u}_i)$;

4 Compute step - size $\alpha \in [0, 1]$ to guarantee descent;

5 Update $(\mathbf{x}_i^{guess}, \mathbf{u}_i^{guess})$ with the Newton step

$$(x_i^{guess}, u_i^{guess}) \leftarrow (x_i^{guess}, u_i^{guess}) + \alpha(\Delta \mathbf{x}_i, \Delta \mathbf{u}_i)$$

6 **end**

return: NMPC solution $(x_i, u_i) = SQP(x_i, u_i) = x_i^{guess}, u_i^{guess}$

The NMPC solution of the $NLP(\hat{x}_i, \mathbf{x}_i^{ref}, \mathbf{u}_i^{ref})$ is the obtained from the SQP Algorithm 1, starting from the initial guess $(x_i^{guess}, u_i^{guess})$. as follows:

$$u_i^{NMPC} = u_{i,0}, \quad (\mathbf{x}_i, \mathbf{u}_i) = SQP(\hat{x}_i, \mathbf{x}_i^{guess}, \mathbf{u}_i^{guess}, \mathbf{x}_i^{ref}, \mathbf{u}_i^{ref}) \quad (3.1.5)$$

The choice of appropriate initial guess input is of great importance since they play a major role in convergence and reliability of the SQP iterations. According to [43], a good choice of initial guess could prevent the algorithm from converging to an infeasible solution and allows for taking full Newton steps, leading to faster convergence of the algorithm. For linear MPC, the initial guess is chosen to be the reference trajectory. However, this might be a poor initial guess since the reference and the actual trajectory maybe significantly diverge. In the present context of SQP for NMPC, a good initial guess from the discrete time instant i can be obtained, provided that a good solution has been obtained at the previous time instant $i - 1$. In essence, the initial guess is obtained by a *shifting procedure*. This procedure assumes that the evolution of system dynamics follows

the predicted trajectory (i.e. $\hat{x}_i \approx x_{i-1,1}$), and can be expressed as:

$$x_{i,k}^{guess} = x_{i-1,k+1}, \quad k = 0, \dots, N-1 \quad (3.1.6)$$

$$u_{i,k}^{guess} = u_{i-1,k+1}, \quad k = 0, \dots, N-2 \quad (3.1.7)$$

$$x_{i,N}^{guess} = f(x_{i,N-1}^{guess}, u_{i,N-1}^{guess}) \quad (3.1.8)$$

It is suggested that if the solution (x_{i-1}, u_{i-1}) is feasible, then the shifted solution should be also feasible, regarding the dynamic constraints. Furthermore, if the guess which was obtained from the shifting procedure is close enough to the real solution of the NMPC problem then according to [44], full Newton steps can be selected for SQP iterations and the first iteration would be an excellent approximation of the exact solution to the NMPC problem. As it can be seen, the above scheme does not provide any information about the last control input guess, since that exceeds the prediction horizon. Several approaches have been proposed to select the input $u_{i,N-1}^{guess}$. If a control law $k(x)$ is available, that stabilizes the system and simultaneously enforces the path constraints, then it can be chosen that $u_{i,N-1}^{guess} = k(x_{i,N-1}^{guess})$. If the model describes the system well enough, the choice would guarantee feasibility in respect to system dynamics and constraints. However, in practice simpler approaches are employed, with the most common being that the last control input is equal to the previous i.e. $u_{i,N-1}^{guess} = u_{i,N-2}^{guess} = u_{i-1,N-1}$.

Considering the above procedure, an important observation could be made. The SQP procedure starts when the new state estimate is obtained. While the iterations of the algorithm are performed, the physical system evolves, and consequently when the SQP finally converges, the information which was used to compute the state estimate \hat{x}_i are outdated. This problem can be overcome by employing prediction algorithms in order to estimate the state when the iterations have been completed. However, since the update of the control law requires the completion of the SQP algorithm and thus large computational delays can occur. The RTI approach which is presented here, chooses to begin the SQP algorithm and constantly incorporate the latest information of the system evolution in the iterations. Here lies a dilemma: whether to compute an exact solution with out-dated information or approximate the solution with the latest data. This is referred to as the *real-time dilemma*.

3.1.1.3 The Real Time Iteration approach (RTI)

The RTI approach is a method which efficiently solves the NMPC problem via the SQP, via performing the Newton steps always using the latest information of the system evolution. The RTI procedure is based on the Algorithm 1 which was previously presented, with some modifications. First it is considered that the initial guess is derived from the shifting procedure. Secondly, the NMPC solution is updated via a single Newton step for every time instant, on the previously constructed initial guess, instead of applying the SQP to full convergence. Assuming, that the solution which was obtained at time instant $i-1$ is a good initial guess, then according to the previous, the solution of the NMPC with $\alpha = 1$ is an excellent approximation of the fully converged solution. Thirdly, besides the above the RTI, divides the calculations into two phases, in order to reduce the *feedback time*. Considering the fact that, shifting procedure and calculation of the sensitivities (linearization of the system) on the initial guess, does not require the knowledge of the state estimate \hat{x}_i , and therefore they can be performed before the state estimate is available. Therefore, the RTI procedure is consisted of two phases which are:

- *the preparation phase*, in which shifting and sensitivity calculations occur prior to obtaining the state estimate

- *the feedback phase*, in which the rest of the calculations occur after obtaining the state estimate

For the above scheme, the Hessian approximation, i.e. $H_{i,k} = W_{i,k}$ is usually used in order not to calculate second order derivatives, receive a positive semi-definite approximation. The RTI algorithm is presented below [43]:

Algorithm 2: RTI for NMPC at discrete time i

- 1 *Preparation Phase* performed over time interval $[t_{i-1}, t_i]$;
Input: previous NMPC solution $(\mathbf{x}_{i-1}, \mathbf{u}_{i-1})$, reference $(\mathbf{x}_{i-1}^{ref}, \mathbf{u}_{i-1}^{ref})$
- 2 Shift $(\mathbf{x}_{i-1}, \mathbf{u}_{i-1})$ in order to construct $(\mathbf{x}_i^{guess}, \mathbf{u}_i^{guess})$;
- 3 Evaluate $r_{i,j}, h_{i,k}$, and sensitivities $A_{i,k}, B_{i,k}, C_{i,k}, D_{i,k}, H_{i,k}, J_{i,k}$ at $(\mathbf{x}_i^{guess}, \mathbf{u}_i^{guess})$ using 3.2.5;
- 4 Form QP omitting \hat{x}_i , prepare all possible calculations (e.g. condensing, matrices factorization) **return:** QP
- 5 *Feedback Phase* performed at time t_i upon availability of \hat{x}_i ;
Input: \hat{x}_i , prepared QP
- 6 Compute $(\Delta x_i, \Delta u_i)$ by introducing \hat{x}_i in QP and solving it ;
- 7 Apply the full Newton step

$$(\mathbf{x}_i^{guess}, \mathbf{u}_i^{guess}) \leftarrow (\mathbf{x}_i^{guess}, \mathbf{u}_i^{guess}) + (\Delta \mathbf{x}_i, \Delta \mathbf{u}_i) \quad (3.1.9)$$

return: NMPC solution (x_i, u_i)

According to [43], some important notifications should be kept in mind:

- The delay introduced by the feedback time can be accommodated as in linear MPC, by including a corresponding prediction in the state estimate
- The overall sampling time $t_i - t_{i-1}$ that can be achieved by the RTI scheme is limited by the total time spent in solving both the feedback phase and the preparation phase.
- The time required to perform the feedback phase is practically the same as the time required to solve the linear MPC problem.
- Part of the computations related to the QP solution can often be moved to the preparation phase, e.g. using a technique called condensing
- The minimum sampling time that can be achieved via RTI-based NMPC increases compared to standard linear MPC by the time required for the preparation phase
- It is typically desirable that the feedback time is only a fraction of the overall sampling time. Because the preparation phase can often fit in the time after the feedback phase and before the next state estimate is available, RTI NMPC can in many cases be applied at the same sampling frequency as linear MPC based on a model pre-linearised offline.

3.1.1.4 Global optimality for the NMPC solution

As it was mentioned before, NMPC optimization is non-convex, and therefore the computation of global solution for each time instant is not guaranteed. However, according to [43], under some specific assumptions, the solution provided from the RTI, can be proved to be global. These assumptions are:

- (1) the RTI scheme is warm-started at the global optimum
- (2) the sampling frequency is sufficiently high
- (3) there is continuity in the reference and the state
- (4) the OCP underlying the NMPC problem fulfills Second Order Sufficient Conditions¹ (SOSC) for every feasible initial condition
- (5) the global optimum depends continuously on the initial state and reference

According to [43], the above statement has been proved for local optimality in [46]. With use of assumption 1, the local optimum followed by RTI is also the global one. It is also remarked that Assumption 4 guarantees that the solution manifold is smooth and has no bifurcation. This entails that the RTI will keep track of the global solution manifold as long as it starts on that manifold and the initial conditions \hat{x}_i are sufficiently close to the predicted ones. The latter is guaranteed by Assumptions 1, 2, and 3. Faster sampling results in a larger set of disturbances for which RTI tracks the global solution manifold. Assumption 5 ensures that the solution manifold is continuous in time. In practice, the warm starting can be performed by setting the system at a reference steady state and initializing the RTI algorithm accordingly. Consequently, RTI is initialized at the global optimum.

3.1.1.5 Application to continuous-time systems

It is obvious that the above algorithm applies for discrete-time systems. RTI procedure requires to compute the dynamic sensitivities, $\nabla f(x, u)$, and this for the above systems is straightforward. However, in most cases, the controlled systems are described by time-continuous, Ordinary Differential Equations (ODE), in form of $\dot{s}(t) = F(s(t), v(t))$, where $s(t)$ and $v(t)$ are the states and controls respectively. Therefore, discretization of the system should be conducted before the RTI algorithm proceeds. In order this to be done, several methods have been proposed. However, the accuracy and the computational efficiency of each method mainly depends on the application. In [43], several methods are presented and analyzed. In the present work, it is chosen that the discretization to be conducted first and then the linearization to be occur at every time instant the previous solution, as the RTI algorithm occurs.

¹For further information about this scheme, [45] is suggested

3.2 Moving Horizon Estimation Theory

In control applications, it is desirable all the control related system parameters and states, to be known for every time instant. However, in most cases, this is not possible, since a number of states cannot be measured directly or it is too costly to do so, and the system parameters are not time constant. For instance, in a marine application, the external torque which applies to the propeller shaft is not usually measured. Therefore various schemes have been proposed in order to estimate the system states, which mostly are referred as *observers*. In this work, the observer which was chosen to be employed, is the *Moving Horizon Estimation* scheme.

Before explain the MHE, an introduction to state and parameter estimation is presented [47]. Consider, a discrete-time dynamic system with the following formulation:

$$x_{k+1} = f(x_k, z_k, u_k, p) + w_k, \quad x_0 = x(t_0) \quad (3.2.1)$$

$$g(x_k, z_k, u_k, p) = 0 \quad (3.2.2)$$

$$y_k = h(x_k, z_k, p) + v_k \quad (3.2.3)$$

where, $x \in \mathbb{R}^{n_x}$ are differential states, $z \in \mathbb{R}^{n_z}$ are algebraic states, $u \in \mathbb{R}^{n_u}$ are the controls, $p \in \mathbb{R}^{n_p}$ the system parameters, $y \in \mathbb{R}^{n_y}$ the system outputs and $w \in \mathbb{R}^{n_x}$, is the noise term which accounts for unmeasured disturbances. Index k denotes the time sample, taken at time t_k . Here, it should be noted that continuous time systems can be discretize in order to be in the above form, via analytic solution or numerical integration. Now, consider a complete array of measurements which is available from initial condition to final time for the system. The procedure in which an estimation of states and parameters for the system is conducted with the use of these measurements is called *full-information estimation*. The traditional formulation of the problem consists of a least-square batch estimation problem, and can solved deterministic way by minimizing a weighted sum of squared errors between initial conditions, model dynamics, and measurements, from time t_0 up to final time t_l as follows [47]:

$$\min_x \|x_0 - \hat{x}_0\|^2 + \sum_{k=0}^{l-1} \|x_{k+1} - f(x_k)\|_{Q_k^{-1}}^2 + \sum_{k=1}^l \|y_k - h(x_k)\|_{R_k^{-1}}^2 \quad (3.2.4)$$

The first term refers to cost related to uncertainty of initial conditions, the second term is a penalization of the state uncertainty, and the third term is a penalization of the measurement uncertainty. The three terms are weighted with confidence matrices P_0^{-1}, Q_k^{-1} and R_k^{-1} . With the solution of the least-squares problem, the optimal state sequence $x = [x_0^T, \dots, x_l^T]^T$. If the system is linear and observable then the least square problem has a unique solution. If the problem is nonlinear, there are multiple solutions that can give the observed output, and the solution to the least square problem requires to perform several Gauss-Newton iterations until convergence.

The above scheme is a deterministic approach, since by solving the least-square problem, indirectly, the unknown states and the measurements disturbances are calculated as the best fit. Thus, there is no need to define any probabilistic distributions in order to define the disturbances, as they redeemed as unknown inputs. However, in linear linear system with zero-mean uncorrelated random variables, the inverse of the weighting matrices are directly related to covariance matrices. In case of nonlinear systems, or the noise is described by a non-Gaussian distributions or there are constraints constraints

enough N . On the other hand, short horizon increases the importance of arrival cost, and in extreme case when $N = 1$, the problem formulation boils down to Extended Kalman Filter. Furthermore, arrival cost is also compensate for no observable systems, or for lack of efficient information, in order the MHE to solve the least square problem. In [49], an efficient way to implement the arrival cost is suggested, which is based on approximating the ideal arrival cost which occurs from dynamic programming. This manner is also used in the current work.

An efficient way to solve the above problem is to use sequential quadratic programming (SQP) techniques based on the generalized Gauss-Newton method, and more specifically Real Time Iteration approach. As explained in the previous section, the RTI process is essentially reduces the computational burden, by implementing only one Gauss-Newton iteration per sample, by coupling the system evolution with the solution. The solving process, is also split into two parts, the preparation phase and the estimation phase as previously explained. Also direct multiple shooting is employed, meaning that the problem is discretize within the considered estimation horizon, and it is solved for all the initial value problems that occurs simultaneously in the resulted time intervals.

The benefits of MHE implementation, regarding other observer types according to [47] are the faster convergence when starting from large initialization errors, and an increased estimation accuracy for nonlinear systems, in some circumstances, with respect to Extended Kalman Filter. Also, simultaneous state and parameter estimation could occur. Furthermore, MHE does not require particular assumptions on the disturbance distributions, it can handle state and parameter constraints that could be imposed for physical reasons. Finally, The ability of the MHE to approximate a full information filter over a finite horizon makes it well suited for online estimation.

3.3 NMPC and MHE Implementation

The NMPC controller and the MHE estimator were both implemented via the *ACADO Toolkit* open source package [50–53]. ACADO Toolkit is software environment and algorithm collection for automatic control and dynamic optimization, written in C/C++. The framework which provides, includes a variety of algorithms for direct optimal control, including model predictive control as well as state and parameter estimation, via direct single or multiple shooting methods. Moreover, it also provides efficiently implemented (stand-alone) Runge-Kutta and BDF integrators for the simulation of ODE's and DAE's. Its design is object oriented, which allows the coupling with other existing optimization packages and user-written code.

All in all, ACADO is a powerful optimization toolbox which can provide NMPC and MHE solvers in form of C/C++ source code, via the code generation tool. According to [54] several advantages of the optimization software have been identified. Firstly, The exported code has hard coded dimensions and uses static global memory only. That way there are no *malloc/free* or *new/delete* statements. This ensures that any segmentation faults and out of memory errors cannot occur while running the algorithm on the embedded device, (such as the dSpace Micro Autobox II DS1401/1511 which is employed for experiments). Loop statements tend to be avoided whenever possible, ensuring code's high efficiency. Furthermore, the precision of the calculation can be regulated to single or double, based on the on the capabilities of the embedded platform which is used. Finally, except the QP solver the generated code does not contain any conditional statements. So the code cannot run into a code that has not been tested before.

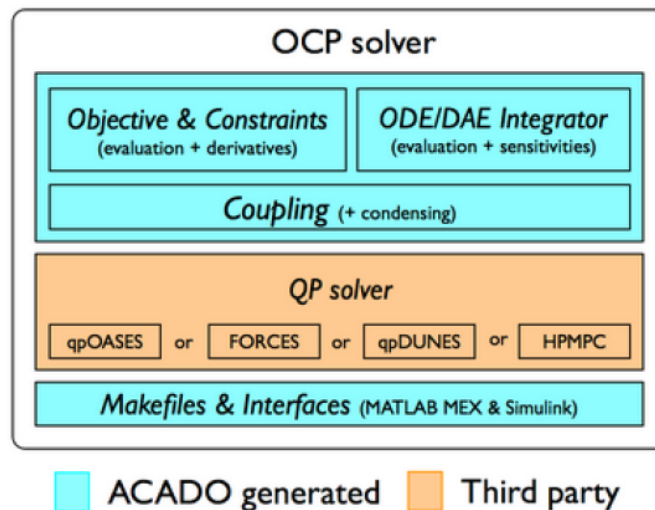


Figure 3.2: ACADO Code Generation Structure [55].

Chapter 4

Controllers Design and Simulations

In this chapter, the design procedure, tuning and simulation of the developed controllers is presented and explained. Like any other control system, the controllers should have the following attributes [56] Minimize steady state errors, respond to transient disturbances acceptably and achieve stability. It is clear that the above objectives are contradictory. For instance, if a controller has increased robustness, then the control actions will be decreased and consequently its performance would be reduced. Therefore, during the controller design and tuning, a compromise of the above takes place. The design procedure was as follows: 1) system identification, 2) modeling, 3) controller design, 4) control system analysis and performance 5) result review and check if the objectives are satisfied. The first two steps regarding system identification and modeling were presented, in Chapter 2, and therefore only the final steps are presented here.

Controllers, were developed in Simulink environment using *ACADO Toolkit's code generation tool*. Although, a brief presentation of ACADO has been shown in Section 3.3, its implementation for the NMPC scheme for this work's applications, is illustrated here.

The purpose of the developed controllers is to efficiently perform power split in the hybrid propulsion plant, operating within a number of predefined limits. These limits refer to the operational outputs (Torque, Rotational Speed), the fuel consumption and emissions. The first two were directly considered during NMPC design, i.e. they were modeled and relevant constraints were implemented. As mentioned before, HIPPO-2 testbed engine CAT C 9.3, is equipped with DPF filter, EGR system and SCR after-treatment systems; therefore, NOx and PM emissions are mostly self-regulated by the engine and the Aftertreatment ECUs. However, if the SCR system is ignored, NOx values during transient operations, even those of medium scale, can reach high values as 800 ppm, as stated in chapter X. Therefore, the controller design was oriented to *reduce the intensity of engine transient behavior during the particular loading profiles*. This is done indirectly, since no efficient computationally ¹ model of NOx value estimation was found applicable for the experimental engine. The main reason for that is the EGR's behavior which, apparently, have great implications on NOx emissions reduction, and it is directly controlled by the ECU of the engine. In light of these evidence, it is decided that the NOx emissions will be indirectly regulated by smoothing the transient operations of the Diesel engine, via the operation of the EM, in order to force the engine to operate in static or quasi-static state,

¹i.e. a mean value model which can be integrated in msec and give reliable information about NOx quasi-static - dynamic behavior

even in the transient loading profiles. This control scheme is presented and implemented in controller cases 2 through 4 and referred to as direct engine control.

Moreover, it must be pointed out that the calculation of NMPC control values emerge from the minimization of a cost function, in which more than one parameters and constraints are involved. Consequently, some times the references values may not be tracked. For instance, if there are two references values or constraints, one for *Fuel Consumption Rate* and one for *SoC*, maybe there is not an operation point which satisfies them both, meaning that the problem is *infeasible*. The risk in this case, is the possibly unstable control inputs, which will provoke the system to respond violently. According to ACADO this case has been considered and special course of action will occur, i.e.: the NMPC input to the plant will be the one which minimizes the cost function, at the particular time (possibly a near constraint operation point), and then the input will remain constant until the in-feasibility is resolved. Considering that this case of poor control design, can prove to be difficult to be distinguished, especially when a number of different constraints are involved, a special case considering the above is tested and presented.

Furthermore, in order the NMPC to solve the semi-optimal control problem, the values of all states, control inputs, disturbances and parameters of the system at the particular time instant, should be measured or at least be estimated efficiently, and be fed to the controller. Of course, these data are not available all the time. In particular, torque load in a marine power plant is not measured/estimated directly in most cases, or measured signals can be tampered with noise or significantly delayed. In section 4.5, an efficient way of estimating the load torque and rejecting the noise, based on a Moving Horizon Estimation scheme, is presented, along with simulation results.

Finally, a power-split application on a marine power plant using the developed controller and estimator is presented and simulated in section 4.6, via a propeller load simulation. The propeller load simulator is derived from [57], and referred to ship, with power needs which are similar to the capabilities of HIPPO 2 test-bed, equipped with fixed or controllable pitch propeller with environmental disturbances to be taken into account.

In the present work, two controller categories were considered. The first case refer to MISO controllers which in general obtain constraints and references regarding the engine and the power plant operation in general, and regulates the EM's torque command in order to satisfy the control objectives. This kind of scheme will be referred to as *indirect engine control*. In the other case, the NMPC conducts the power splitting directly, by controlling both the EM and the ICE. This scheme will be referred to as *direct engine control*. These two kinds controllers were developed, with several variations, and simulated on the hybrid propulsion plant model which is described in next section. One case from the first scheme and two from the second were selected and tested in a real time application on the HIPPO 2 experimental test-bed. The results are presented in the next section. For the evaluation of NMPC and comparison regarding their performance at reference tracking and constraints handling of those with the same control object, the *Integral Square Error Criterion (ISE)* was employed, which formulation is the one below:

$$ISE = \int_0^{\infty} \epsilon^2(t) dt \quad (4.0.1)$$

4.1 NMPC Strategy and Implementation

In this section, the attributes of the developed NMPC are explained as the controller application using the *ACADO Toolkit* have specifications and limitations which have to be considered. NMPC problem follows the formulation

$$\min_{\substack{x_0, \dots, x_N \\ u_0, \dots, u_{N-1}}} \sum_{k=0}^{N-1} \|h(x_k, u_k) - \hat{y}_k\|_{W_k}^2 + \|h_N(x_N) - \hat{y}_N\|_{W_N}^2 \quad (4.1.1)$$

$$s.t \quad x_0 = \hat{x}_0 \quad (4.1.2)$$

$$x_{k+1} = F(x_k, u_k, z_k), \quad for \quad k = 0, \dots, N-1 \quad (4.1.3)$$

$$x_k^{lo} \leq x_k \leq x_k^{up}, \quad for \quad k = 0, \dots, N \quad (4.1.4)$$

$$u_k^{lo} \leq u_k \leq u_k^{up}, \quad for \quad k = 0, \dots, N-1 \quad (4.1.5)$$

$$r_k^{lo} \leq r_k(x_k, u_k) \leq r_k^{up}, \quad for \quad k = 0, \dots, N-1 \quad (4.1.6)$$

$$r_N^{lo} \leq r_N(x_n) \leq r_N^{up} \quad (4.1.7)$$

where $x \in \mathbb{R}^{n_x}$ is the differential states, $u \in \mathbb{R}^{n_u}$ are the control inputs, $z \in \mathbb{R}^{n_z}$ are the algebraic variables and $x_0 \in \mathbb{R}^{n_x}$ is the current state measurement. The reference functions are denoted as $h \in \mathbb{R}^{n_y}$ and $h_N \in \mathbb{R}^{n_y, N}$ and weighting matrices are denoted with $W_N \in \mathbb{R}^{n_y \times n_y}$ and $W_k \in \mathbb{R}^{n_y, N \times n_y, N}$. The stage costs in this are restricted to quadratic positive (semi- definite matrices, in order to ensure closed loop stability [58]). Variables $y_k \in \mathbb{R}^{n_y}$ and $y_N \in \mathbb{R}^{n_y, N}$ denote the time-varying references. In ACADO environment, the bounds for the states and control variables, described in (4.1.4) and (4.1.5), can be varying for every time instant or may change along the prediction horizon, or may be chosen to be hard-coded. System equations are defined in continuous time, and discretization along with online linearization is conducted by the solver. In this section, a number of attributes which are implemented for all the NMPC's solvers are presented in a form compatible that is compatible with the ACADO Toolkit.

A. Soft Constraints

Infeasibility poses a serious problem for online controllers. Although, ACADO considers this case and provides an acceptable solution, further action can be performed to overcome this problem. According to [39] an efficient way to eliminate this case is to implement *Soft Constraints*. The term hard constrains is applied to states or control inputs which cannot be softened in any way. For instance, the engine load command cannot exceed 80 % in any case due to factory setting. In order to change that, ECU of the engine has to be reset. On the other hand soft, constraints refer to bounds which have been set by the controller designer and are not derived directly by the physical limitations of the system. E.g. if it is preferable to limit the shaft speed below 2000 rpm, while the engine can reach 2200 rpm.

Soft constraints in ACADO, and in optimization applications in general, can be implemented with the use of extra variables, which called "*slack variables*". These are defined in a way that they are positive, non-zero only if the soft constraints are violated. The non-zero values are heavily penalized in the cost function with a, relatively to the other components, higher value in the cost matrix, in order for the optimizer to have a strong

incentive to keep them at zero if possible and as a result make the constraint to be satisfied. Soft constraints are defined in affine form as follows:

$$x_k + \varepsilon \leq x_k^{up} \quad (4.1.8)$$

$$x_k - \varepsilon \geq x_k^{low} \quad (4.1.9)$$

where $\varepsilon \geq 0$ is the slack variable, which is considered as the rest of input vectors. If the state is below the lower limit, the the slack variable increased, and therefore the constraint is valid (i.e. the problem remains feasible). Similarly, when the state is above the limit the slack variable increases.

B. Control Law

Another attribute of NPMCs is that the system control inputs are treated as differential states. In essence, the control variables $u(k)$ of the controller are obtained by adding the control law $\Delta u(k)$ to the previous output $u(k-1)$. In ACADO environment this is implemented by adding extra differential equations, as many as the manipulated variables, with the following formulation

$$\dot{u} = du \quad (4.1.10)$$

where u is the vector of the manipulated variable du is the vector of the controller output. The reason why control variables are chosen to be implemented in this way, is to penalize the control command change and avoid oscillating behavior.

C. Control horizon

Several of the developed NPMCs were chosen to have different control N_c and prediction horizon N_p , with $N_p \geq N_c$. The control horizon is a tuning parameter, and it is desirable to be as small as possible, in order to reduce computational cost. In ACADO environment there is no direct option for the choice control horizon, and it is considered to be the same as the prediction horizon. However, ACADO gives the option to manipulate constraints at each prediction horizon step. Consequently, control horizon was implemented by setting $\Delta u(i) = 0$ for $i = N_c, \dots, N_p$.

D. Kickback constraint

It was observed that, when the propulsion plant operates near/on a state constraint (e.g. engine speed constraint), oscillations (kickbacks) occurs. This phenomenon can be explained as follows: The model which is integrated into the NMPC is not perfect, although it's high accuracy. Furthermore, the signals are affected with disturbances and noise. Consequently, when the plant operates near a constraint, it is very possible that this constraint may be violated (or it is predicted to be violated within N_p). In response, the NMPC will produce an input which will tend to restore the the system inside the allowable operation limits. In order, for the above to be avoided, a constraint regarding the changing rate of the controller input is applied. This constraint has two stages. In the first stage when the state is near a constraint, between two values, the manipulated variable change rate constraint is reduced. If the state value comes closer to the constraint, the maximum rate value decreases even more. The simple algorithm which was previously described, has been performed in ACADO environment by implementing affine constraints for the control rates using a parameter which is regulated externally, and is considered static for the N_p in accordance to the above.

4.2 Propulsion Plant Simulation

In order to develop reliable controllers for the experimental propulsion test-bed, several simulations were conducted and results evaluated. The simulation of propulsion plant model was based on the high fidelity models which were presented in Chapter 2.

The power plant consists of the *Internal Combustion Engine (ICE) Model*, the *Electric Motor (EM) Model*, the *Load Component*, the *Shaft Inertia* and the *Battery (BAT)*. The components, which are described here are the load component and the shaft inertia. The first component describes the external torque which is applied at the shaft. In most scenarios, it is represented by a signal which varies according to the case requirements (constant, pulse, etc.). There is a scenario though, in which this component describes a propeller load. The Simulink adaption was derived directly from [57] and therefore will be described in the corresponding case scenario. The shaft inertia represents the systems mechanical dynamics, and it is mathematically described by Newton's second law. The block diagram of the propulsion plant and the Simulink adaption are shown in Figure 4.1 and 4.2.

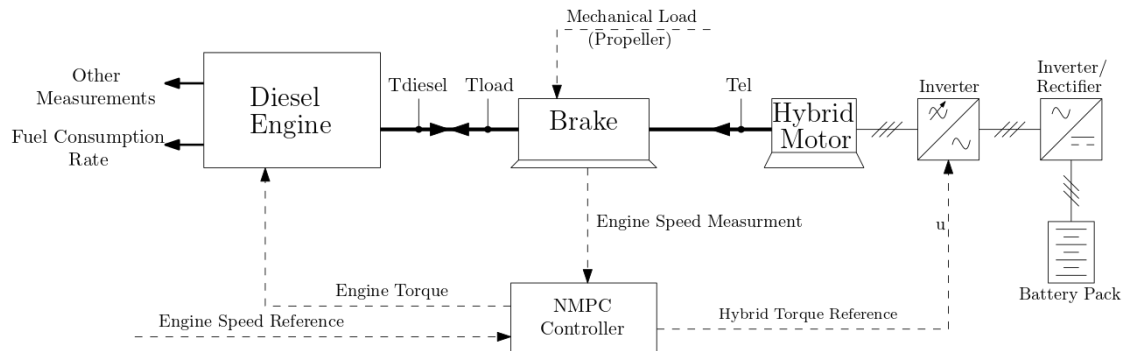


Figure 4.1: Block Diagram of engine direct torque control scheme of HIPPO 2 with battery consideration.

Another attribute of the Simulink model is that the signals which are fed to the controller, are obtained with the same sample time and the same time delay as they are measured on the HIPPO 2 experimental test-bed. The sample rates obtained from the manufacturer guide books of the various components, wherever these were available or by direct measurements. Time delays were estimated from data measurements. Time delays and sample times for the signals is shown in table 4.2.

<i>Signal</i>	<i>Sample Time (sec)</i>	<i>Time Delays (sec) (Signal Measurement)</i>
<i>EB Torque</i>	0.01	0.1
<i>Engine Torque</i>	0.01	0.1
<i>EM Torque</i>	0.1	0.1
<i>Engine Speed</i>	0.01	0.1
<i>Fuel Consumption Rate</i>	0.5	0.5

Table 4.1: HIPPO's 2 measured signal sample times and time delays relative to load application.

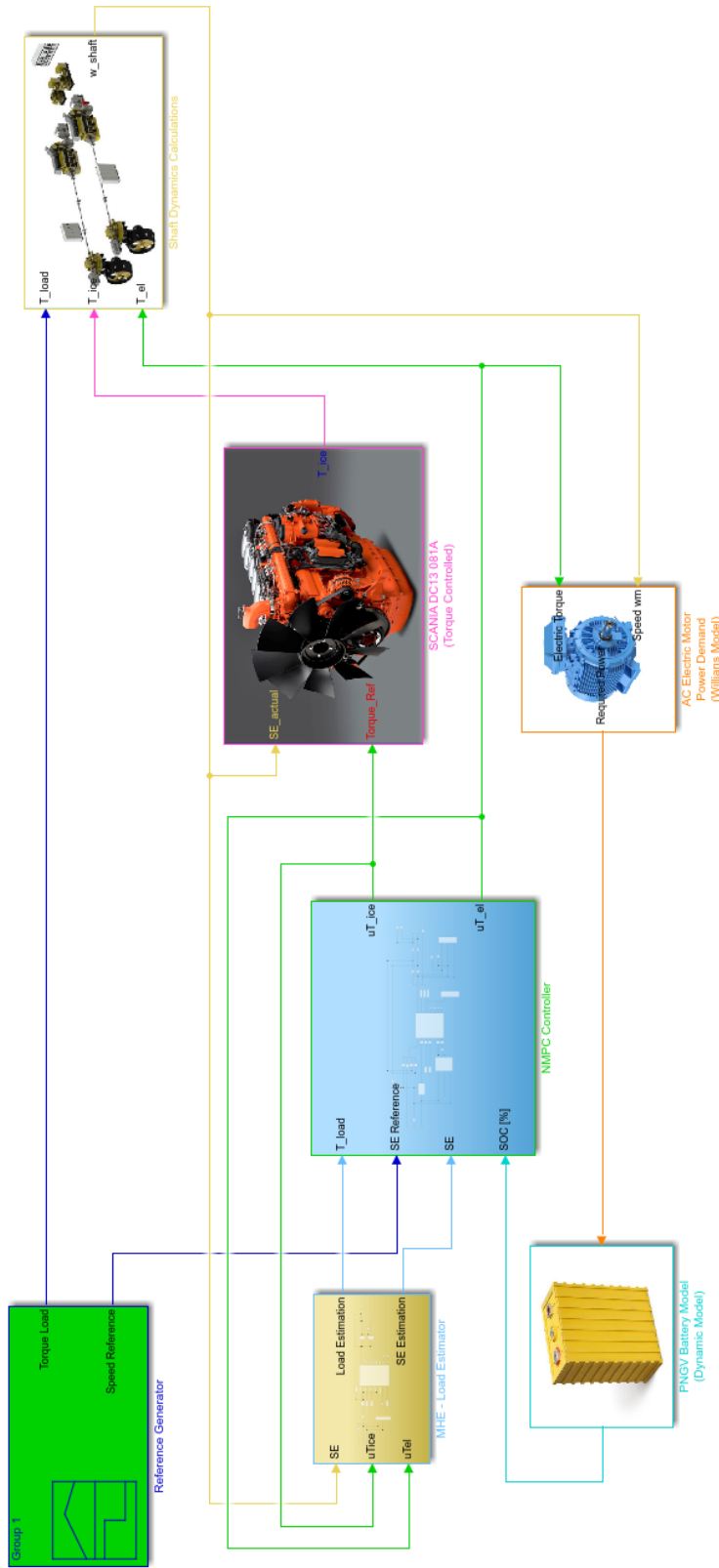


Figure 4.2: Simulink set up of Marine Hybrid Diesel Electric Propulsion Plant

4.3 Indirect Control of ICE

The aim of the first set of controllers and simulations is to control indirectly the ICE with regulation of EM torque. The NMPC controller receives references and constraints for the control and the prediction horizon, which are related to engine operation such as the *Fuel Consumption Rate*. The controller also, obtains the operational profile of the plant (i.e. the shaft rotational speed and torque)². The operational profile is considered to be static within the future steps (predictive horizon). The controller solves the nonlinear optimal control problem for the finite time period of the prediction horizon, and calculates the appropriate input for the EM (Torque). In essence, the NMPC alters the ICE operation point (alters the required ICE Torque with speed remains unchanged), so that ICE tracks the appropriate references, or be in accordance with the preset constraints.

4.3.1 Fuel Rate control

The operation scenario for this controller is to regulate the control input to EM, in order to manipulate the fuel oil consumption so this remains inside the predefined limits, or track a reference value. This case resembles a diesel driven generator or cargo pump which is required to operate within certain consumption limits (e.g. for economic reasons). The block diagram of the control scheme is presented below

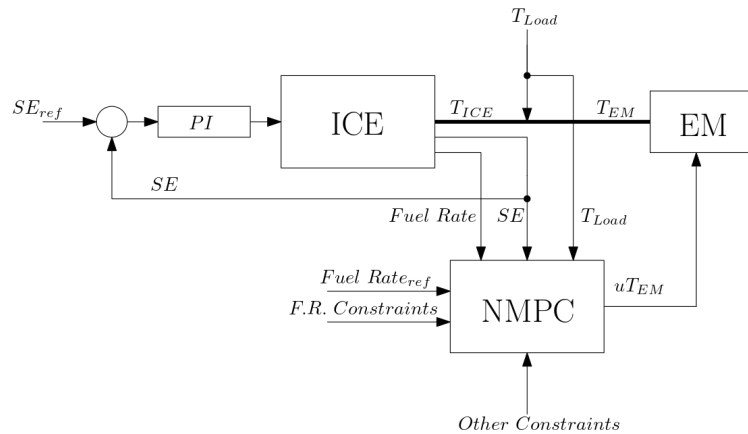


Figure 4.3: Block Diagram of indirect fuel rate scheme

Considering the mathematical formulation of the problem in the form which is described above (eq: 4.1.1), the problem components using the same symbolism are the following

- Differential states are the Fuel Rate Consumption FR and the EM Torque command uT_{EM} . The first is the system output variable and the second is the manipulated system input variable.
- the controller output is the rate of change of EM torque command duT_{EM} . (For the the controller this is the calculated command as explained above)
- the time varying reference is $\hat{u}T_{EM}$ in the first case and \hat{FR} in the second.

²An alternative proposal for the estimation of Torque Load, is discussed later in this chapter

- The cost function is the following:

$$\min_{\substack{FR(0), \dots, FR(N) \\ duT_{EM}(0), \dots, duT_{EM}(N-1) \\ \varepsilon(0), \dots, \varepsilon(N-1)}} \sum_{k=0}^{N-1} \|h(FR(k), duT_{EM}(k), \varepsilon(k)) - \hat{y}_k\|_{W_k}^2 + \|h_N(FR(k)) - \hat{y}_N\|_{W_N}^2$$

- the main implemented constraints for all controllers of this section are:

- $0 \leq FR \leq 40$ [1/h] (Hard Constraint)
- $FR - \varepsilon \leq 35$ [1/h] (Soft Constraint)
- $0 \leq T_{ICE} = T_{load} - T_{EM} \leq 800$ [Nm]
- $-90 \leq uT_{EM} \leq 90$ [%]
- $-50 \leq duT_{EM} \leq 50$ [%/s]

Additional constraints were also implemented

- the kick-back constraint:

- $-50 \leq duT_{EM} - k_c$ [%/s]
- $50 \leq duT_{EM} + k_c$ [%/s]

- the control horizon constraint:

$$g. \quad duT_{EM}(k) = 0 \quad \text{for } k \in H_c + 1, \dots, H_k$$

In this scheme, two NMPC controllers are presented which differ in the control horizon. The first controller, was design to have equal control and prediction horizon, where the second has much smaller control horizon (3 steps N_c and 10 stpes N_p).

The loading scenario refers to static and dynamic reference tracking; results are shown in Figure 4.4. Comparing the two controllers, the differences are not significant. However, the control command of the first is sharper than the others, leading to a faster response of the system. For example at time instant 28s, where speed reference changes, the engine speed controller reacts by reducing the fuel rate. As a result, the FC diverge from the predefined reference. Both NMPCs detects that and applied regenerating torque in order to increase the fuel consumption. Meanwhile, the speed reference is reached and the speed controller increases the torque in order to stabilize the speed to its reference. The NMPCs respond by decreasing the regenerating command. However, the controller with the smaller control horizon, achieves a faster stabilization due to its faster responds. The reason of this behavior was explained previously. The above explanation can be illustrated with the help of ISE criterion, which for the first approach is 3891 and for the second is 3449. Therefore, control horizon scheme is employed since it reduces the computational costs, and favors stability.

NMPC with adaptive model

Based on the above controller, another scenario was also considered, in which the plant operates in a region which is not enclosed in the data-set where the model was tuned. Consequently, the model will diverge from the real plant, and a permanent offset during reference tracking is expected. This phenomenon can also occur when the plant

is operating in an environment with different conditions (e.g different temperature) from those that it was tuned, or with an alteration to the engine setup. These are scenarios which are mostly likely to happen in an actual application. The solution which is examined here, is that the controller employs an adaptive polynomial model, which is re-calibrated online, via the algorithm of chapter 2, in order to adapt in the new conditions. In the scenario, the model is updated every 1 s. From the results, which are shown in Figure 4.5, it is clear that online model adaptation is an efficient way to deal with plant alteration, and uncertainty regarding the model. Although both controllers originally were tuned with the same parametric model, there is a significant difference between the results. With the adaptive model, the offset completely disappears, and the reference is tracked down correctly. This also is highlighted from the ISE criterion value, which decreases from 175 to 114 by applying the online model adaptation.

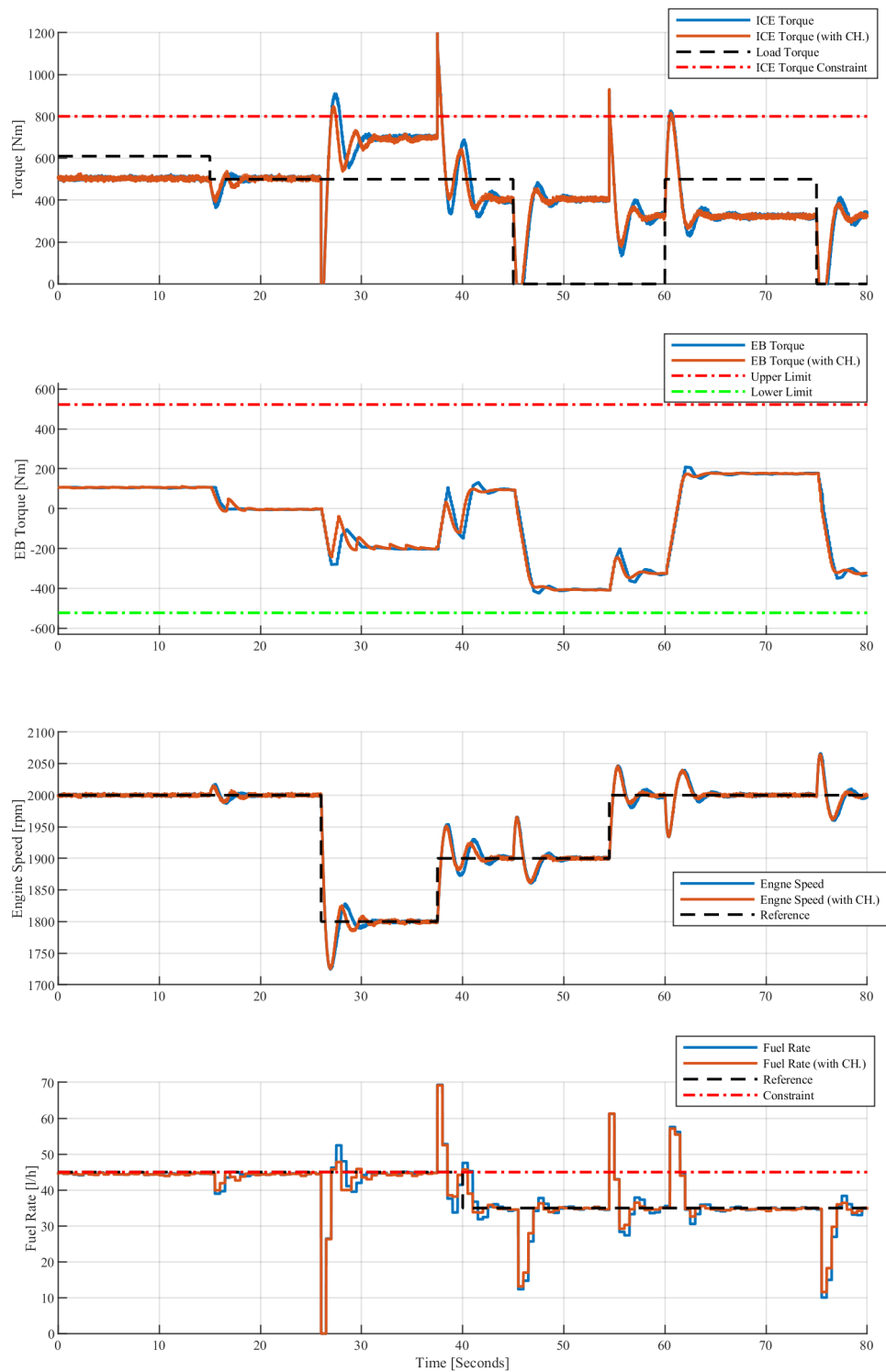


Figure 4.4: Simulation results of Fuel Rate control with and without control horizon NMPC

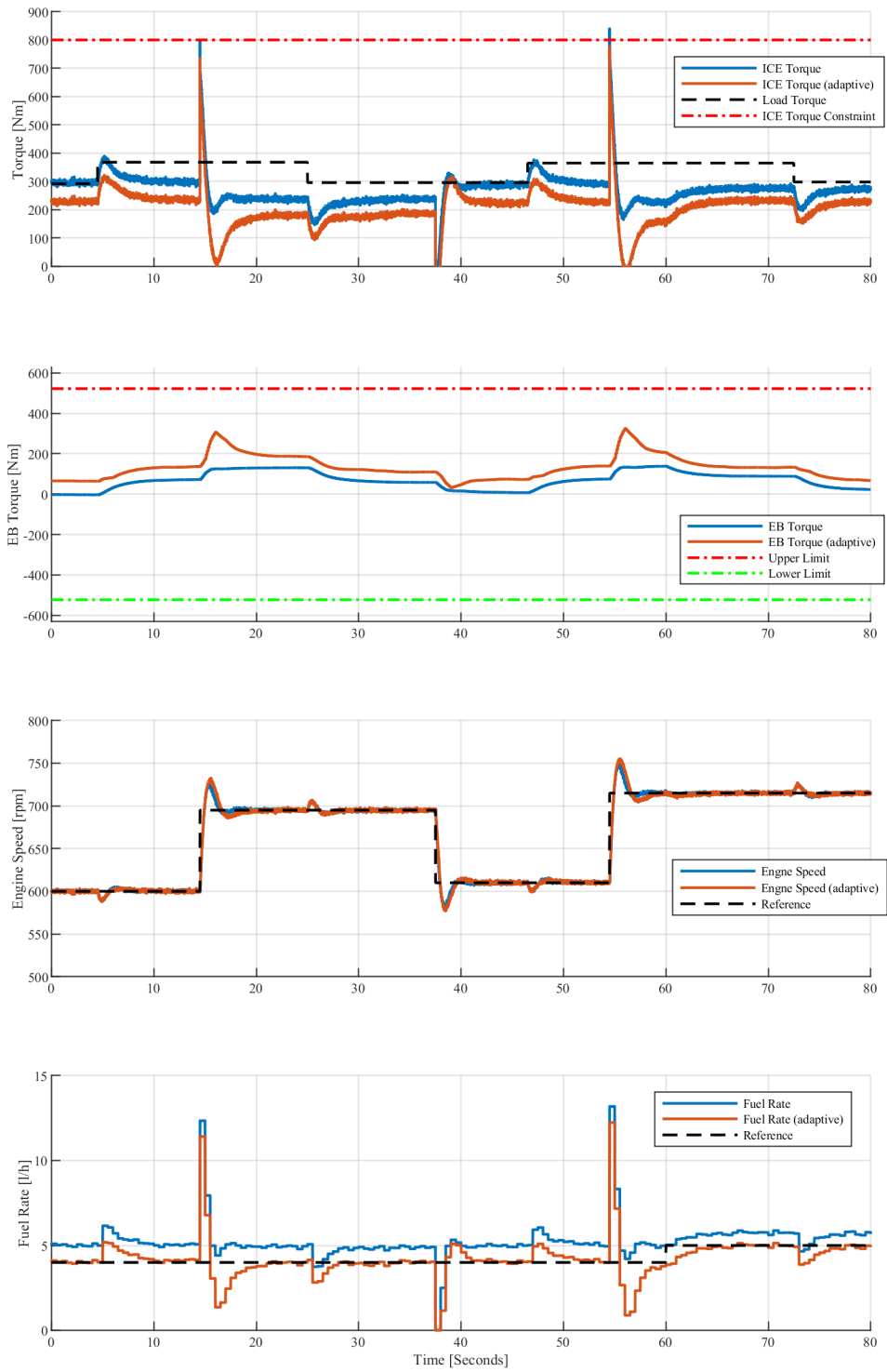


Figure 4.5: Simulation results of Fuel Rate control with and without adaptive NMPC

4.4 Direct Control of ICE

In the previous section, an indirect control scheme, via the EM torque, was employed in order to regulate the operating point of the engine. However, the system tends to surpass the limits during transient operations, due to the faster dynamics of the engine speed controller. Therefore, in order to increase the transients behavior of the hybrid plant, a different control approach adopted: NMPCs apply direct control to both ICE and EM, by manipulating the torque production of each. At the HIPPO-2 experimental test-bed this can be done by giving a control command to each component, as the percentage of the nominal torque of the EM and the indicated load of the engine. The EM is controlled by a DTC scheme and therefore, the EM command is applied instantly. On the other hand, engine torque command is calculated through an open loop map which regulates the injected fuel. The purpose of this control scheme is to "reduce" the engine dynamic response so as to behave like it was in steady state conditions. In this section two kinds of controllers are presented. The first scenario is to operate the propulsion plant in transient loads, with no limitation regarding the electric power, and in the second, a battery keeps the SoC inside predefined limits as an additional control task.

4.4.1 Engine Speed Reference Tracking

NMPC calculates the torque commands of both the EM and the ICE. The control objective is that during transient operation, e.g. the sudden application of a torque load or speed reference alteration, the controller initially gives a control input to EM which will be enough to counter the load or bring the system to the desired reference. The block diagram of the control scheme is presented in Fig. 4.6

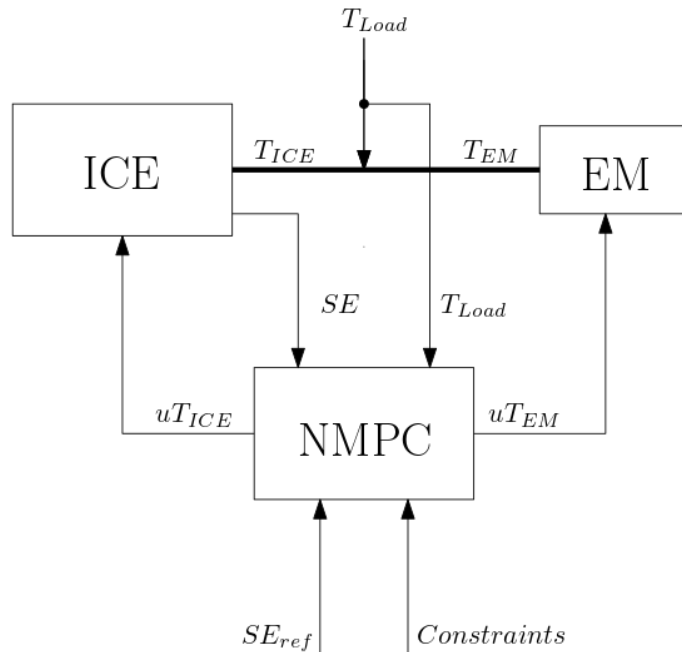


Figure 4.6: Block Diagram of direct SE control scheme

As previously mentioned, the EM has a very fast dynamic response, and can reach the desired reference in practice instantly, with negligible transient phenomenon. At the same time, the NMPC will also start to alter the control input of the ICE, in the same logic as the above. However, the rate of this change would be much lower from that of the EM. Hence, the ICE operation would be or at least resemble to that of the steady state, with

all the benefits which have been described before. Gradually the EM control input would decrease and be counter by the ICE, until the the latter will able to support the whole load alone. The main differential equation which describes the problem is Newton's second law. In order to test the above, a NMPC controller with two version was developed. The difference between the two controllers is that in the second version an extra constraint is employed which referrers to engine Fuel Rate. The constraint is implemented via an open loop - steady state map which was constructed from data, and integrated to NMPC in form of a 3rd degree polynomial function of engine Speed and Torque. Similarly, other steady state maps is possible to be implemented (e.g. NOx maps). Furthermore, the engine maximum torque depends on the engine speed. A variable limit was also considered, with the use of an affine constraint over Np. The problem can be illustrated mathematically in the standard form as

- the differential states are the Engine Speed SE , the ICE ind. torque command uT_{ICE} and the EM Torque command uT_{EM} . The first is the system output variables and the second and third are the manipulated system input variables.
- the controller output is the rate of change of ICE torque command duT_{ICE} and EM torque command duT_{EM} .
- the time varying references are the speed reference \hat{SE} , the EM torque reference $u\hat{T}_{EM}$ and the command references. Beside the speed reference, all the others are zero, in order the EM torque to be zero in steady state condition, and penalize the frequent change of the manipulated variables.
- the cost function which has to be minimized for this problem is:

$$\begin{aligned} \min_{\substack{SE(0), \dots, SE(N) \\ uT_{EM}(0), \dots, uT_{EM}(N) \\ duT_{ICE}(0), \dots, duT_{ICE}(N-1) \\ duT_{EM}(0), \dots, duT_{EM}(N-1) \\ \varepsilon(0), \dots, \varepsilon(N-1)}} \sum_{k=0}^{N-1} \|h(SE, uT_{EM}(k), duT_{ICE}(k), duT_{EM}(k), \varepsilon(k)) - \hat{y}_k\|_{W_k}^2 \\ + \|h_N(SE(N)) - \hat{y}_N\|_{W_N}^2 \end{aligned}$$

- the main implemented constraints the problem is subjected to:
 - a. $950 \leq SE \leq 2100$ [rpm] (Hard Constraint)
 - b. $SE + \varepsilon \geq 1000$ [rpm] (Soft Constraint)
 - c. $SE - \varepsilon \leq 2050$ [rpm] (Soft Constraint)
 - d. $uT_{ICE,limit} - uT_{ICE} \geq 0$ [%]
 - e. $-90 \leq uT_{EM} \leq 90$ [%]
 - f. $-50 \leq duT_{EM} \leq 50$ [%/s]
 - g. $-20 \leq duT_{ICE} \leq 5$ [%/s]
 - h. $FR \leq FR_{Limit}$ [l/h]

From the above formulation, it is clear that the controller task is to track down a reference, (rotational speed), with respect to a number of constraints. Although the model is simple, the constraints especially those which depend on the operation point of plant, introduce a great complexity to the system. The simulation results are shown in Figures 4.7.

From the results, it is obvious that the NMPC achieves its control goal. During transient loads, unlike the previous scheme, the system does not have overshoot and the constraints are mostly satisfied, even the open loop constrain of Fuel Consumption Rate (e.g. the time periods of 1-20 s, 40-50 s and 130-140 s). When load is applied or the speed reference is changed, the controller immediately responds, and regulates the EM torque so as to track the predefined reference. Then the ICE torque is regulated with much lower rate than with the speed controller alone, so as its operation to be like the steady state. Moreover, the SE is regulated to its reference value in a satisfactory rate, with relatively lower overshoot (no more than the PID).

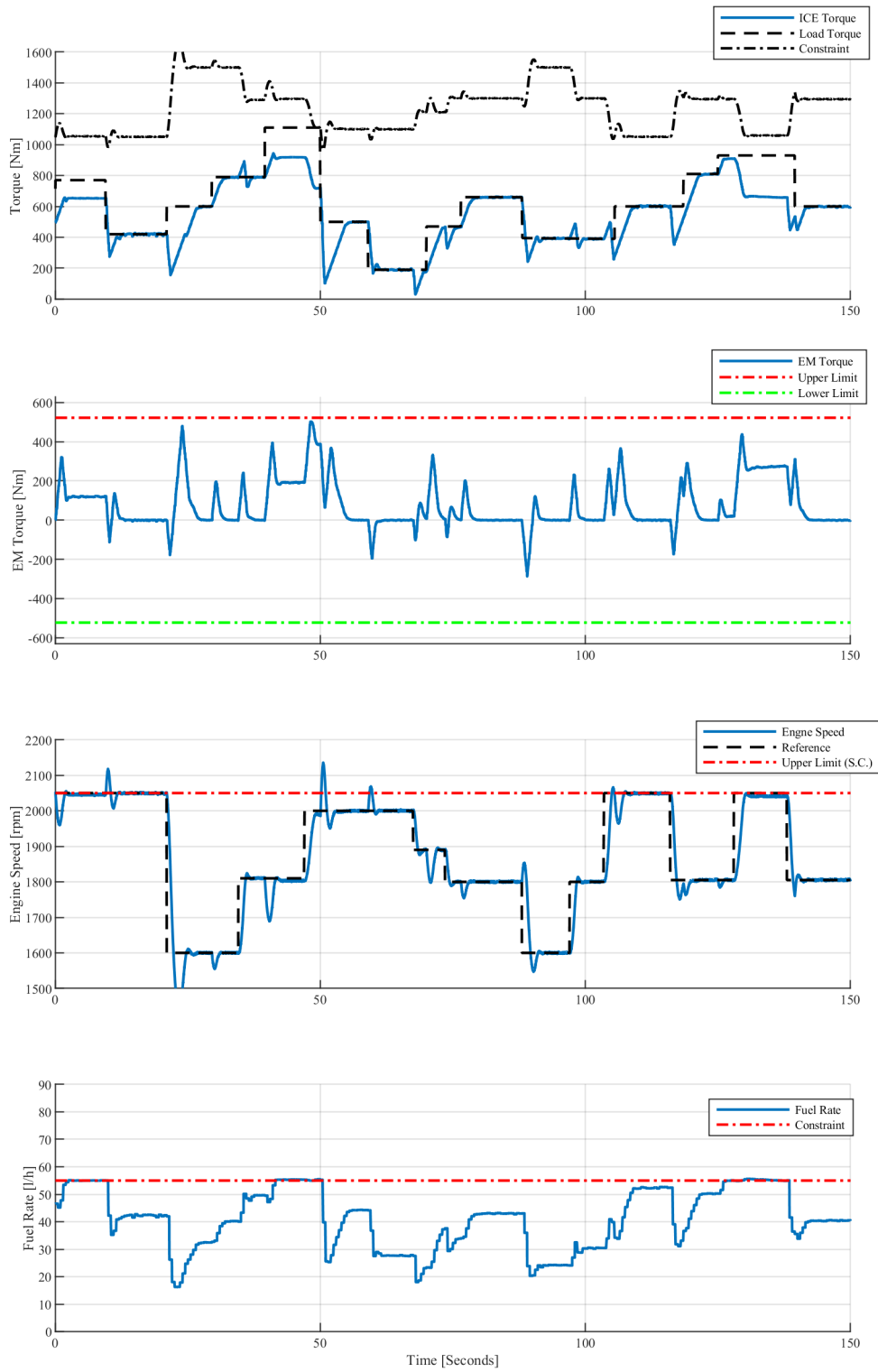


Figure 4.7: Simulation results engine control with Fuel Consumption Rate constraint

4.4.2 Engine Speed Reference Tracking with Battery Consideration

Previously, there were no considerations regarding the electric energy which the EM consumed, in order to produce the required torque. However, in real propulsion applications, the EMs are not connected to any electrical power grid which can provide "unlimited" power and the required energy for their operation is stored in special devices, e.g. batteries, super-capacitors etc. Thus, limitations regarding the use of EM usually applied. These limits have to do with the amount of stored energy, or the limits of the storing device itself. In this work, only batteries were considered as the energy storage devices. The block diagram of the control logic is illustrated at 4.8.

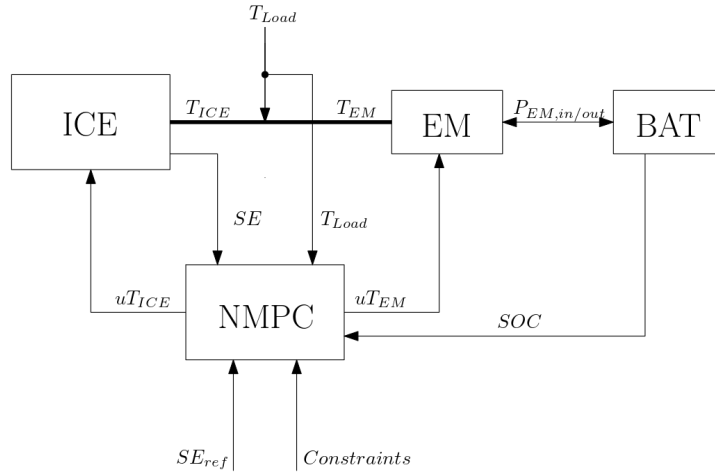


Figure 4.8: Block Diagram of direct SE control scheme with battery consideration

Battery modeling and limitations have been explained in Section 2.4.2. The purpose here was to develop a NMPC which would regulate the engine operation with smoother transients, as previously, and in addition, SOC reference and battery limitations would also be taken into account. The battery which was selected for simulations, was of small capacitance (2.5 Ah), and it is described by the quasi-static approach inside the NMPC, and by the dynamic PNGV model for the simulation model. The battery parameters for each model are shown in the Table 4.2.

The tuning of the controller was such that the primary object is to keep the speed reference, and the secondary when during steady state operation, the NMPC slightly increase the engine torque, in order to charge the battery. The scenario which was tested, resemble a diesel-electric generator on-board a ship. The loading of the plant is pulse loads, and the battery is of small capacitance which is used only to assist the hybrid plant during transient operations. The mathematical formulation of the problem resembles the previous, with two modifications. First, an additional term in cost function, is considered, the differential state of the battery State of Charge (SOC), and also additional constraints are applied regarding the battery operation, compared to the previous one. These are

- i. $15 \leq SOC \leq 85$ [%] (Hard Constraint)
- ii. $SOC + \varepsilon \geq 20$ [%] (Soft Constraint)
- iii. $SOC - \varepsilon \leq 80$ [%] (Soft Constraint)
- iv. $k_1^2 - 4R_i P_b \geq 10000$ [Volt²]

<i>Parameter</i>	<i>Value</i>	<i>Unit</i>
<i>PNGV Model</i>		
<i>OCV</i>	1400	Volts
<i>R_O</i>	0.9640	Ohms
<i>R_P</i>	1.0840	Ohms
<i>1/OCV'</i>	4400	Farads
<i>C</i>	240	Farads
<i>Quasi - Static Model</i>		
<i>k₁</i>	1400	Volts
<i>k₂</i>	40.9091	Volts/% SoC
<i>R_i</i>	2.0480	Ohms

Table 4.2: PNGV and quasi-static ECM parameters for simulation

where P_b is the required power from the EM. The first three constraints are referring to the operational limits of the battery. The last constraint defines the maximum power which the can feed the EM. This power is obtained via the Willan's model which was described in Section 2.3.2, and fitted to HIPPO 2 EM data. The controller was simulated in the same loading profile as before and the results are shown in Figure 4.9.

As it can be seen from the results in Fig. 4.9, the NMPC fulfills its objective, and conducts the power split with the same logic as in the previous case. However, the NMPC behavior here is slightly different. When load torque is applied the controller begin to regulate the output torque of ICE and EM as previously. Although, when the ICE torque equals the load, the NMPC increases the torque command even more, in order the EM to start generating power. This power charges the battery and compensates the energy which was previously consumed by the EM, during the transient loading. In that way the control scheme is repeated. As for the battery SOC, some remarks are useful to be noted here. At first, tracking SOC reference is not the primary objective of the NMPC, and therefore, the battery is regenerated only when the deviation from the reference is greater than 10% or there are no transient operations i.e. the SE reference is tracked down with nearly zero deviation. This behavior is a result of the NMPC tuning, which was conducted in this way on purpose. This operational manner of the controller, ensures the minimum transient loading of the engine, and simultaneously that the deviation of SOC from the reference is kept in acceptable levels, since after a point, intensive regeneration commence (e.g. time instant 50 s). This can be explained by the nature of the cost function. The cost for the NMPC is calculated through a quadratic equation which penalizes the deviation from reference. I.e. the cost is increasing accordingly with the square of the difference. Therefore, after a certain point (about 15%), the cost is high enough to force the NMPC to recharge the battery with an increased rate.

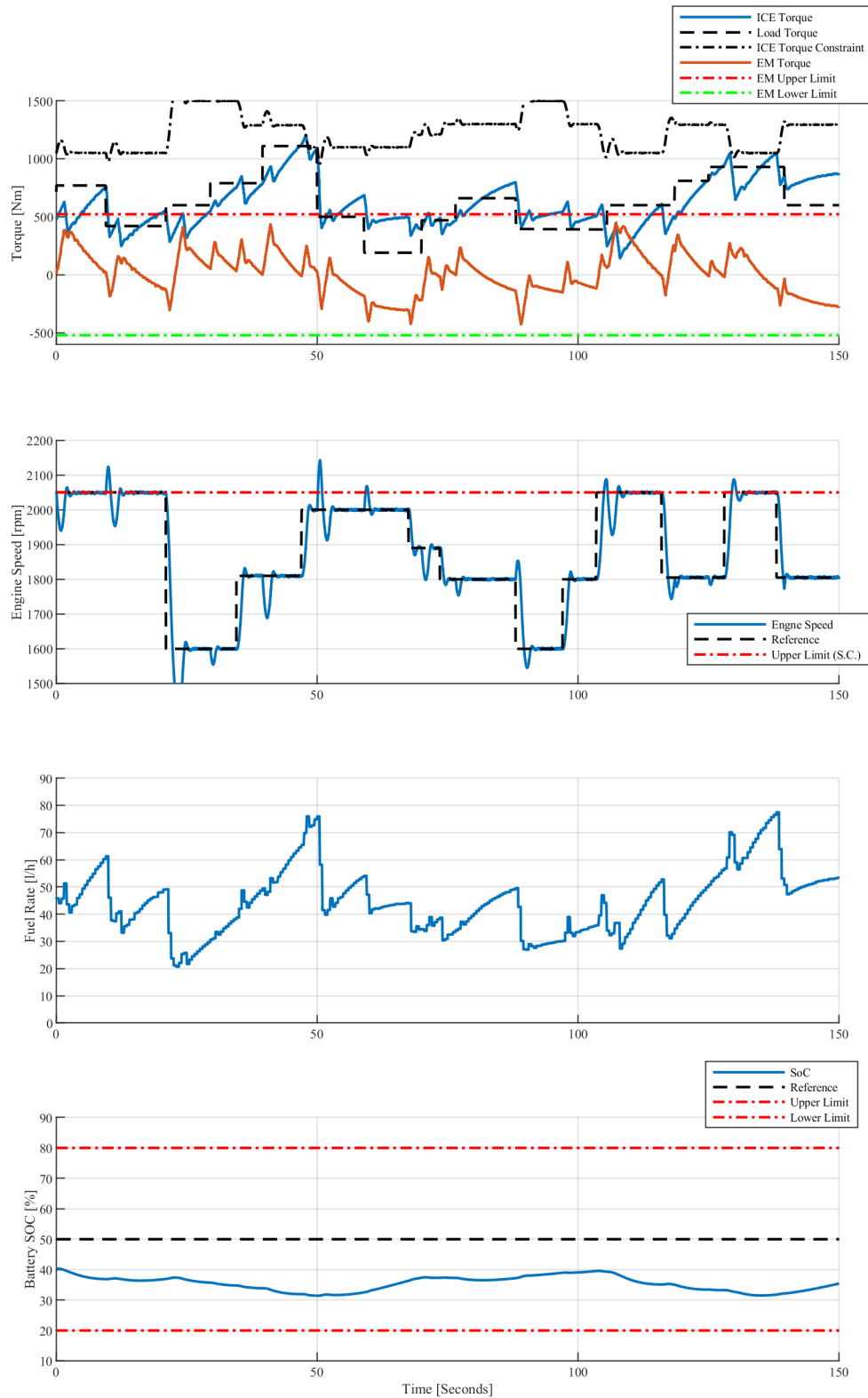


Figure 4.9: Simulation results of direct engine control with consideration of battery

4.5 Load Estimation - MHE

As it was previously mentioned, load torque was considered to be obtained by an estimator and fed to the NMPC, in order to calculate the optimal torque commands. An efficient estimator of plant load which can be used is a MHE scheme. The MHE has been explained and analyzed in Section 3.2.1, and as it is stated its problem formulation is similar to those of the NMPC. ACADO Toolkit's code generation tool, has also the option to generate MHE solvers, which operate similarly to NMPC. The problem formulation according to ACADO has the following form:

$$\min_{\substack{x_0, \dots, x_N \\ u_0, \dots, u_{N-1}}} \|x_0 - x_{AC}\|_{S_{AC}} + \sum_{k=0}^{N-1} \|h(x_k, u_k) - \hat{y}_k\|_{W_k}^2 + \|h(x_N) - \hat{y}_N\|_{W_N}^2 \quad (4.5.1)$$

$$s.t \quad x_{k+1} = F(x_k, u_k, z_k), \quad for \quad k = 0, \dots, N - 1 \quad (4.5.2)$$

$$x_k^{lo} \leq x_k \leq x_k^{up}, \quad for \quad k = 0, \dots, N \quad (4.5.3)$$

$$u_k^{lo} \leq u_k \leq u_k^{up}, \quad for \quad k = 0, \dots, N - 1 \quad (4.5.4)$$

$$r_k^{lo} \leq r_k(x_k, u_k) \leq r_k^{up}, \quad for \quad k = 0, \dots, N - 1 \quad (4.5.5)$$

$$r_N^{lo} \leq r_N(x_N) \leq r_N^{up} \quad (4.5.6)$$

The above symbols have the same meaning with the NMPC formulation which is presented in Section 4.1. The only difference here is that h , h_N denote measurement functions. Furthermore, the parameter x_{AC} denotes the apriori estimate of state vector, S_{AC} is the inverse of convolution matrix of the system. The first term denotes the total the arrival cost. The problem formulation of MHE in ACADO environment is regulated in the same way as the NMPC scheme.

An application of the above scheme is to estimate the external load of the hybrid propulsion plant. In most applications which involves hybrid plants, including marine propulsion plants, the exact load torque is unknown and it is difficult to be measured in real time. However, it was previously implicated that a good estimation of torque load is critical for the NMPC scheme. Therefore, the application of a reliable observer to estimate the system states is necessary. The MHE scheme can be efficiently applied in order to estimate the load. Moreover, the MHE algorithm can take into account the signal noise, and reject it, providing in this way, a better estimation for signals which are already measured, but tampered with noise and disturbances. In order to evaluate the above, a simulation was set up, using the previous NMPC scenario. The block diagram is shown at Figure 4.10.

Furthermore a second scheme was tested, in which apart from the torque load, the MHE feeds also the SE state estimation. As it was referred, the speed signal exhibits high frequency oscillations, which are affecting the behavior of the NMPC, in a low degree of course. The MHE rejects the oscillations as noise, and estimates a more smooth signal, which is fed to the NMPC. Consequently, the controller manipulates the control variables in a smoother way. The MHE problem set up is rather simple. The model which is fed to the MHE is consisting only by the second Newton's Law. As states, SE and Torque Load were considered, and as controls, the ICE and the EM output Torque. The measurements which were fed to MHE are the SE, with low measurement cost, due to the noise which tampers the signal, and the manipulated torque variables, with high measurement cost,

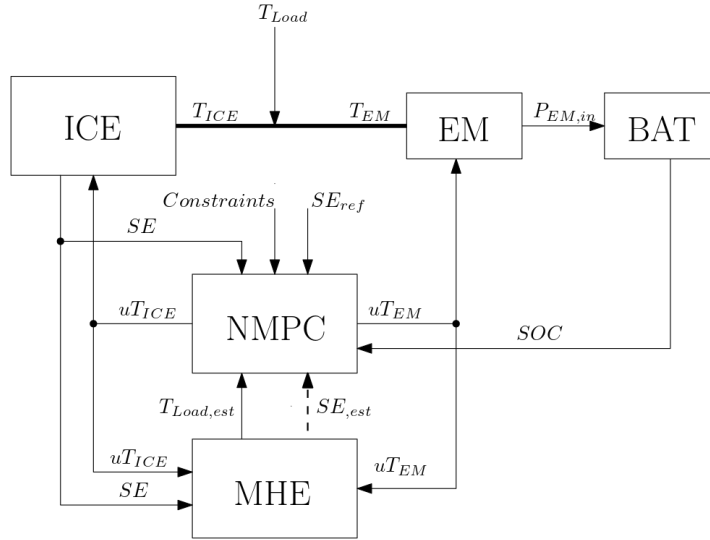


Figure 4.10: Block Diagram of direct SE control scheme with battery consideration and MHE estimator

since they are obtained directly by the controller. The constraints and the cost function which were applied are the following

Cost Function:

$$\begin{aligned} \min_{\substack{SE(0), \dots, SE(N) \\ uT_{ICE}(0), \dots, uT_{ICE}(N-1) \\ uT_{EM}(0), \dots, uT_{EM}(N-1)}}} & \|SE(0) - SE_{AC}, T_{load}(0) - T_{load,AC}\|_{S_{AC}} + \\ & \sum_{k=0}^{N-1} \|h(SE(k), uT_{ICE}(k), uT_{EM}(k)) - \hat{y}_k\|_{W_k}^2 + \|h(SE(N)) - \hat{y}_N\|_{W_N}^2 \end{aligned}$$

Constraints:

- i. $600 \leq SE \leq 2500$ [rpm]
- ii. $0 \leq uT_{ICE} \leq 90$ [%]
- iii. $-90 \leq uT_{EM} \leq 90$ [%]
- iv. $0 \leq T_{Load} \leq 2500$ [Nm]

The results of two applications (one with only load torque feedback and another with both SE and load torque) are presented in Figures 4.11. In both cases the MHE can satisfactory estimate the load torque and consequently the NMPC is efficiently regulates the hybrid plant operation. The SE signal is efficiently filtered by the MHE. In particular, in the second case which the SE feedback to the NMPC is obtained by the MHE, the efficiency of the control setup is increased. Since the system response is smoother, the control inputs of the system would also be gentle. This can be illustrated in specific time instances, when transient operations occurs. For instance, at time instance 50 s, the load torque is reduced and consequently at the same time the SE starts to increase. The actual signal of the SE is step, and in the first case which is fed to the controller, provokes an abrupt respond of the controller, and consequently the overshoot of the system is larger. At the same time instant, the SE signal of the MHE is filtered and thus the increase of the

speed is fed to the NMPC gradually, with a satisfactory rate. Therefore, the controller response is gentle leading to an overshoot, which is nearly half as the previous. The efficiency of the MHE scheme can be illustrated by the ISE criterion. For the scheme of the previous section, where the load torque is fed directly to the NMPC, the ISE is 542670, for the MHE scheme which only the load torque is fed is 1099200 and for the scheme which both the load torque and SE are fed is 795830.

Consequently, the MHE is an effective method to estimated unmeasured states, and reject the noise and disturbance from the measurements. Its efficiency is increased when both of these options are adopted, especially where one or more signals are tampered with noise.

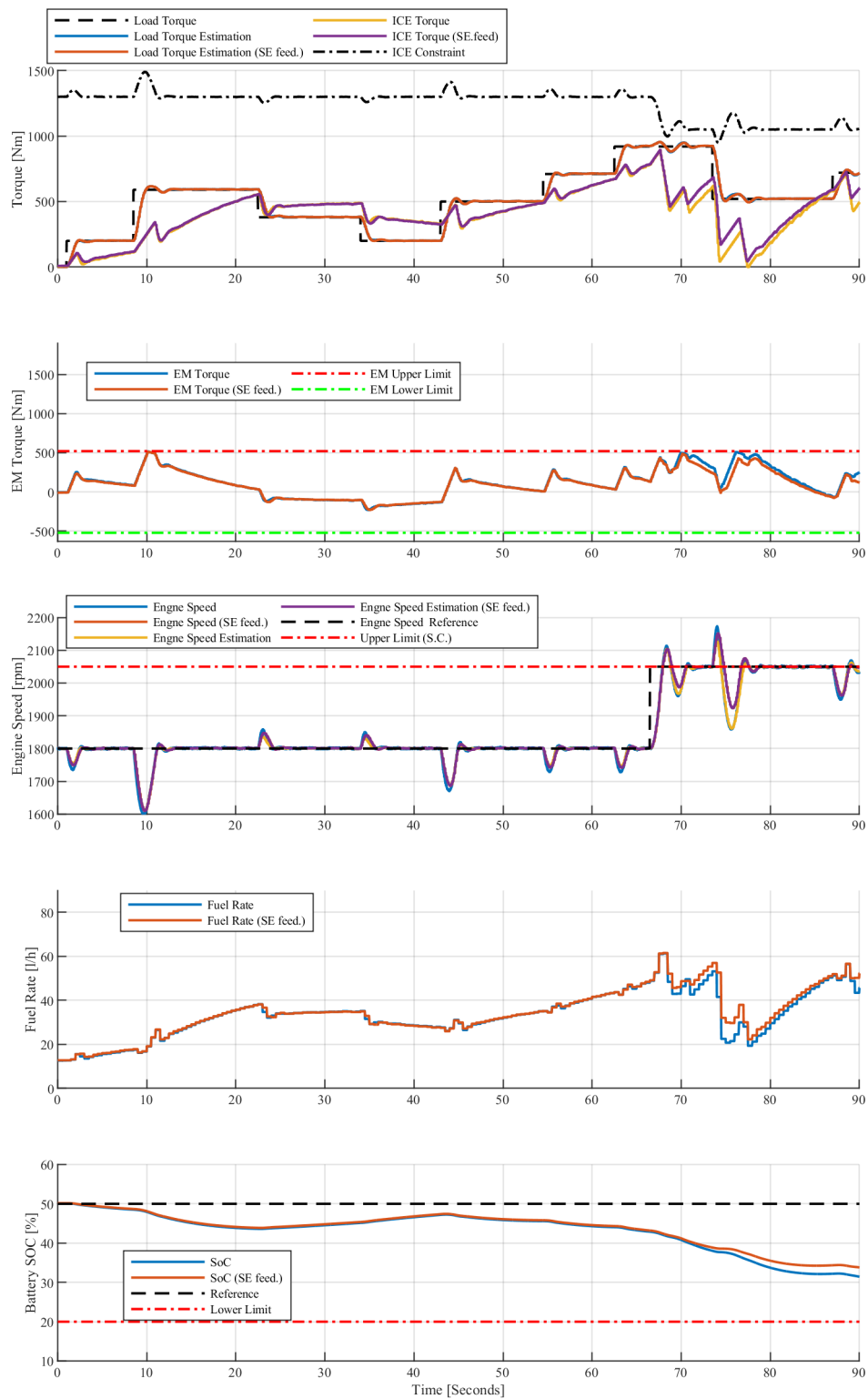


Figure 4.11: Simulation results and comparison of MHE-NMPC scheme with and without SE feedback from the MHE

4.6 Marine Application: Propeller Loading

In order to validate the above control scheme, a real marine application, was chosen to be simulated. The simulation was conducted by employing a propeller load simulator which can be found here [57]. The model refers to a controllable pitch propeller (CPP) load, which also accounts the environmental disturbances, along with the ship Resistance. The scenario was chosen to represent a fast acceleration of a tug boat, which employs a similar size engine. The control scheme which is implemented, is chosen to be the latest one, with battery consideration, and MHE scheme as load estimator. The purpose here is the EM to initially accelerate the ship, by compensating the required torque, and the engine to follow but with a lower rate of torque increase. When the requested speed is achieved, the EM would go to generating mode, in order to recharge the battery. The operating profile and the results are shown in Figs. 4.12 and 4.12 respectively.

From these results, it clear that the NMPC-MHE scheme can efficiently be implemented for vessel speed control, during transient operation. The control objective to track the speed reference while smoothing the engine operation is achieved. Also, the implemented constraints are satisfied. Battery *SoC* reference is also tracked, since after the transient operation the EM goes to generator mode in order to compensate the lost charge. The above scheme has a great impact in NOx reduction, while the fuel consumption penalty is nearly zero.

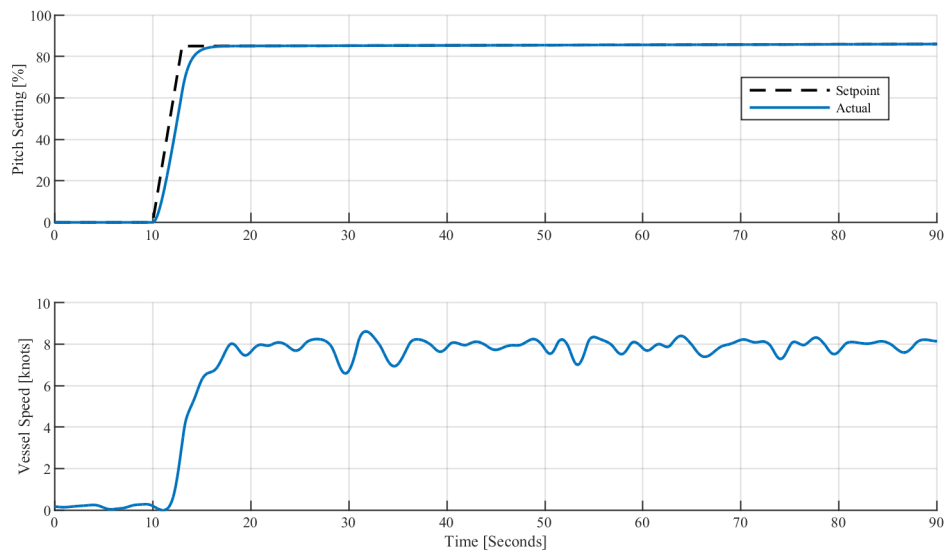


Figure 4.12: Vessel operation profile

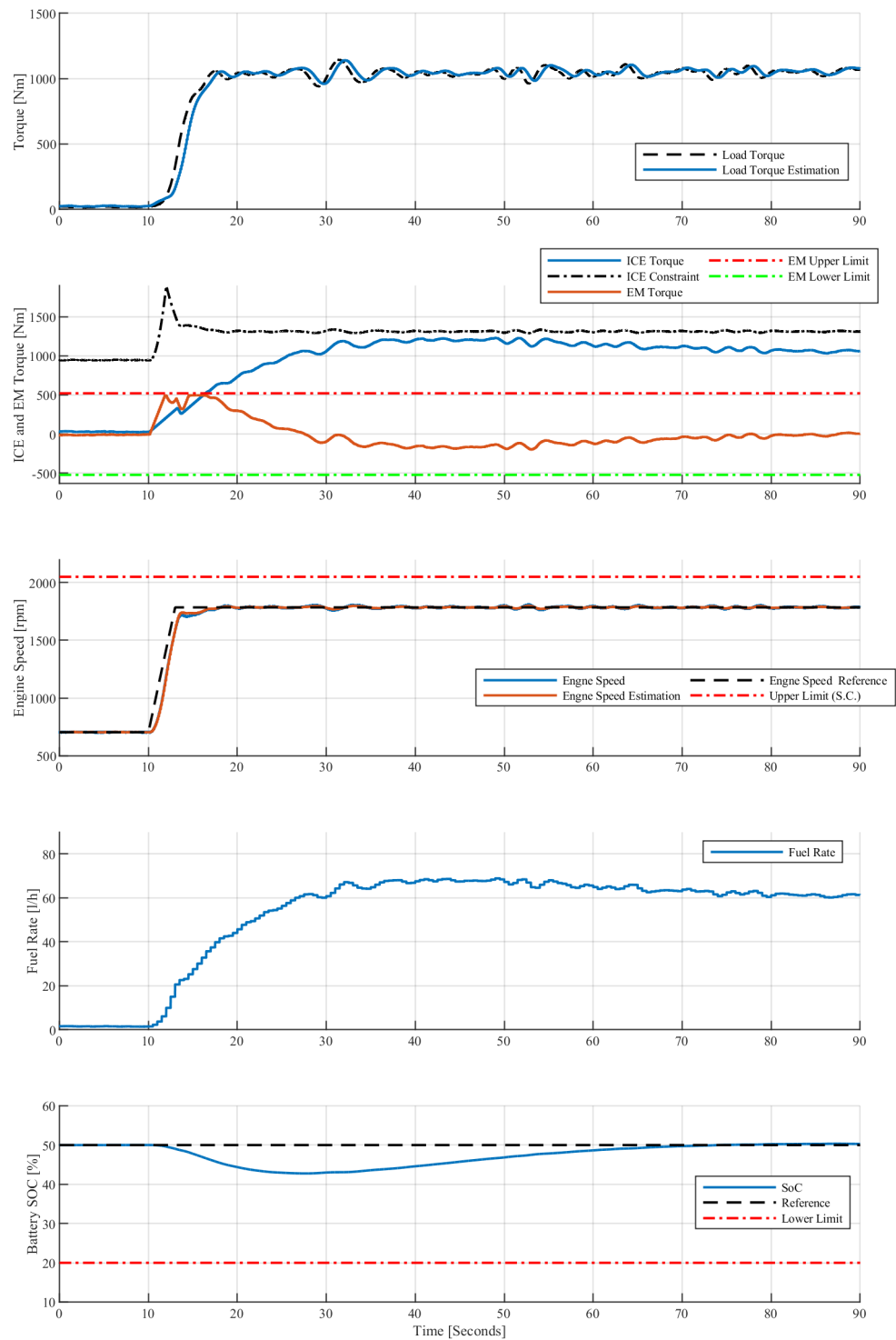


Figure 4.13: Simulation results of NMPC and MHE performance during transient propeller load

Chapter 5

Experimental Results

In order to validate the efficiency and the performance of the developed NMPC controllers, various experiments were conducted, using the experimental hybrid diesel-electric facility *HIPPO-2* at LME. The scenarios experiment, were in the operational area of 1700 to 2000 rpm and up to 800 Nm of Load Torque. The controller references were both static and dynamic. The characteristics of the presented experiments, are shown in Table 5.

<i>Exp. No</i>	<i>Purpose</i>	<i>Load [Nm]</i>	<i>Engine Speed [rpm]</i>	<i>Type of Reference</i>	<i>Duration [sec]</i>
1	Fuel Consumption Regulation	300-600	1800	FR Constant- Step changed	140
2a	Speed Control (Sole ICE - Hybrid Comparison)	300-700	1800	SE Constant	160
2b	Speed Control (Sole ICE - Hybrid Comparison)	400-600	1800-200	SE Step changed	140
3a	Speed Control with respect to Battery SoC	300-600	1800-1900	SE Constant- Step changed	160
3b	Speed Control with respect to Battery SoC (Sole ICE - Hybrid Comparison)	300-700	1800	SE Constant	160
3c	Speed Control with respect to B attery SoC (Sole ICE - Hybrid Comparison)	400-600	1800-200	SE Step changed	140

Table 5.1: Index of experiments which were conducted on HIPPO 2 test-bed

5.1 Experiment 1: Indirect Fuel Rate Control

In the first experiment, the indirect engine control scheme, which was presented in Section 4.3.1, is implemented on the hybrid experimental facility. The control purpose of the NMPC was to track a fuel consumption rate reference, in respect to a group of certain constraints, via the regulation of the EM torque. The reference was constant for large time periods with a few increasing and decreasing interval steps, while step loads of various amplitudes applied to the system from the electric brake. Engine speed was kept constant at 1800 rpm, via the engine speed controller. The implemented constraints were related to maximum fuel consumption rate, load distribution between the ICE and the EM and controller operational parameters such as the control horizon and kickback prevention constraint.

5.1.1 Controller Set Up

The NMPC which was implemented for this experiment, is the same which was presented in Section 4.3.1, with slight modifications due to the differences between the dynamic simulation model and the experimental engine. The NMPC's attributes and constraints are listed below:

- The controlled differential state is the Fuel Consumption Rate FR .
- The manipulated differential state is the EM Torque Command uT_{EM} .
- The *NMPC* $1i$ input of the controller is the rate of change of manipulated variable duT_{EM} .
- Slack Variable ε is implement for soft constraints.
- Fuel oil consumption rate was modeled via a 2nd degree MISO differential polynomial model with inputs the speed SE and the dynamic load which the engine has to compensate $T_{Load,ice}$.
- The control constraints were:
 - i $0 \leq FR \leq 50$ [l/h] (Hard Constraint)
 - ii $FR - \varepsilon \leq 30$ [l/h] (Soft Constraint)
 - iii $0 \leq T_{ICE} = T_{load} - T_{EM} \leq 1200$ [Nm]
 - iv $-90 \leq uT_{EM} \leq 90$ [%]
 - v $-70 \leq duT_{EM} - k_c$ [%/s]
 - vi $70 \leq duT_{EM} + k_c$ [%/s]
 - vii $\varepsilon \geq 0$ (Slack Variable)
 - viii $duT_{EM}(k) = 0$ for $k \in H_c + 1, \dots, H_k$
- The cost function of the NMPC, was formulated as in Section 4.3.1 in the quadratic predefined form of the solver, and the weight tuning was kept the same as the simulation.

The sample time of the controller was set up to 0.1 s. The prediction horizon length was chosen to be 10 time instances, i.e. 1.0 s. The control horizon was regulated to be 3 time instances. In the next section, results from the experiment are presented.

5.1.2 Experimental Results

Figures 5.1, 5.2 and 5.3 are corresponding to experiment 1 results. The measurements are referring to output torques of the ICE, the EM and the electric brake (load), the engine speed, the FR, the λ value and the emission related measurements NO_x (ppm), EGR valve cmd (%) and exhaust gas flow.

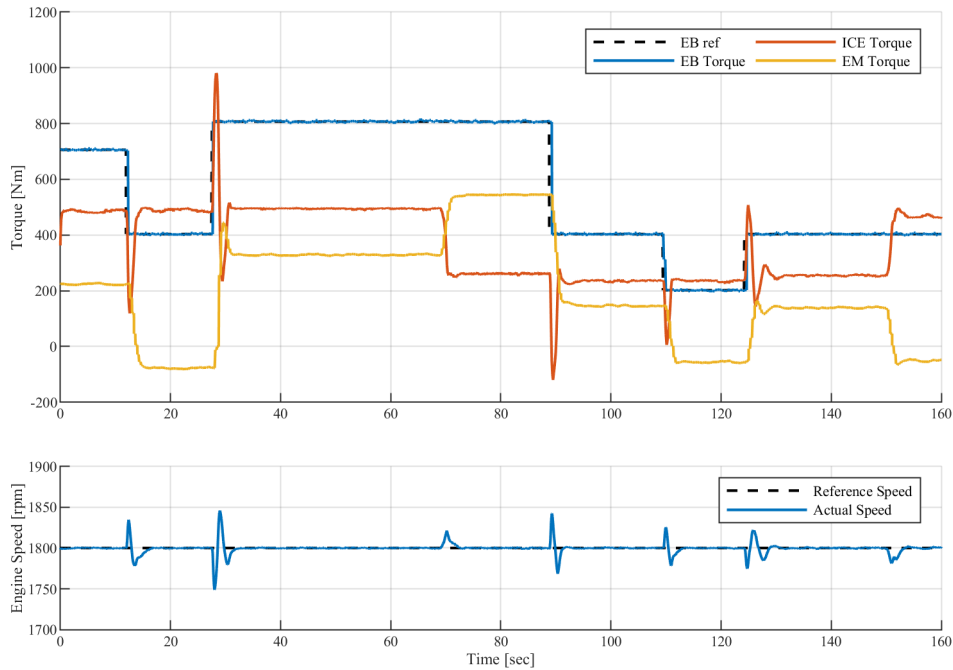


Figure 5.1: Exp 1: Applied EB torque, EM torque and ICE torque.

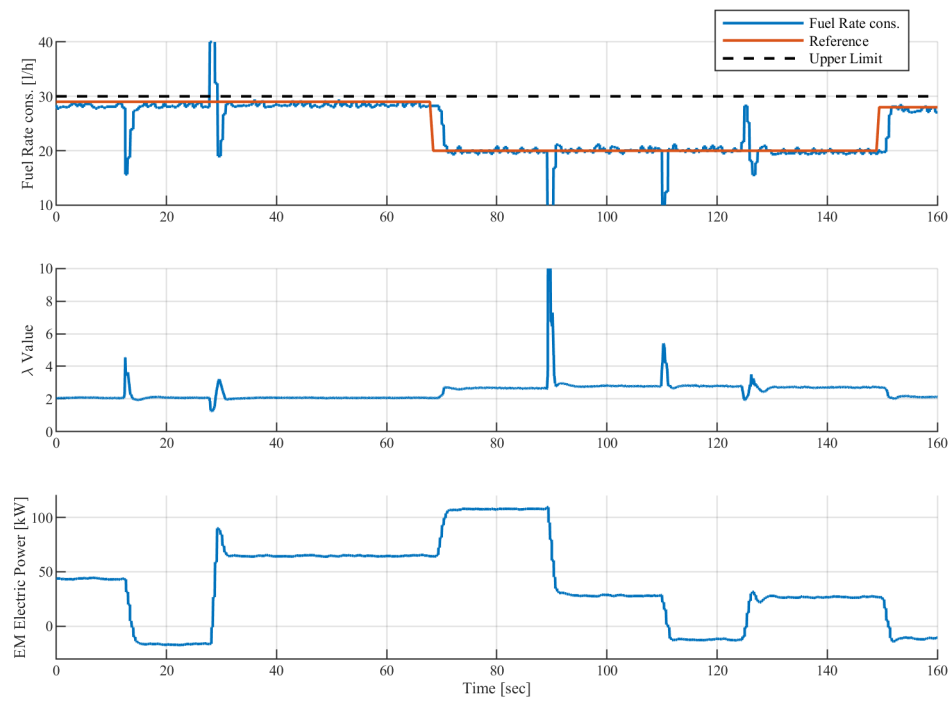


Figure 5.2: Exp 1: Measured fuel rate consumption and reference, λ value and EM requested power.

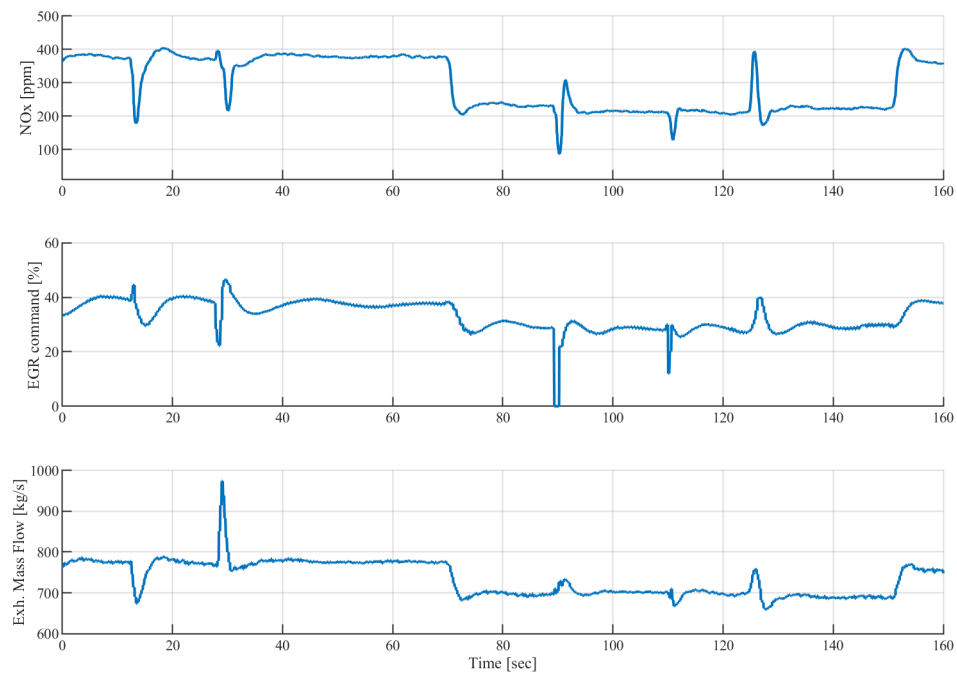


Figure 5.3: Exp 1: NO_x concentration, EGR valve command and Exhaust Gas Mass Flow.

5.1.3 Results Analysis

From the previous results, it is obvious that the NMPC achieved its control objective. In all cases, the fuel consumption rate trajectory was successfully tracked down, while the constraints were satisfied, leading to a steady state behavior for the engine regardless the load variances. From figures 5.2 and 5.3, it can be seen that engine operation is relatively steady, since all operational parameters are converging to a single value. For instance, NOx concentration converges to 200 ppm for FR 20 l/h, to 300 ppm for FR 25 l/h and to 400 ppm for FR 29 l/h, at 1800 rpm. The same also applies for other engine parameters such as λ , and the exhaust mass flow.

However, the behavior of the system during transient conditions is different. In cases, in which step load is applied to the system or fuel oil consumption reference is altered, engine speed controller instantly increases/decrease the fuel flow in order to track the speed reference, as expected. As the engine speed controller dynamics are way faster than those of the NMPC, this results that the engine accelerates/decelerates faster than the NMPC is able to respond, and spontaneously the FR is heavily diverges from the defined reference and the constraints are violated (e.g. Fig 5.2 time instant 32 s). That leads to instant changes for other parameters too. For example, at Fig. 5.2 at time instant 90 s, the load torque decreased by 300 Nm, leading to an over-speed. Instantly the engine torque decreases, and NMPC also does the same. Consequently, when the speed decreases more than the reference, the speed controller responds by increasing the injected fuel, and the ECU closes the EGR valve in order to boost the engine performance. Therefore NOx concentration is instantly increased. During these violations, the NMPC responds by manipulating the EM torque, and regulates again the FR according to the reference, in relatively small time period (1 to 3 s).

All in all, from the previous results, the NMPC prove to handle non-linear problems, with ease in real time applications with the indirect engine control scheme all the control objectives were satisfied. However, in transient operations due to the faster engine speed controller, instant reference diversions and constraint violations occur. This problem is efficiently being addressed in the next type of experiments.

5.2 Experiments 2a and 2b: Direct Engine Speed Control

In these experiments, the NMPC controls both the of the power sources of the hybrid plant. The controller development and attributes are explained in Section 4.4. Here the control objective is to follow a specific speed reference, regardless the torque load, satisfying nonlinear constraints and minimizing the transient engine behavior. The experiments included transient loading with step loads at constant speed and speed steps at constant torque. The applied torque load were pulses of variant amplitudes. The main purpose of these experiments was to evaluate the benefits of the engine operation in a nearly steady state condition, during the transient loading conditions for the system. As explained in Section 4.4, this can be achieved by enforcing constraints regarding the rate of change of ICE command input (i.e. fuel regulator) and the extra torque required to achieve the rapid transient operation is provided by the EM motor (*"Phlegmatisation"*). Moreover, the results are additionally compered with those which are obtained from similar loading profile with the use of the ICE only controlled by its speed controller.

5.2.1 Controller Set Up

The development of the NMPC which employed for this experiment, is presented at Section 4.4.1. Here, the control objective is to regulate both the ICE and EM command, in order to track the speed reference, under certain constraints. The attributes of the NMPC are the following:

- The controlled differential state is the Engine Speed SE .
- The manipulated differential states are the ICE Torque Command uT_{ICE} and the EM Torque Command uT_{EM} .
- The NMPC inputs of the controller is the rate of change of manipulated variables duT_{ICE} and duT_{EM} .
- Slack Variable ε is implement for soft constraints.
- The engine output torque was modeled as the difference between the net torque and the engine losses.
- A dynamic torque constraint, regarding the output engine torque was also implemented. The limit was modeled as a linear function of SE . However, by introducing the relation between the command and the output torque, the constraint is in fact non-linear, considering the NMPC command.
- The other control constraints were:
 - i. $1600 \leq SE \leq 2100$ [rpm] (Hard Constraint)
 - ii. $SE - \varepsilon \leq 2000$ [rpm] (Soft Constraint)
 - iii. $SE + \varepsilon \geq 1700$ [rpm] (Soft Constraint)
 - iv. $0 \leq T_{ICE} \leq T_{limit}(SE)$ [Nm]
 - v. $0 \leq uT_{ICE} \leq 80$ [%]
 - vi. $-20 \leq duT_{ICE} \leq 3$ [%/s]
 - vii. $-50 \leq duT_{EM} - k_c$ [%/s]
 - viii. $50 \leq duT_{EM} + k_c$ [%/s]
 - ix. $\varepsilon \geq 0$ (Slack Variable)

- The cost function of the OCP problem, is formulated in the standard quadratic form and employs the rotational speed SE , the electric torque command uT_{EM} , the rates of the output commands and the slack variable. ICE torque could also be employed in order to optimize the relation between the electric torque, however it was chosen its weight to be zero since no criterion for optimum power split for electric and diesel component was considered. (e.g. cost for diesel fuel and kWe).

The sample time of the controller was set up to 0.1 s. The prediction horizon length was chosen to be 10 time steps, i.e. 1.0 sec. The control horizon was regulated to be the same as the prediction horizon.

Furthermore, FR and λ constraints could also have been applied, using the constant models which were presented in Chapter 2 and validated here. The form of the models are 3rd degree polynomial relations, which depends on uT_{ICE} and SE . However the results would be the same as the dynamic torque constraint implemented here, and is shown in the Fig. 5.10. This can be explained from the fact that these quantities are expressed as algebraic functions uT_{ICE} and SE . In fact, it should be noted that fuel injection is regulated by ECU directly by a same-logic map with (main) inputs the above, in order to achieve the requested torque. Consequently, by regulating uT_{ICE} , the NMPC actually regulates the fuel injection. The quantities which depend on the dynamic states of the engine, in steady and quasi-static state, can be also described as functions uT_{ICE} and SE . Here the engine dynamics are reduced to a point in which ICE can be considered as a quasi-static system. Therefore, FR and λ constraints, are actually a constraint for uT_{ICE} , just as the torque constraint which is implemented here, since SE is a control state which have to track a reference, or else it is penalized inside the cost function. As a result, the behavior of the system when it operates near constraints as those which described above, would be the same as shown in Fig. 5.10. Moreover, a simulation of the above scheme is presented in Section 4.4.1.

5.2.2 Experimental Results

In the following figures the experimental results are shown. Fig. 5.4, 5.5 and 5.6 are corresponding to experiment 2a, in which the speed reference is constant and equals 1800 rpm, and Fig. 5.7, 5.8 and 5.9 to experiment 2b which the reference is step changed. The presented measurements are referring to the output torques of the ICE, the EM and the electric brake (load), the engine speed, the FR, the λ value and the emission related measurements NOx (ppm), the EGR valve cmd (%) and the exhaust gas flow. Moreover, the results of hybrid operation are compared to those which were obtained from operation of ICE only, with similar loads. Also two steady state maps for Fuel Consumption Rate and λ Value were validated. Finally, a near constraint operation is presented.

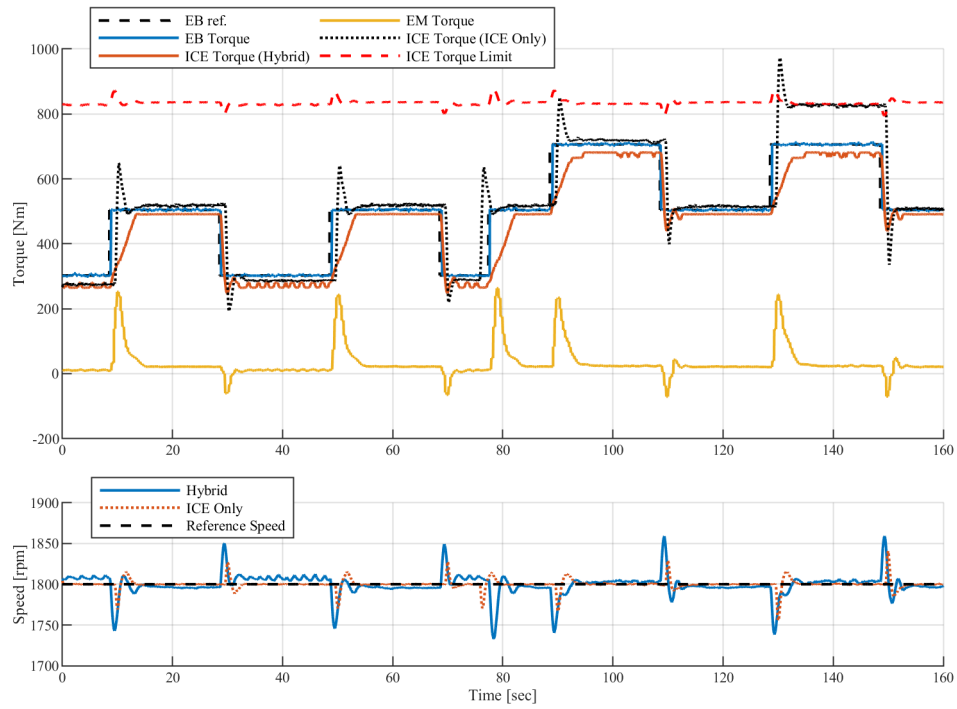


Figure 5.4: Exp 2a: Applied EB torque, EM torque and ICE torque.

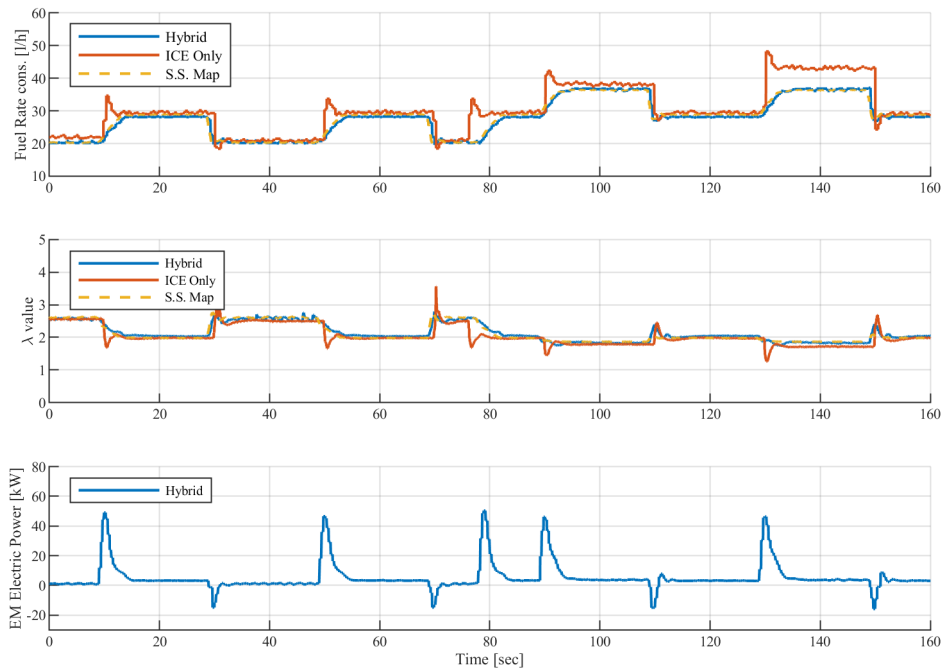


Figure 5.5: Exp 2a: Measured fuel rate consumption and reference, λ value and EM requested power.

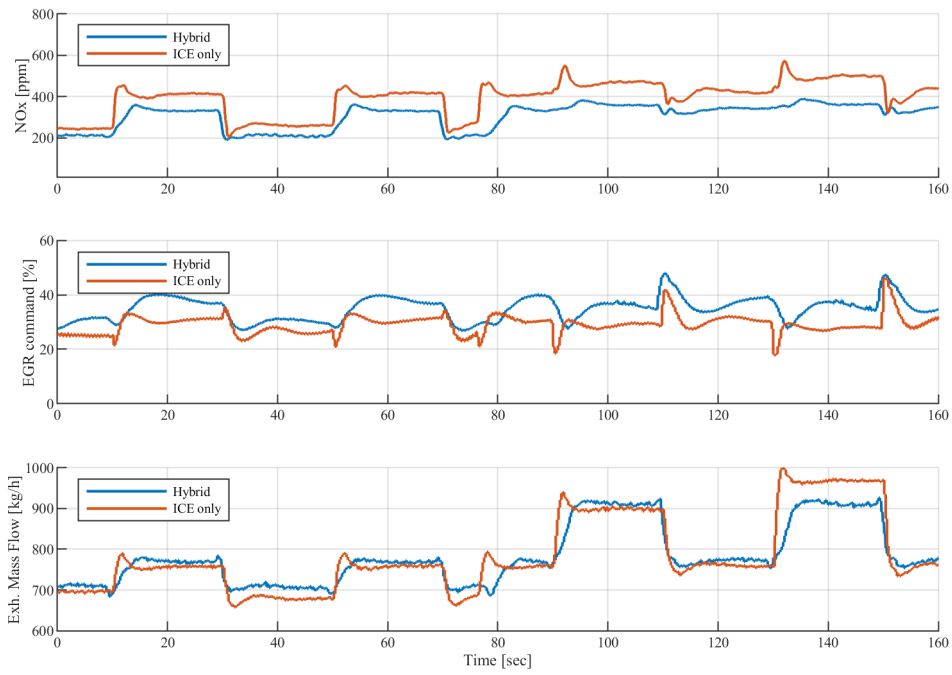


Figure 5.6: Exp 2a: NOx concentration, EGR valve command and Exhaust Gas Mass Flow.

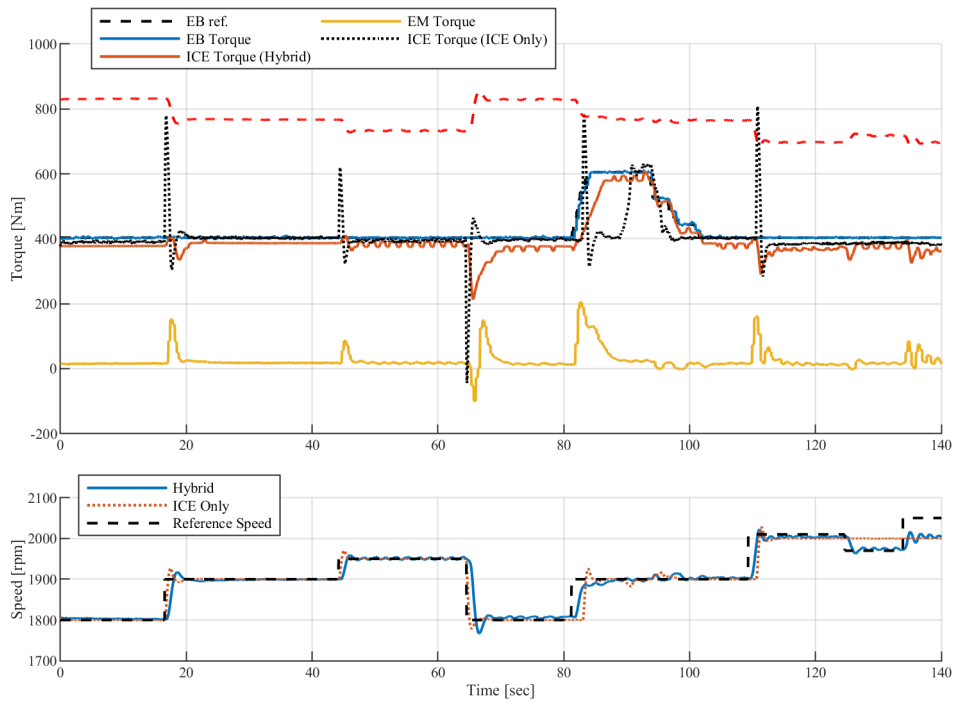


Figure 5.7: Exp 2b: Applied EB torque, EM torque and ICE torque.

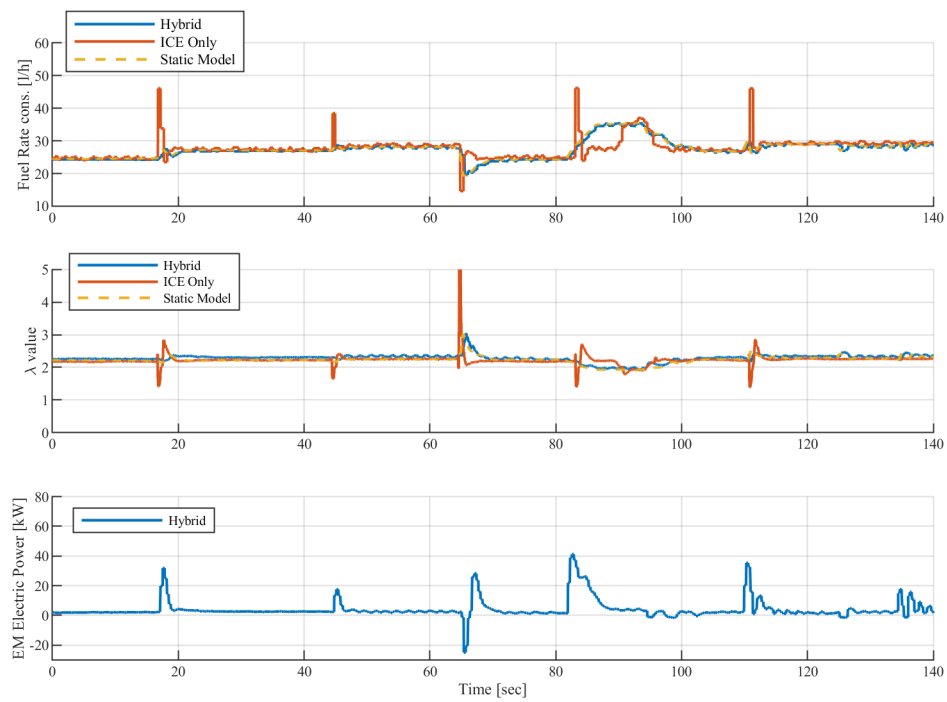


Figure 5.8: Exp 2b: Measured fuel rate consumption and reference, λ value and EM requested power.

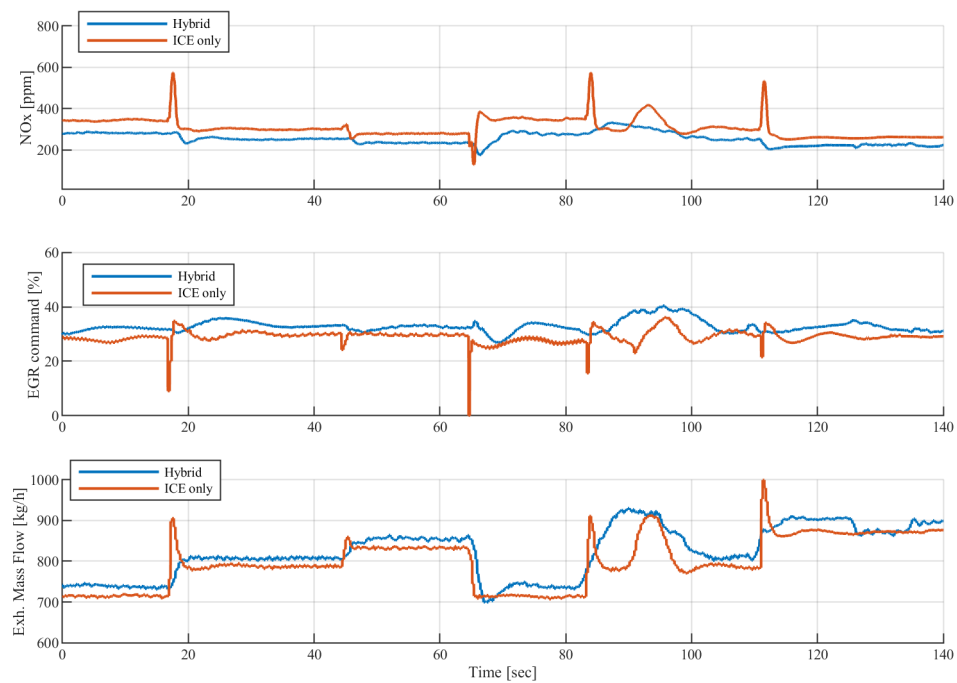


Figure 5.9: Exp 2b: NOx concentration, EGR valve command and Exhaust Gas Mass Flow.

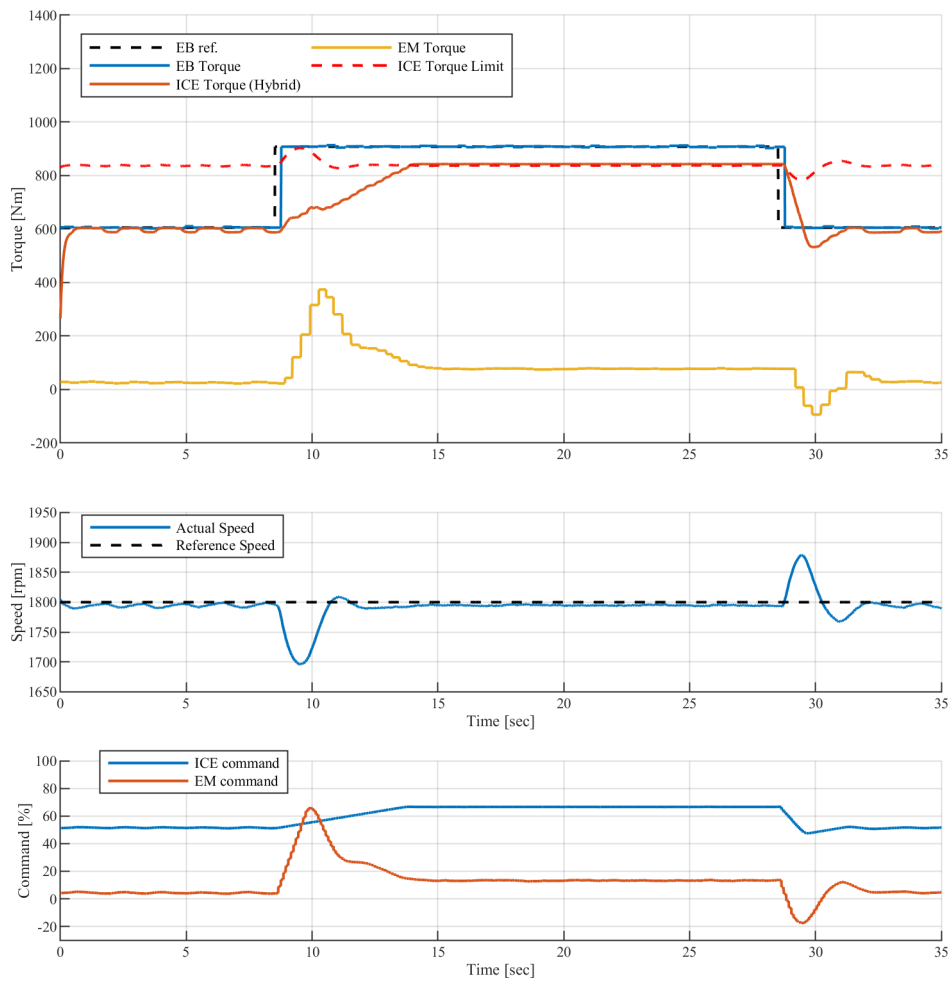


Figure 5.10: Exp 2b: Near constraint (ICE torque) operation.

5.2.3 Result Analysis

The purpose of the experiments presented in this section, was to evaluate the performance of the NMPC which controls directly both the components of the propulsion plant. Moreover, special constraints are implemented regarding the ICE operation, in order to force its behavior to resemble to a nearly steady state condition. In steady state, the efficiency of the ICE is increased and its emissions are mostly regulated by the engine internal and after-treatment systems (EGR, SCR) [59], as previously explained. In transient loads, these systems usually have lower efficiency. The performance of the hybrid plant is also compared to those of the engine if it was operating alone, with a similar loading profile.

From the results, it is obvious that NMPC, given the previous specifications, is able to conduct the power split successfully. In all cases, the controller was able to give the appropriate inputs to the system in order to track down the given speed reference. The constraints were, successfully, kept by the NMPC, for both control inputs and states. Furthermore, the other main objective of this scheme which was to reduce the transient operation of the ICE by implementing constraints regarding the rate of change the engine torque, was effectively achieved. For instance, in experiment 2a, at time instant 7 s, a pulse load with magnitude of 200 Nm, is applied to the hybrid system. Instantly, the NMPC highly increases the EM torque in order to compensate the drop of the engine speed. Simultaneously, the ICE torque command also increases, but with a much slower rate. In that way, engine operation is relatively stable. This can be shown from Fig. 5.8 and 5.3, in which the engine performance is plotted. At the same time instant, Fuel Consumption, which was steady, increases with a relative slow rate in accordance with the engine torque, while λ value decreases with the same rate. The EGR valve, although it briefly closes for a little during the begging of the torque command increase, in the next period the higher EGR command is than it would be if the engine was operating alone, leading to much lower NOx concentrations. When the speed reference is tracked, the EM torque starts to decrease at the same rate as the ICE toque increases. At time instant 14 s, the engine torque completely compensates the load, while the EM torque converges to zero. The above procedure is mostly the same for speed reference increasing, however the transient phenomena are much more aggressive and brief for the sole ICE operation. This is explained from the fact that the engine is controlled by a PID speed controller. Therefore speed reference alteration, means an abrupt error and consequently a large controller response. This leads instantly to a heavy increase of the injected fuel amount. Moreover, the engine ECU recognizes the intense power demand and fuel injection is increased, and instantly decreases the EGR command, in order to reduce the resulted soot and boost the engine. E.g. at experiment 2b, at time instant 17 s, a reference alteration occurs. Considering the engine sole operation, the EGR valve closes, and the NOx concentration is heavily increased, along with fuel consumption and exhaust mass flow. The above are completely eliminated by the engine steady state operation, which the NMPC applies. The values of the above are changing as the rate of the engine torque does and no "spikes" at any value appears.

A quantification of the above can be conducted by comparing the total amount of NOx, the Fuel Oil and the Electric Power, which were emitted or consumed, for both ICE sole and Hybrid operation. The time windows which were examined are from 0 to 120 s and from 0 s to 80 s for the first and the second experiment, respectively. The NOx production in $[g/kWh]$, for both cases is shown in the Fig. 5.11 and 5.12. Also the total NOx production and the total fuel consumption is shown in Table 5.2. The conversion from ppm (volume) to g and g/s and g/kWh respectively is conducted by using the following

formulas [60]. Here, it should be noted that the molar mass of exhaust gas was considered steady and equal to those of air, since its substance is nearly the same, in accordance with [61].

$$\dot{m}_{NO_x} = \frac{ppm_{NO_x}}{10^6} \cdot \frac{MW_{NO_x}}{MW_{exhaust}} \cdot \dot{m}_{exhaust} \quad [g/s] \quad (5.2.1)$$

$$NO_{x,g/kWh} = \frac{\dot{m}_{NO_x} \cdot 3600}{P_{eng,out}} \quad [g/kWh] \quad (5.2.2)$$

where \dot{m}_{NO_x} , $\dot{m}_{exhaust}$, the NO_x and the exhaust mass flow respectively in [g/s] and $NO_{x,g/kWh}$ the specific emissions at g/kWh.

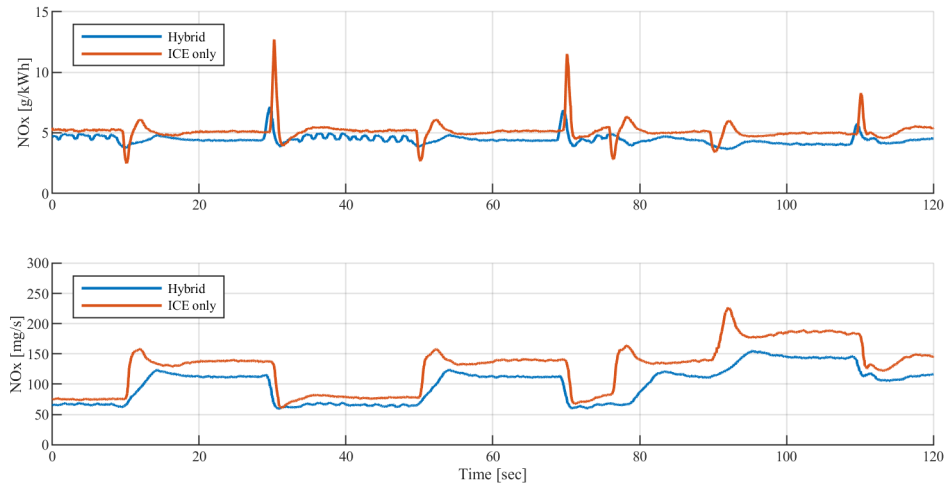


Figure 5.11: NO_x production for static reference in g/kWh (Exp 2a)

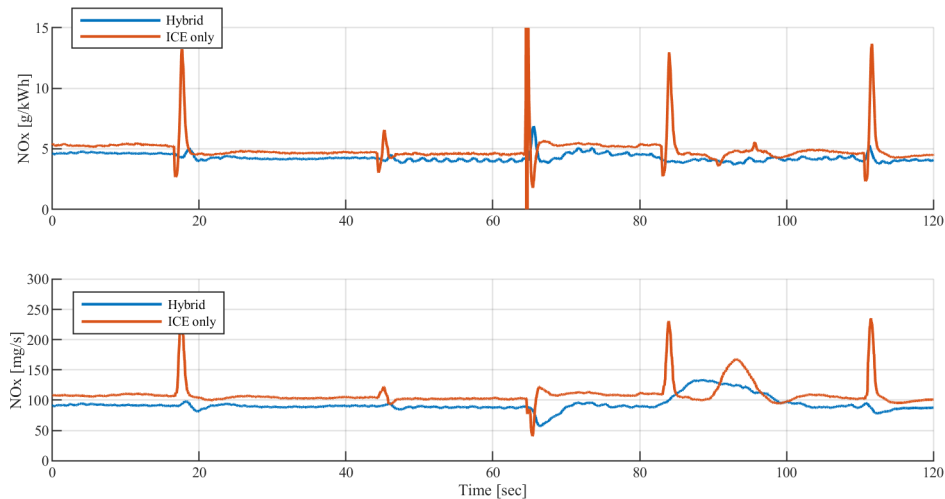


Figure 5.12: NO_x production for dynamic reference in g/kWh (Exp 2a)

As it can be shown, during hybrid operation the NO_x production is noticeably lower by 21.17 % in the first case, and by 16.36% compared to the conditional setup. If NO_x emissions are expressed in g/kWh¹, then the reduction 13.56% and 8.25 %, for constant

¹g/kWh are the units in which the NO_x limits are expressed by the regulations of IMO for marine applications

<i>Case</i>	<i>Constant SE Reference</i>			<i>Step Change SE Reference</i>		
	ICE only	Hybrid	Difference [%]	ICE only	Hybrid	Difference [%]
<i>Quantities</i>						
<i>Mean Emissions NO_X [mg/s]</i>	127.69	100.69	21.14	106.47	89.039	16.34
<i>Total Emissions NO_X [g]</i>	15.32	12.08	21.14	8.52	7.12	16.36
<i>Mean Emissions NO_X [g/kWh]</i>	5.12	4.43	13.47	4.73	4.34	8.25
<i>Fuel Consumption [l]</i>	0.9488	0.8859	6.62	0.5941	0.5767	2.93
<i>Electric Power Consumption [kJ]</i>	-	621	-	-	252	-

Table 5.2: Comparison Hybrid vs ICE sole operation for the same load cycle

and step changed references respectively. Also a lower decrease can be observed for the fuel consumption. In order for the above to be achieved the hybrid plant consumes 621 and 252 kJ of electric energy, respectively. Of course the significance of these reductions, depends on the manner of the consumed electric energy it is acquired. Moreover, an another factor which contributes for the above, is the lack of ICE transient operations in the Hybrid scheme. A part of NO_x emissions, mainly, and fuel consumption, secondly, is produced during acceleration of the engine (i.e. the "spikes" on the diagrams). Considering a case where, the electric power which is consumed from the EM, is replenished from the engine and stored to battery, in a time instant which the engine efficiency is high enough (around 40%) and considering an efficiency of 90% for the EM, and 85% for the battery, it would required 0.0563 L for the first case and 0.0229 L in the second case to restore a battery's charge. In essence, the actual fuel consumption would be 0.9422 and 0.5996 respectively. In essence, the fuel consumption would be the same. This particular case was considered in the experiments which are presented in the next section. However, the NO_x emissions would not increase that much. In fact it is observed, that in heavy duty loading, i.e. in regions where the efficiency is high and can reach 40%, minor output torque increases such as 100 Nm, does not affected the resulted NO_x emissions at all, since the EGR system can completely neutralize them. Therefore, the above NO_x emissions reductions can be occur unchanged, and consequently the NO_x emissions are reduced without any fuel consumption increase. According to [62], the NO_x emission reduction can reach 21 % without influencing fuel consumption.

An another point worth to be mentioned, is that the static models of fuel consumption rate and λ are efficiently describing the above engine operation, even in transient conditions. Even λ value which depends on the air mass flow after the compressor, which is a function of SE and intake manifold pressure, both of which are dynamic states of the engine, can be efficiently described by the static model. As mentioned these models, are function of the two engine inputs, uT_{ICE} and SE , the first of which is manipulated by the NMPC directly and the second is controlled indirectly. The use of the these models have certain advantages. Firstly, they are of a low computational burden for the NMPC, since no integration is required, (they are characterized as algebraic states). Secondly, keeping a constraint or following reference which is related to quantities they describe is much more easier. Since, the NMPC here tracks a speed reference, diverges from this reference would mean an increase of cost function. Therefore in order to follow a reference

or keep a constraint for the above algebraic states, the NMPC would firstly, regulate the uT_{ICE} command, which is rather easy since this is been done directly, i.e. constraints and references regarding the engine quantities are considered by the NMPC as manipulated variable constraints of uT_{ICE} . This kind of constraints is much more easier to be handled, as it was previously illustrated, and effects such as kickback would not occur as occurs with state constraint. In Fig.5.10, the hybrid plant operates in respect to a torque constraint. At time instant 27s step load of 250 Nm occurs, and the total torque load rises to 850 Nm. However, this load is above the constraint which is been set. Consequently, the NMPC regulates the command of the engine in order to achieve the maximum allowed torque production. Then EM torque is manipulated in order to produce the rest of the required torque. During this time period, the engine operation is stable, the constraints are kept and no kickback is observed. The only limitations of the above models are, obviously the engine should work in a nearly steady state operation, and also the validity of these models is satisfying since no feedback is provided to the controller for algebraic states.

5.3 Experiments 3a, 3b and 3c: Direct Engine Speed Control with Battery Consideration

The experiments which are presented here, are based on the previous control scheme, with the addition of a Battery in the system. The control objective of this scheme was, also, to follow a speed reference with reduced ICE dynamics, respect the previous constraints and, simultaneously, to keep the State of Charge of the battery around a desired level. Also, the efficiency of *phlegmatisation*, considering the NOx emissions is examined, regarding the extra power the ICE have to produce in order to replenish the battery charge, which was consumed during transients operations.

5.3.1 Controller Set Up

The structure of the controller is based on the previous one, with additional modifications for battery consideration. This was conducted by integrating additional models and constraints for the battery and the EM into the NMPC. The manipulated variables were also the ICE and EM torque command. The control purpose here, besides following a specific *SE* reference, is also to follow a reference for battery *SoC* too. Considering the attributes and constraints of the previous scheme, the extra characteristics are:

- State of Charge *SoC* is also a controlled differential state.
- The required power of the electric motor is model via Willan's Model. However, this model is consisted of a two branch function of T_{EM} and ω . The first branch refers to motoring and the second to generating mode. However, this form is not acceptable by the solver since it is required all the relations to be continuous functions of differential states and controls. Thus, the approximation via the sigmoid function, is employed.
- Battery is modeled via the quasi-static approach, expressed as the derivative of state of charge. Also, an algebraic state for open source voltage U_{oc} is introduced, which is expressed as function of state voltage.
- The maximum ICE torque rate of increase duT_{ICE} was considered to be 3%/s in experiment a, as previously, and 5%/s in experiments b and c.
- The extra constraints for the controller are:
 - a. $20 \leq SOC \leq 80$ [%] (Hard Constraint)
 - b. $SOC + \varepsilon \geq 25$ [%] (Soft Constraint)
 - c. $SOC - \varepsilon \leq 75$ [%] (Soft Constraint)
 - d. $k_1^2 - 4R_iP_b \geq 10000$ [Volts²]
- The cost function is the same as in the previous experiment, with the alteration that instead of the EM torque command uT_{EM} , the diversion of *SoC* from the reference is penalized.

Constraints regarding the operational parameters of the engine, were decided not to be included, since they would set additional limits for engine torque, and consequently, it would probably required extensive EM operation in higher loads, something which would lead to extensive drop of battery state of charge.

HIPPO-2 experimental test-bed does not integrate any battery configuration yet. Therefore, the battery was decided to be virtual, which was employed on the dSpace Micro Autobox II control platform. The battery was simulated dynamically according to the PNGV model which is described in Section 2.4.2. The battery consists of 250 battery cells, connected in series, with total capacitance of 2 Ah. The parameters for both quasi-static model for the controller and the dynamic simulated model, are given in Table 5.3.

<i>Parameter</i>	<i>Value</i>	<i>Unit</i>
<i>PNGV Model</i>		
OCV	875	Volts
R_O	0.6025	Ohms
R_P	0.6775	Ohms
$1/OCV'$	140	Farads
C	7.7	Farads
<i>Quasi - Static Model</i>		
k_1	875	Volts
k_2	51.13	Volts/% SoC
R_i	1.28	Ohms

Table 5.3: PNGV and quasi-static ECM parameters for experiment

5.3.2 Experimental Results

In the following figures the experimental results are shown. The first experiment, which is presented in Fig. 5.13, 5.14 and 5.15 and corresponds to experiment 3a, is conducted in order to validate the controller behavior regarding the battery charging and discharging operations and the engine's with allowed rate of torque increase (3%/s). The other two experiments, besides the validation of the NMPC, were also conducted in order to compare the *phlegmatistion* strategy of NOx reduction emissions, in present of a battery of small capacitance which requires to be charged during the operation. Therefore the loading scenarios, which were conducted, are the same as previous, one for constant speed reference and one for step changed. These experiments are corresponding to experiment 3b, Fig. 5.1, 5.2 and 5.3, in which the speed reference is constant and equals 1800 rpm as previously, to experiment 3c, Fig. 5.1, 5.2 and 5.3, in which the reference is dynamic. The quantities which are measured and shown are the same as previously with the addition of battery SoC. The results are also compared with the ones of the solely operation of ICE.

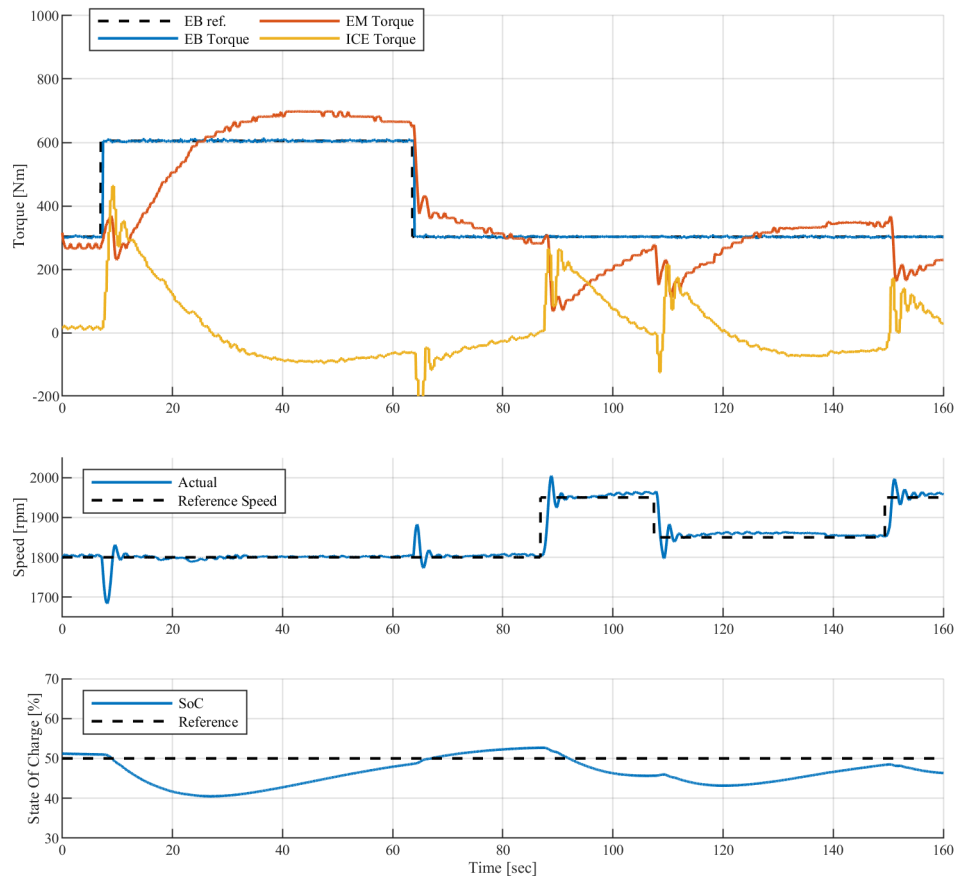


Figure 5.13: Exp 3a: Applied EB torque, EM torque and ICE torque.

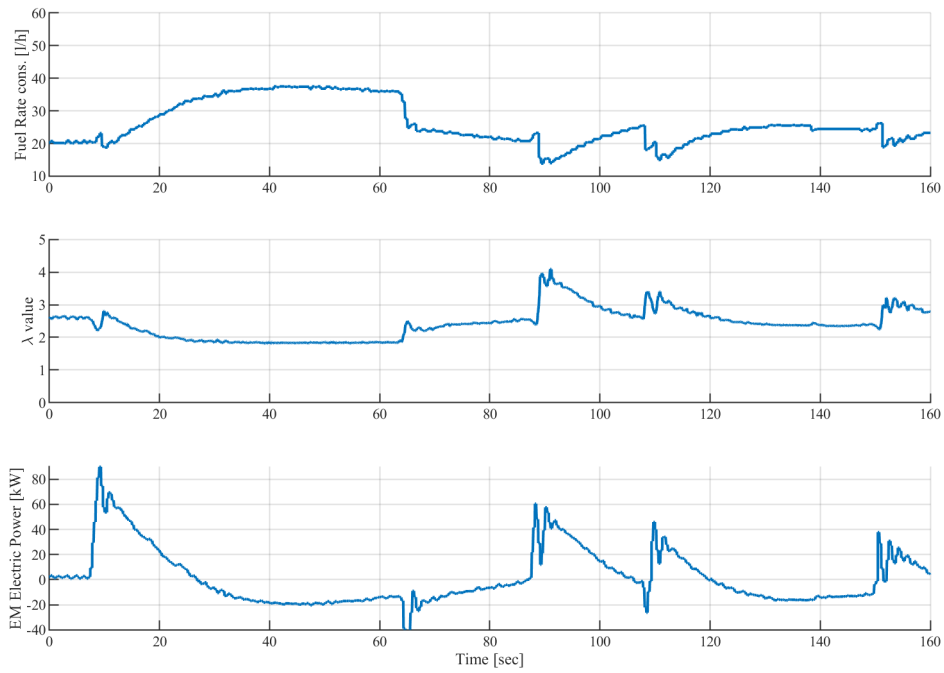


Figure 5.14: Exp 3a: Measured fuel rate consumption and reference, λ value and EM requested power.

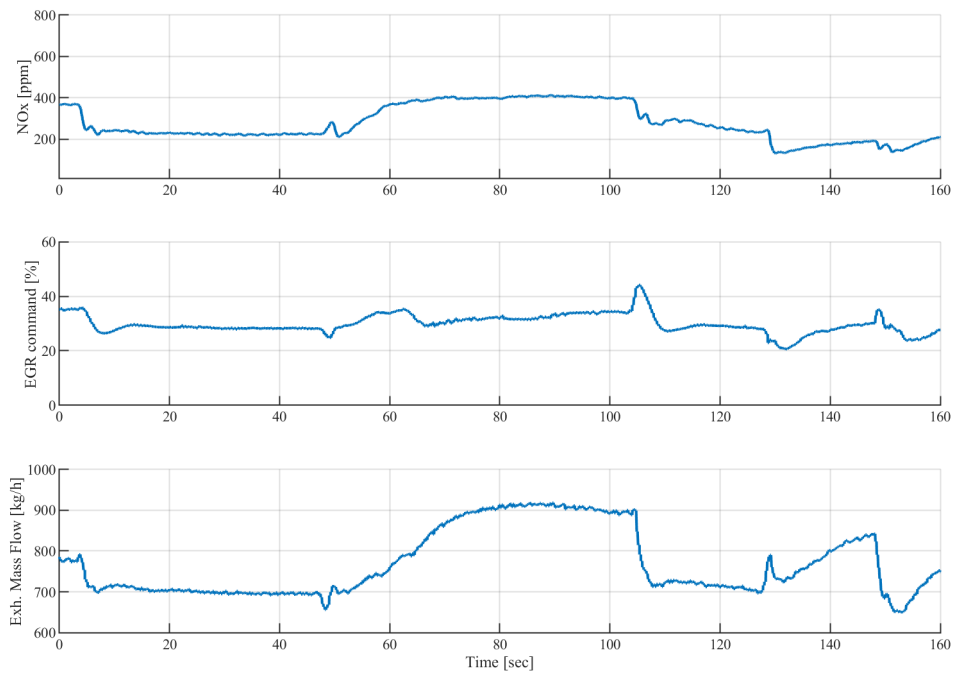


Figure 5.15: Exp 3a: NOx concentration, EGR valve command and Exhaust Gas Mass Flow.

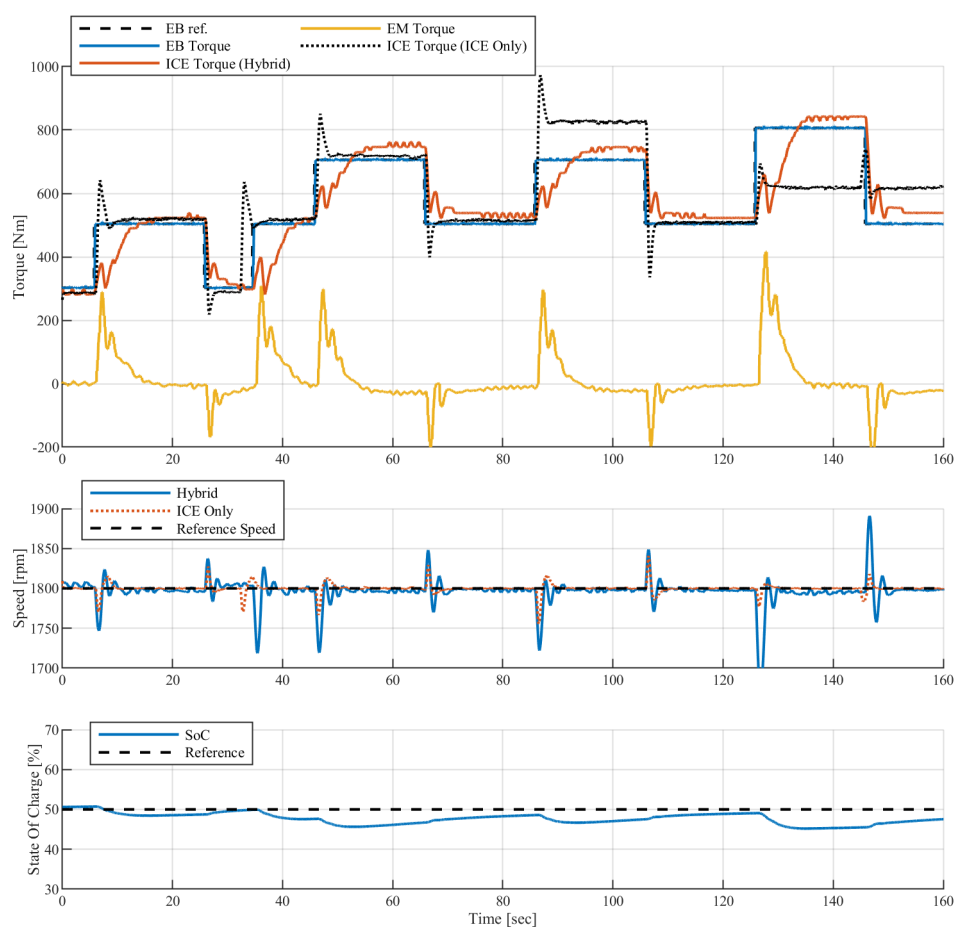


Figure 5.16: Exp 3b: Applied EB torque, EM torque and ICE torque.

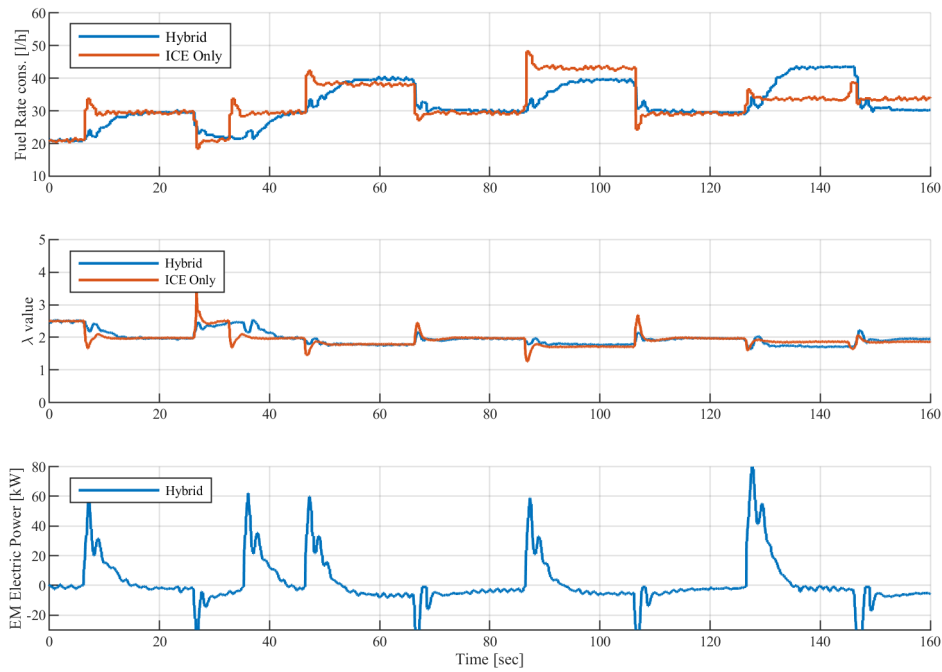


Figure 5.17: Exp 3b: Measured fuel rate consumption and reference, λ value and EM requested power.

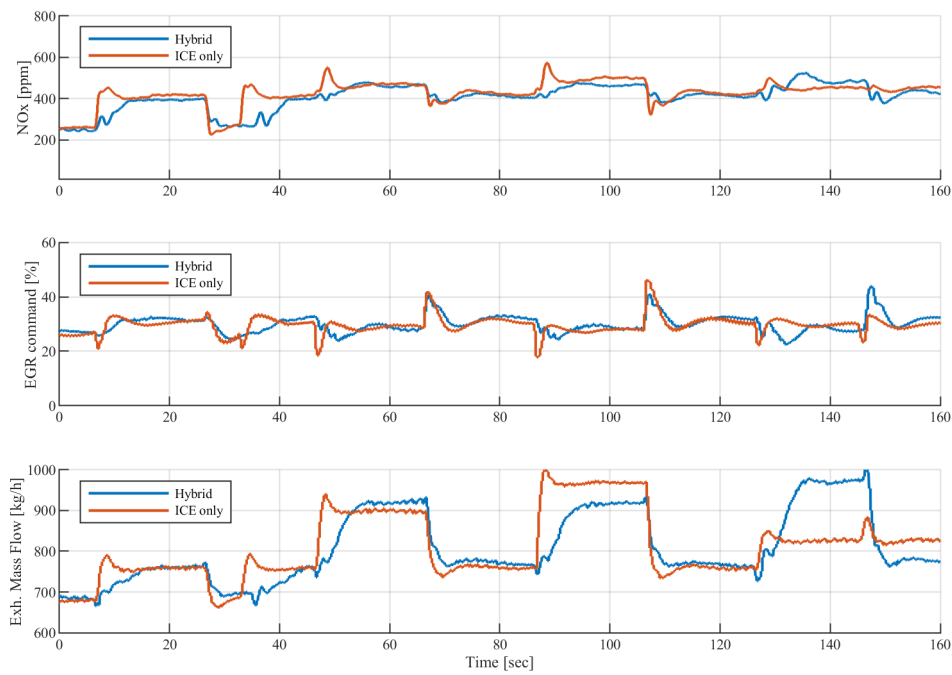


Figure 5.18: Exp 3b: NOx concentration, EGR valve command and Exhaust Gas Mass Flow.

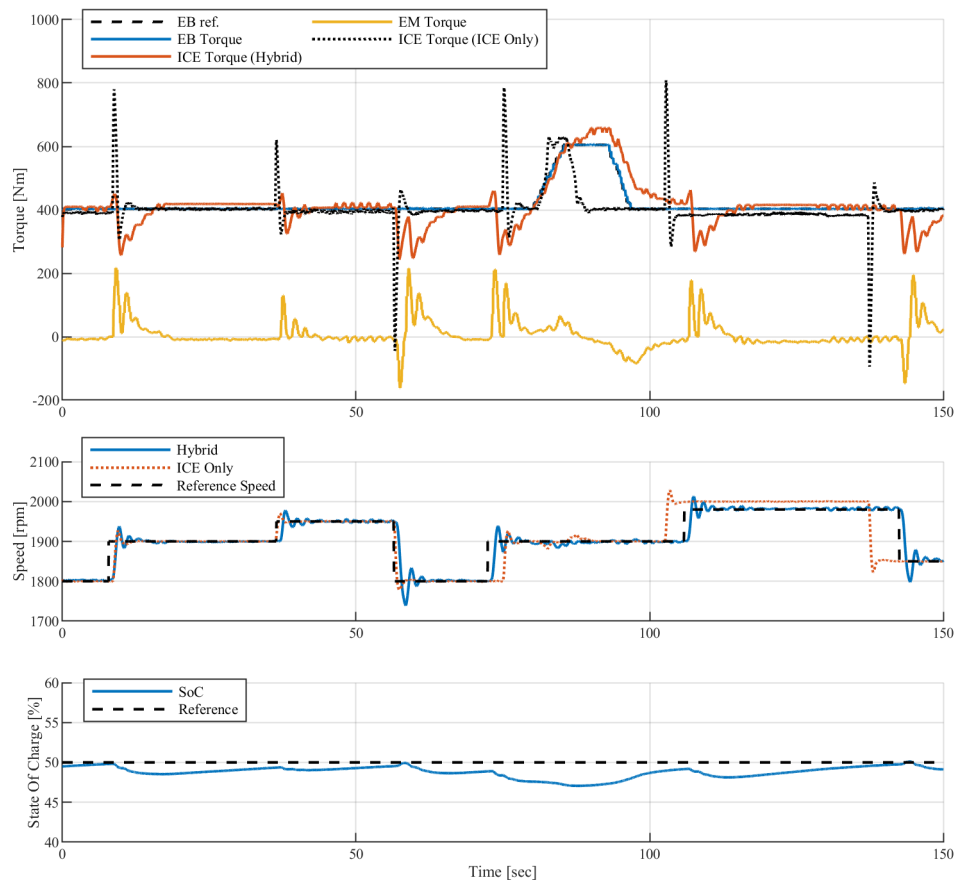


Figure 5.19: Exp 3c: Applied EB torque, EM torque and ICE torque

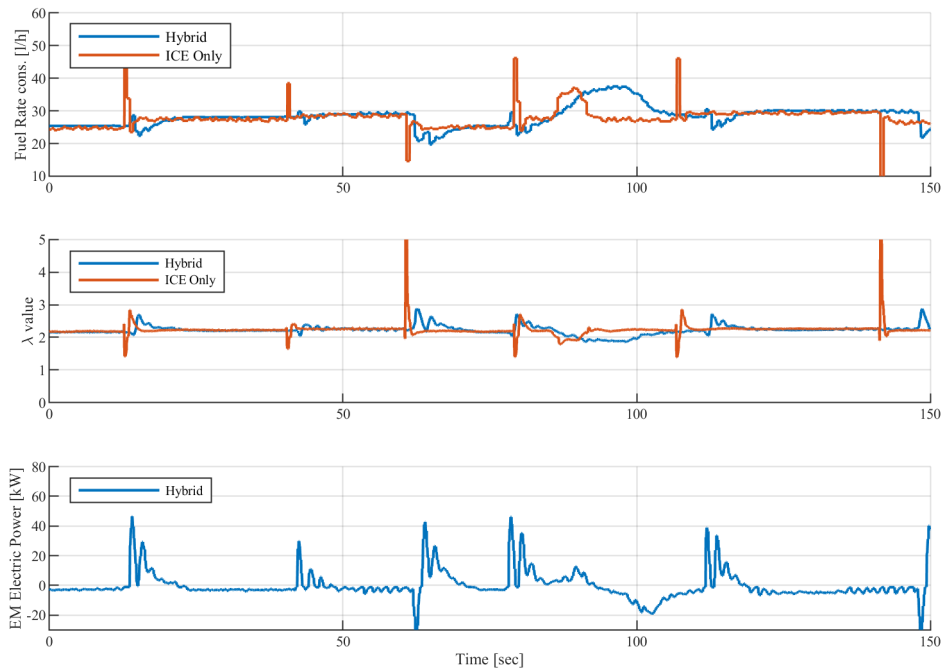


Figure 5.20: Exp 3c: Measured fuel rate consumption and reference, λ value and EM requested power.

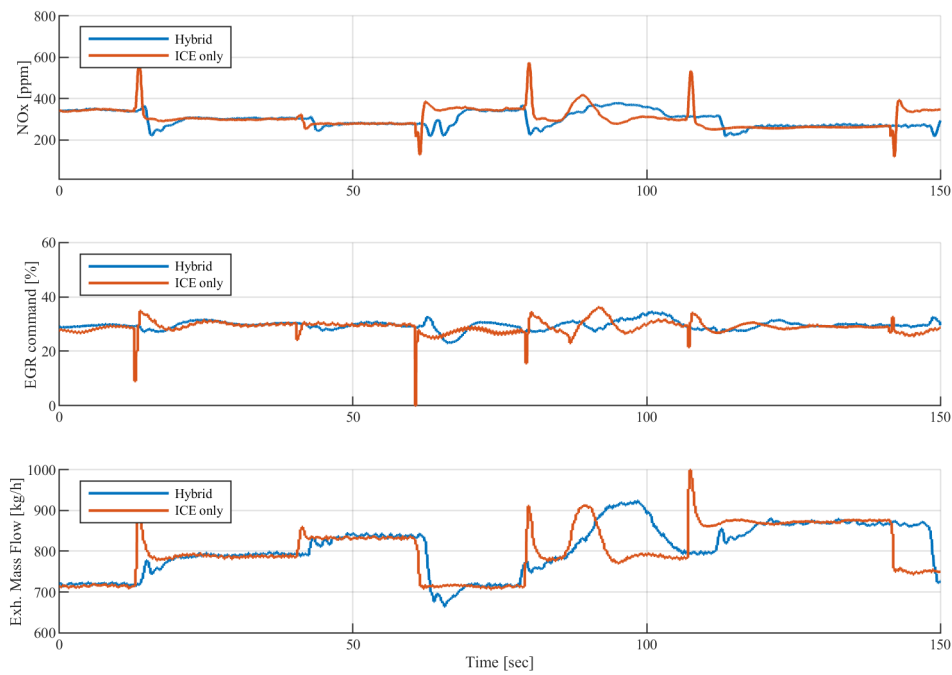


Figure 5.21: Exp 3c: NO_x concentration, EGR valve command and Exhaust Gas Mass Flow

5.3.3 Results Analysis

NMPC behavior analysis regarding battery configuration

From the results of the previous figures, it is obvious that the NMPC can efficiently address the power split problem, considering restricted power source for the EM, as the battery is, while charge level have to be maintained inside predefined limits. In transient conditions, the plant behavior is the same as in the previous experiment. When a load pulse, or an alteration of speed reference occurs, for instance at instant 47 s, Fig. 5.14, a step load of 300 Nm is applied to the plant, the NMPC increase the command of EM rapidly, in order to restore the system to the current reference. The ICE command is also increased, with a much slower rate of course, in order to compensate gradually the EM torque. When this occurs, in contrast to the previous scheme, the torque command of ICE is further increased, and the extra torque is absorbed by the EM, which operates in generator mode. With the produced power, the EM charges the battery so as to be restored to its reference SoC level. When this happens the EM torque command tends to be restored in zero position.

In steady condition, the EM remains in generating mode, due to the losses (e.g. friction and iron losses, etc.), in order to not consumed the battery. The required power for the EM, to overcome these losses, has been calculated via Willan's model to be around 0.3 kW. Therefore, as regarding the extra fuel consumption, this can be considered negligible. Furthermore, when the EM passes from generating mode to motor and the opposite, there is an hysteresis of 0.4 resulting a slightly higher overshoot for the rotational speed, than in the previous scheme. However, as it can be shown from the experimental results, this overshoot can be consider acceptable.

Another point which is worth to be mentioned is the behavior of the controller with different tuning parameters. The NMPC, which was used in the first experiment, was tuned with heavier penalization of the diversion of SoC charge from the reference (i.e. 10% decrease) and with reduced engine dynamics (i.e. the ICE command rate limit from 3%/s for the first experiment 5 %/s for the second). From the previous results, it is clear that in the first case battery, SoC is replenished with a faster rate. When transient operation is conducted the engine increases even more the ICE command in order the SoC to reach its reference point. In the second and third case, the controller although it regulates the ICE command in the same logic, the extra generating torque is not as high as before, and SoC converges to its reference with much slower rate, and in some cases, this would never be reached, as the recharging would stop in a near SoC value. This can be explained from the fact that, in the cost function the rate of change, and the EM torque (motoring and generative) are penalized. Thus in some cases the cost function reaches its minimum before the SoC reaches its reference. The opposite applies in the first case. It is observed that when the depth of discharge is large enough after a transient operation, the EM torque can be high enough that would result the engine speed to diverge from the reference value, and would not be restore until the battery charge is replenished. For instance in Fig. 5.13 for time period 120 -140 s, the engine speed is increased due to the increased ICE torque which have to be absorbed by the EM. It is only restored, after the torque is stabilized. The reason for that, is the same as before.

Plant behavior analysis regarding NOx emissions and phlegmatisation

As in the previous scheme, reduced ICE dynamics were applied, in order to force the engine to operate in steady state. As it was shown in the previous experiment, NOx emis-

sions reduction for this kind of loads can reach as high as 21%. However, in this scheme the consumed electrical energy is derived from the battery storage, and it is replenished immediately by the ICE in order to maintain the SoC according the reference. As it was mentioned the loads were also similar to those of experiments 2a and 2b, in order to compare the results. The NOx production is shown in Fig. 5.22 and 5.23. As in the previous section, the experiment results are compared in time periods which the operational profiles of the solely ICE and the Hybrid configuration are the same. The results are presented in Table 5.4.

<i>Case</i>	<i>Constant SE Reference</i>			<i>Step Change SE Reference</i>		
	ICE only	Hybrid	Difference [%]	ICE only	Hybrid	Difference [%]
<i>Quantities</i>						
<i>Mean Emissions NO_X [mg/s]</i>	147.52	138.95	5.81	106.23	102.23	3.30
<i>Total Emissions NO_X [g]</i>	10.030	9.45	5.78	4.57	4.42	3.30
<i>Mean Emissions NO_X [g/kWh]</i>	5.12	4.91	4.01	4.76	4.62	2.99
<i>Fuel Consumption [l]</i>	0.5901	0.5806	1.61	0.3331	0.3312	0.57
<i>SoC difference [%]</i>	-	+0.7	-	-	-0.1	-

Table 5.4: Comparison Hybrid vs ICE sole operation for the same load cycle and battery configuration.

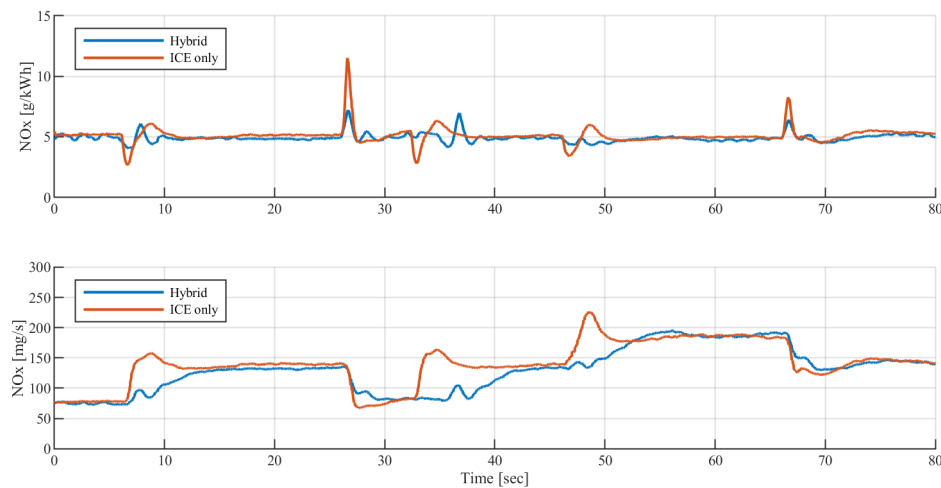


Figure 5.22: Exp 5b: NOx production for static reference in mg/s and g/kWh .

In regard to these results, a number of observations should be noted. Firstly, it is observed that the reduction of NOx emissions is 3% to 6%, while the fuel consumption is slightly decreased or it is nearly the same. Considering that in the previous scheme, this reduction could reach 21 % without increasing the fuel consumption (under some specific assumptions), it is clear that the efficiency of this control scheme regarding the NOx emissions reduction is significantly lower. The main reason for that is the battery regeneration is conducted in low-efficiency operation regions. That means that more fuel is been consumed in order torque to be produced and battery to be charged, resulting more

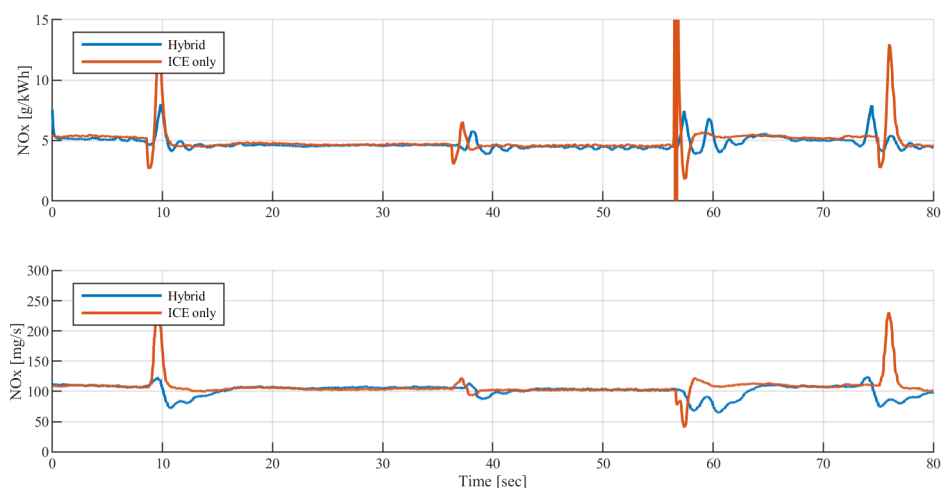


Figure 5.23: Exp 5c: NOx production for dynamic reference in mg/s and g/kWh .

NOx emissions. Furthermore, the dynamics of the engine are increased. According to [62] this contributes further to increase the NOx production. However this control logic has a major advantage, that contrary to the schemes 2a and 2b, the battery regeneration is been conducted during the transient load conditions. Therefore, this algorithm is appropriate for slightly NOx reduction and battery regeneration, in cases which the power plant is not going to work in higher efficiency, or there is uncertainty about the future load cycles.

Chapter 6

Conclusions and Future Work

Conclusions

In this work, the potential of using nonlinear model predictive control for conducting efficient real time power split in a hybrid diesel-electric marine power plant has been investigated. Initially, polynomial differential and static models for the engine were investigated and validated via several experiments. Electric motor/generator was model using a quasi-static model, since it was determined that its dynamics are much more faster than those of the controller. Furthermore, a virtual battery was considered, and modeled dynamically for simulations, while a quasi-static model was employed for the NMPC. As far as the controller design procedure concerned, two approaches were consider. The first approach, is referred as indirect engine control, and its purpose to regulate the EM torque in order to manipulate the engine operation point. The second, is referred as direct engine engine control, as both of the power sources of the plant are controlled directly from the NMPC. In the second scheme, reduction of engine dynamics (phlegmatising) was also performed in order to reduce the NOx emissions. Furthermore, an efficient observer, using the moving horizon estimation technique, was also developed, in order to estimate the applied load. The performance of the developed controllers and observer were tested in simulations, using a hybrid diesel-electric simulation set-up, which was developed for this reason.

The performance of controllers were verified experimentally on the diesel-electric testbed at LME, under realistic transient loads. Experimental results showed that NMPC is capable of controlling the power plant in real time, in respect to the references and constraints which have been set. Moreover the phlegmatising strategy which was implemented, led to significant reduction of NOx emissions. Finally, the controller efficiency led to slightly fuel consumption reduction, during transient operations.

Conclusively, it was verified that NMPC controller and MHE estimator can be successfully applied in real time for control applications regarding the operation of hybrid powertrains. Their ability to handle nonlinear equations, constraints and multiple references makes them a powerful tool for efficient control of such plants.

Future Work

In this thesis, nonlinear model predictive control was employed with primary objective to track the speed reference and satisfy the implemented constraints. The consider objective was to reduce the engine dynamic response during transient operations via the electric motor.

It can be suggested that fuel reduction strategies could also be implemented. These strategies, are based on the load circle prediction, and optimization of power split via the equivalent fuel consumption. In this scheme, a multilevel control configuration could control the plant, in which the developed NMPC would receive the optimal control reference trajectory, and regulate the power plant operation accordingly.

Furthermore, NO_x static models could be constructed and integrated in the NMPC along with constraints regarding, the maximum allowed emissions (e.g. regulation limit). Considering the behavior of the NMPC in near constraint operation, the plant would operate near the constraints, achieving maximum efficiency. Moreover, the after-treatment system could also be taken into account, by penalizing the urea consumption, in order to achieve an economic reduction of NO_x.

Finally, the MHE scheme could also be investigated further for estimating other plant parameters which are not available or are tampered by disturbances, such as the turbocharger speed etc.

Appendices

Appendix A

Simulation Engine Model Symbols and Parameters

The symbolism and parameters of SCANIA engine simulation model were derived from [12]. In table A.1, the symbolism of the model are explained, in A.2 the physical constants are shown, and in A.3 the engine parameters are presented.

Model Nomenclature

E_{req}	= required energy (J)	T_{ig}	= indicated gross torque (N m)
\dot{m}_{ac}	= massflow after compressor (kg/s)	T_{pump}	= pumping torque (N m)
\dot{m}_c	= compressor massflow (kg/s)	u_f	= injected fuel mass (mg/cycle)
$\dot{m}_{c,corr}$	= corrected compressor massflow (kg/s)	u_{wg}	= wastegate position
\dot{m}_f	= fuel flow (kg/s)	x_p	= pressure quotient from combustion
\dot{m}_t	= turbine massflow (kg/s)	λ	= air/fuel ratio
\dot{m}_{wg}	= wastegate massflow (kg/s)	Π_c	= pressure ratio over compressor
P_c	= compressor power (W)	$\Pi_{c,max}$	= pressure ratio for zero massflow
P_t	= turbine power (W)	Π_t	= pressure ratio over turbine
p_{em}	= exhaust manifold pressure (Pa)	Π_t^*	= useful pressure ratio over turbine
p_{im}	= intake manifold pressure (Pa)	Π_{wg}	= pressure ratio over wastegate
q_{in}	= specific energy of the charge (J/kg)	phi_{λ}	= smoke-limiter (kg/s)
T_{em}	= exhaust manifold temperature (K)	Psi_t	= massflow parameter
T_{fric}	= friction torque (N m)	Psi_{wg}	= massflow parameter
T_{ice}	= engine torque (N m)	ω_{ice}	= engine speed (rad/s)

Table A.1: Nomenclature for engine model [12].

Constants			
Symbol	Description	Value	Unit
p_{amb}	Ambient pressure	1.011×10^5	Pa
T_{amb}	Ambient temperature	298.46	K
p_{ref}	Reference pressure	1.011×10^5	Pa
T_{ref}	Reference temperature	298.46	K
c_{pa}	Specific heat capacity of air, constant pressure	1011	$J/(kgK)$
c_{va}	Specific heat capacity of air, constant volume	724	$J/(kgK)$
γ_e	Specific heat capacity ratio of air	1.3964	-
R_a	Gas constant, air	287	$J/(kgK)$
c_{pe}	Specific heat capacity of exhaust gas, constant pressure	1332	$J/(kgK)$
γ_e	Specific heat capacity ratio of exhaust gas	1.2734	-
R_e	Gas constant, exhaust gas	286	$J/(kgK)$
γ_{cyl}	Specific heat capacity ratio of cylinder gas	1.35004	-
T_{im}	Temperature intake manifold	300.6186	K
p_{es}	Pressure in exhaust system	1.011×10^5	Pa
$(A/F)_s$	Stoichiometric oxygen–fuel ratio	14.57	-
q_{HV}	Heating value, diesel	42.9^6	J/kg

Table A.2: Constant that were applied for engine model [12].

Parameters			
Symbol	Description	Value	Unit
n_{cyl}	Number of cylinders	6	-
V_D	Engine displacement	0.0127	m^3
r_c	Compressor Ratio	17.3	-
J_{set}	Inertia of the engine-brake-electric motor	3.5	kgm^2
V_{is}	Volume of intake system	0.0218	m^3
R_c	Compressor radius	0.04	m
Ψ_{max}	Maximum compressor head parameter	1.5927	-
$\dot{m}_{c,corr,max}$	Maximum corrected compressor massflow	0.5462	kg/s
n_c	Compressor efficiency	0.5376	-
n_{vol}	Volumetric efficiency	0.8928	-
$n_{ig,ch}$	Combustion chamber efficiency	0.6774	-
$c_{fr,1}$	Friction coefficient	8.4100×10^{-5}	-
$c_{fr,2}$	Friction coefficient	-5.6039×10^{-3}	-
$c_{fr,3}$	Friction coefficient	0.4758	-
n_{sc}	Nonideal Seliger cycle compensation	1.0540	-
x_{cv}	Ratio of fuel burnt during constant volume	0.4046	-
V_{em}	Volume of exhaust manifold	0.0199	kgm^2
J_{tc}	Turbocharger inertia	1.9662×10^{-4}	m^3
w_{fric}	Turbocharger friction	2.4358×10^{-5}	kgm^2/rad
$A_{t,eff}$	Effective turbine area	9.8938×10^{-4}	m^3
n_t	Turbine efficiency	0.7278	-
$c_{wg,1}$	Wastegate parameter	0.6679	-
$c_{wg,2}$	Wastegate parameter	5.3039	-
$A_{wg,eff}$	Effective wastegate area	8.8357×10^{-4}	m^3
λ_{min}	Minimum air/fuel ratio, smoke-limit	1.2	-

Table A.3: Parameters that were applied for engine model [12].

Bibliography

- [1] R. Geertsma, R. Negenborn, K. Visser, and J. Hopman, “Design and control of hybrid power and propulsion systems for smart ships: A review of developments,” *Applied Energy*, vol. 194, pp. 30 – 54, 2017.
- [2] R. A. of Engineering, *Future Ship Powering Options Exploring alternative methods of ship propulsion*. IMO, 2013.
- [3] G. Sulligoi, S. Castellan, M. Aizza, D. Bosich, L. Piva, and G. Lipardi, “Active front-end for shaft power generation and voltage control in fremm frigates integrated power system: Modeling and validation,” in *International Symposium on Power Electronics Power Electronics, Electrical Drives, Automation and Motion*, pp. 452–457, June 2012.
- [4] S. K. Topaloglou, G. Papalambrou, K. Bardis, and N. Kyrtatos, “Transient load share management of a diesel electric hybrid powertrain for ship propulsion,” *International Journal of Powertrains*, vol. 7, p. 341, 01 2018.
- [5] N. Planakis, G. Papalambrou, and N. Kyrtatos, “Predictive control for a marine hybrid diesel-electric plant during transient operation,” pp. 989–994, 04 2018.
- [6] H. T. Grimmelius, P. D. Vos, M. Krijgsman, and E. van Deursen, “Control of hybrid ship drive systems,” 2011.
- [7] *Internal Combustion Engine Fundamentals*. McGraw-Hill, 1988.
- [8] L. Guzzella and A. Amstutz, “Control of diesel engines,” *Control Systems, IEEE*, vol. 18, pp. 53 – 71, 11 1998.
- [9] *Handbook of Diesel Engines*. Springer, 2010.
- [10] L. Eriksson, “Modeling and control of turbocharged si and di engines,” *Oil and Gas Science and Technology - Revue de l'IFP*, vol. 62, 07 2007.
- [11] J. Wahlstrom, L. Casacca, and W. A. Eriksson, “Modelling diesel engines with a variable-geometry turbocharger and exhaust gas re-circulation by optimizing of model parameters of model parameters for capturing non-linear system dynamics. proceedings of the institution of mechanical engineers, part d,,” *Journal of automobile engineering*, vol. 7, no. 225, pp. 960–986, 2011.
- [12] M. Sivertsson and L. Eriksson, “Optimal transient control trajectories in diesel–electric systems—part i: Modeling, problem formulation, and engine properties,” *Journal of Engineering for Gas Turbines and Power*, vol. 137, p. 021601, 02 2014.

- [13] M. Huang, H. Nakada, K. Butts, and I. Kolmanovsky, "Nonlinear model predictive control of a diesel engine air path: A comparison of constraint handling and computational strategies," *IFAC-PapersOnLine*, vol. 48, pp. 372–379, 12 2015.
- [14] M. Herceg, T. Raff, R. Findeisen, and F. Allgöwe, "Nonlinear model predictive control of a turbocharged diesel engine," pp. 2766 – 2771, 11 2006.
- [15] J. Aspriona, O. Chinellato, C. Onder, and L. Guzzella, "From static to dynamic optimisation of diesel-engine control," pp. 6824–6829, 12 2013.
- [16] *Robust Adaptive Control*. Dover Publications. Dover Publications Inc., 1995.
- [17] L. Guzzella and A. Sciarretta, *Vehicle Propulsion Systems: Introduction to Modeling and Optimization*. 01 2007.
- [18] A. Parmar and A. Patrel, "Speed control techniques for induction motor - a review," in *International Journal for Scientific Research and Development*, vol. 2, 2014.
- [19] B. Ozpineci and L. M. Tolbert, "Simulink implementation of induction machine model - a modular approach," in *IEEE International Electric Machines and Drives Conference, 2003. IEMDC'03.*, vol. 2, pp. 728–734 vol.2, 2003.
- [20] A. Haintham, I. Atif, and J. Guzinski, *High Performance Control of AC Drives with MATLAB/SIMULINK Models*. Wiley, 2012.
- [21] *DTC: A motor control technique for all seasons*. ABB, 2013.
- [22] P. Dietrich, "Gesamtenergetische bewertung verschiedener betriebsarten eines parallel-hybridantriebes mit schwungradkomponente und stufenlosem weitbereichsgetriebe für einen personenwagen /," 07 2019.
- [23] W. Lee, D. Choi, and M. Sunwoo, "Modelling and simulation of vehicle electric power system," *Journal of Power Sources*, vol. 109, no. 1, pp. 58 – 66, 2002.
- [24] V. Johnson, "Battery performance models in advisor," *Journal of Power Sources*, vol. 110, no. 2, pp. 321 – 329, 2002.
- [25] V. Shagar, S. Jayasinghe, and H. Enshaehi, "Effect of load changes on hybrid shipboard power systems and energy storage as a potential solution: A review," *Inventions*, vol. 2, p. 21, 08 2017.
- [26] *The Handbook of Lithium-Ion Battery Pack Design Chemistry, Components, Types and Terminology*. Elsevier, 2015.
- [27] T. Hartley and A. Jannette, "A first principles battery model for the international space station," vol. 2, 08 2005.
- [28] *Use of Lithium Batteries in the Marine and Offshore Industries*. American Bureau of Shipping. ABS, 2018.
- [29] H. Mu and R. Xiong, *Modeling, Evaluation, and State Estimation for Batteries*, pp. 1–38. 01 2018.
- [30] R. Hartman, *An Aging Model for Lithium-Ion*. University of Akron, 2008.
- [31] *NGV Battery Test Manual. Partnership for a New Generation of Vehicles*. PNGV, 2001.

- [32] “A simplified model of the lead/acid battery,” *Journal of Power Sources*, vol. 46, no. 2, pp. 251 – 262, 1993, note = Proceedings of the International Conference on Lead/Acid Batteries: LABAT ’93,.
- [33] Z. M. Salameh, M. A. Casacca, and W. A. Lynch, “A mathematical model for lead-acid batteries,” *IEEE Transactions on Energy Conversion*, vol. 7, no. 1, pp. 93–98, 1992.
- [34] S. Buller, M. Thele, E. Karden, and R. De Doncker, “Impedance-based non-linear dynamic battery modeling for automotive applications,” *Journal of Power Sources*, vol. 113, pp. 422–430, 01 2003.
- [35] M. Sivertsson and L. Eriksson, “Optimal transient control trajectories in diesel–electric systems—part ii: Generator and energy storage effects,” *Journal of Engineering for Gas Turbines and Power*, vol. 137, p. 021602, 02 2014.
- [36] S. Xiang, G. Hu, R. Huang, F. Guo, and P. Zhou, “Lithium-ion battery online rapid state-of-power estimation under multiple constraints,” *Energies*, vol. 11, p. 283, 01 2018.
- [37] X. Liu, W. Li, and A. Zhou, “Pngv equivalent circuit model and soc estimation algorithm for lithium battery pack adopted in agv vehicle,” *IEEE Access*, vol. 6, pp. 23639–23647, 2018.
- [38] *Modeling, Simulation and Implementation of Li-Ion Battery Powered Electric and Plug-In Hybrid Vehicles*. University of Akron, 2011.
- [39] J. Maciejowski, *Predictive Control with Constraints*. Prentice Hall, 2000.
- [40] B. Kouvaritakis and M. Cannon, *Model Predictive Control Classical, Robust and Stochastic*. Springer, 2014.
- [41] H. J. Ferreau, C. Kirches, A. P. H. G. Bock, and M. Diehl, “qpOASES: A parametric active-set algorithm for quadratic programming,” *Mathematical Programming Computation*, p. 327 – 363, 2014.
- [42] A. Z. A. Domahidi, M. Zeilinger, M. Morari, , and C. Jones, “Efficient interior point methods for multistage problems arising in receding horizon control.,” *IEEE Conference on Decision and Control (CDC)*, p. 668 – 674, 2012.
- [43] S. Grosa, M. Zanona, R. Quirynen, A. Bemporad, and M. Diehl, “From linear to nonlinear mpc: Bridging the gap via real-time iteration,” *International Journal of Control*, 2015.
- [44] M. Diehl, H. G. Bock, P. S. Johannes, R. Findeisen, Z. Nagy, and F. Allgower, “Real-time optimization and nonlinear model predictive control of processes governed by differential-algebraic equations,” *Journal of Process Control*, 2002.
- [45] J. Nocedal and S. Wright, *Numerical Optimization*. Springer Series in Operations Research and Financial Engineering, 2006.
- [46] M. Diehl, *Real-Time Optimization for Large Scale Nonlinear Processes*. PhD thesis, Universitat Heidelberg,, 2001.
- [47] M. Boegli, *Real-Time Moving Horizon Estimation for Advanced Motion Control Application to Friction State and Parameter Estimation*. PhD thesis, KU Leuven – Faculty of Engineering Science,, 2014.

- [48] P. Kühnl, M. Diehl, T. Kraus, J. P. Schlöder, and H. G. Bock, “A real-time algorithm for moving horizon state and parameter estimation,” *Computers and Chemical Engineering*, vol. 35, no. 1, pp. 71–83, 2011.
- [49] P. Kühnl, M. Diehl, T. Kraus, J. P. Schlöder, and H. Bock, “A real-time algorithm for moving horizon state and parameter estimation,” *Computers and Chemical Engineering*, vol. 35, pp. 71–83, 01 2011.
- [50] B. Houska, H. Ferreau, and M. Diehl, “ACADO Toolkit – An Open Source Framework for Automatic Control and Dynamic Optimization,” *Optimal Control Applications and Methods*, vol. 32, no. 3, pp. 298–312, 2011.
- [51] B. Houska, H. Ferreau, and M. Diehl, “An Auto-Generated Real-Time Iteration Algorithm for Nonlinear MPC in the Microsecond Range,” *Automatica*, vol. 47, no. 10, pp. 2279–2285, 2011.
- [52] B. Houska, H. Ferreau, M. Vukov, and R. Quirynen, “ACADO Toolkit User’s Manual.” <http://www.acadotoolkit.org>, 2009–2013.
- [53] H. Ferreau, T. Kraus, M. Vukov, W. Saeys, and M. Diehl, “High-speed moving horizon estimation based on automatic code generation,” in *Proceedings of the 51th IEEE Conference on Decision and Control (CDC 2012)*, 2012.
- [54] E. Kanellis and G. Vasov, *Real time NMPC for fixed wing UAV applications*. Master Thesis, Aalborg University – Electronics and IT, 2016.
- [55] D. Ariens, B. Houska, and H. Ferreau, “Acado for matlab user’s manual.” <http://www.acadotoolkit.org>, 2010–2011.
- [56] G. Papalambrou, *Introduction to Control Systems, Lecture Notes*. Zografou, Athens: NTUA, 2011.
- [57] D. Vasrsamis, *Load Simulation during ship propulasion and application in experimental marine hybrid Diesel-Electric testbed*. Zografou, Athens: NTUA, 2019.
- [58] J. Rawlings, D. Angeli, and C. Bates, “Fundamentals of economic model predictive control,” *51st IEEE Conference on Decision and Control*, p. 3851–3861, 2012.
- [59] E. Giakoumis, *Diesel Engine Transient Operation*. 04 2009.
- [60] J. R. Hagena, Z. Filipi, and D. N. Assanis, “Transient diesel emissions: Analysis of engine operation during a tip-in,” in *SAE Technical Paper*, SAE International, 04 2006.
- [61] H. Jaaskeläinen, “Diesel exhaust gas.” <https://www.dieselnet.com>.
- [62] N. Lindenkamp, C.-P. Stöber-Schmidt, and P. Eilts, “Strategies for reducing no x - and particulate matter emissions in diesel hybrid electric vehicles,” 04 2009.